T2R2 東京科学大学 リサーチリポジトリ
Science Tokyo Research Repository

論文 / 著書情報
Article / Book Information

題目(和文)	平均場模型の量子アニーリングにおける量子相転移の制御
Title(English)	Control of quantum phase transitions in mean-field models for quantum annealing
著者(和文)	関優也
Author(English)	Yuya Seki
出典(和文)	学位:博士(理学), 学位授与機関:東京工業大学, 報告番号:甲第10061号, 授与年月日:2016年3月26日, 学位の種別:課程博士, 審査員:西森 秀稔,斎藤 晋,古賀 昌久,西田 祐介,竹内 一将
Citation(English)	Degree:Doctor (Science), Conferring organization: Tokyo Institute of Technology, Report number:甲第10061号, Conferred date:2016/3/26, Degree Type:Course doctor, Examiner:,,,,
学位種別(和文)	博士論文
Type(English)	Doctoral Thesis

Powered by T2R2 (Science Tokyo Research Repository)

Dissertation
Control of quantum phase transitions in mean-field models for quantum annealing

Yuya Seki
Department of Physics, Tokyo Institute of Technology

February 19, 2016

Abstract

The present thesis studies statistical-mechanical properties of mean-field models to reveal an effect of various types of quantum fluctuations against the efficiency of quantum annealing.

Quantum annealing is a quantum computation model to search the ground state of Ising spin systems by taking advantage of quantum fluctuations. The quantum fluctuations are usually induced by the transverse-field term. However, it has been reported that the quantum annealing with the transverse-field term has a difficulty of exponentially long running time for certain problems. For example, quantum annealing cannot find even the ground state of a simple ferromagnetic system. The difficulty is closely related to the phenomena of quantum phase transitions. Quantum annealing typically requires exponentially long time to find the ground state of a system, if the system undergoes a first-order quantum phase transition in the thermodynamics limit. Hence, avoiding first-order quantum phase transitions is a critical issue for quantum annealing.

A solution to avoid the difficulty mentioned above is to use a degree of freedom of quantum annealing. Although many studies adopt the transverse-field term to induce quantum fluctuations, there is no restriction to use the term. The present thesis shows that the difficulty for the simple ferromagnetic system can be avoided by using transverse antiferromagnetic interactions. Furthermore, the antiferromagnetic term turns out to be also effective for a random spin system. We next focus on the macroscopic degeneracy of the ground states of the antiferromagnetic term. In order to reveal the effect of the macroscopic degeneracy, the Wajnflasz-Pick model is analyzed. The Wajnflasz-Pick model is interesting also in terms of providing an alternative way to control the order of quantum phase transitions.

Acknowledgments

I would like to thank my supervisor Prof. Hidetoshi Nishimori for his guidance and revisions of the thesis and the papers we co-authored. The studies in the present thesis could not have been accomplished without his insightful advice. I am also grateful to Dr. Kazutaka Takahashi for fruitful discussions. I would like to thank the current and previous members of the Nishimori group for discussion stimulating my study. I would like to thank Dr. Shu Tanaka for giving me an idea of the Wajnflasz-Pick model. Thank all my colleagues for sharing nice days at Tokyo Institute of Technology. I acknowledge the financial support from the Global Center of Excellence Program by MEXT, Japan through the "Nanoscience and Quantum Physics" Project of Tokyo Institute of Technology and the financial support provided through the Research Fellowship of the Japan Society for Promotion of Science. Finally, I would like to show my gratitude for my family for their unfailing support.

Publications

1. Y. Seki and H. Nishimori, "Quantum Annealing with Antiferromagnetic Fluctuations", Phys. Rev. E **85**, 051112 (2012).

2. Y. Seki and H. Nishimori "Quantum Annealing with Antiferromagnetic Fluctuations for Mean-Field Models", Kinki University Series on Quantum Computing **9**, 103 (2013).

3. Y. Seki and H. Nishimori "Quantum Annealing with Antiferromagnetic Transverse Interactions for the Hopfield Model", J. Phys. A: Math. Theor. **48**, 335301 (2015).

Contents

Chapter 1.

Introduction

The present thesis analyzes quantum phase transitions of discrete quantum systems from a point of view of quantum annealing. Quantum annealing [1–6] stems from development of algorithms for combinatorial optimization problems [7], where researchers in various field such as physics, mathematics, and computer science contributes. In this chapter, we briefly review the development of quantum annealing in order to understand the motivation of the present study. Detailed explanation is given by the subsequent chapters. We start the present chapter with background of combinatorial optimization problems. Next, Sec 1.2 explains a contribution from physics to combinatorial optimization problems. We then describe quantum annealing in association with quantum phase transitions in Sec. 1.3. Finally, Sec. 1.5 is devoted to the overview of the present thesis.

1.1. Combinatorial optimization problems

Combinatorial optimization problems [7] originate in our lives. One would try to find the shortest route from their home to workplace, and minimize the cost for the commuting. Combinatorial optimization problems are considered as problems to find an option from among a set of options so that the option minimizes cost. In economic point of view, such problems are important to save money, time, and resources. Furthermore, combinatorial optimization problems are interesting topic also in scientific context. Investigating a low-energy state of a physics system is helpful to understand low-temperature properties of the system. Here, the energy corresponds to cost, and the low-energy state to the best option.

In a computer science context, combinatorial optimization problems are formulated in the following way. First, one should convert the options of combinatorial optimization problems to bit strings with an injective mapping. Second, one should construct a function representing the cost of the problem. The function must be a scalar function of binary variables whose values correspond to the bit strings denoting the options. The function is referred to as the cost function. Although the construction of the cost function is not trivial, we can find examples of the cost function of combinatorial optimization problems such as the traveling salesman problem [8] and the protein folding problem [9]. The task of combinatorial optimization problems is to obtain a bit string that minimize the cost function. For example, the task of the traveling salesman problem is to find the shortest route from among the possible routes that visits all cities once, and returns to the first city.

A central issue for combinatorial optimization problems is development of an algorithm to solve the problems as fast as possible. In general, combinatorial optimization problems requires much time to solve themselves. The reason is twofold: One is the huge number

of possible options of combinatorial optimization problems. For example, the number of possible routes of the traveling salesman problem grows factorially as the number of cities increases. This means that it is impracticable to check all routes to find the shortest one for the problem with many cities. The other reason is complex dependency of cost functions on binary variables. A cost function of a difficult problem looks like a jagged mountain; that is, the value of the cost function changes rapidly with a little change of the binary variables, and the function has many-valley structure. This attribute makes it difficult to find the optimal solution through a simple algorithm such as the method of steepest descend.

The combinatorial optimization problems can be classified into two classes according to the necessary computational time to solve the problem. Since a large-scale problem naturally requires a long computational time, the point is the scaling of the computational time as a function of the problem size. Here, the problem size is the number of binary variables needed to represent the problem. In theoretical computer science, a problem is considered to be easy if the problem can be solved by an algorithm in a time upper bounded by a polynomial of the system size for all possible problem sizes. In this case, the algorithm is called to be efficient. On the other hand, one considers problems as hard or intractable if the optimal solution cannot be found by any algorithm in a polynomial time. Unfortunately, intractable problems are not rare. Although no proof of intractability is obtained, it is generally believed that, for instance, the traveling salesman problem is intractable because efficient algorithms have not been found despite a lot of studies being carried out.

An effective solution to deal with intractable problems is using approximate algorithms. An approximate algorithm can find the optimal solution of a given problem with a probability. Even though the approximate algorithm fails to find the optimal solution, the algorithm is expected to return an solution that is close to the optimal solution. An approximate algorithm for the traveling salesman problem is the combination of a greedy algorithm followed by the 2-opt algorithm. First, the greedy algorithm constructs an initial guess by connecting nearest cities one after another. The algorithm is based on our heuristics that visiting the nearest city is more efficient than going to a far city and coming back. Next, the 2-opt algorithm refines the initial guess by a local flip of paths. Roughly speaking, the algorithm removes crosses of paths that make the route longer. Since the approximate algorithm do not need to search all routes, the computational time can be significantly reduced. However, the drawback is that the approximate algorithm cannot be applied to other optimization problems. One have to devise an effective approximate algorithm for each problem.

1.2. Statistical mechanics in combinatorial optimization problems

Combinatorial optimization problems can be translated into physics problems of finding the ground state of an Ising spin system by identifying the binary variables with the Ising spins, and cost function with a Hamiltonian [7–11]. The transformation enables us to study combinatorial optimization problems by using ideas and methods developed in statistical physics. Since our focus is on a scaling of a computational time for large-size problems, investigation of statistical-mechanical properties of the system makes sense.

A representative contribution to computer science from statistical physics is the devel-

opment of simulated annealing (SA) [8]. The idea comes from the analogy of the annealing process of metal: when a piece of heated metal is cooled slowly enough, it eventually takes a sturdy and stable structure corresponding to the global minimum of the energy. We introduce artificial temperature into the Ising spin system whose ground state is the desired optimal solution, and reduce the temperature slowly from a high value to zero. Simulated annealing makes the system stay close to the thermal equilibrium state at each temperature by means of the Markov chain Monte Carlo method, and finally, at zero temperature, outputs the lowest-energy state, i.e., the optimal solution. Simulated annealing can be regarded as an algorithm to avoid local minima by using thermal fluctuations.

What matters is the schedule of annealing of SA. Too-fast cooling causes failure of relaxation of the system, leading wrong solution, as a metal cooled rapidly has defects. Although the appropriate annealing schedule depends on each problem, a certain sufficient condition valid for any problems has been found by Geman and Geman [5,12]. The paper has reported that an inverse-logarithmic annealing schedule ensures the success of SA for any problems in the limit of infinitely long time.

An important nature related to the appropriate annealing schedule of SA is phase transition phenomena. Divergence of relaxation time at a phase transition point indicates the failure of SA. Precisely speaking, the relaxation time in SA does not diverge, since SA is a method for finite size systems. However, finite but large systems have a long relaxation time that can be actually regarded as an infinitely long time.

1.3. Quantum annealing

Quantum annealing (QA) is a quantum computation model to solve combinatorial optimization problems by taking advantage of quantum fluctuations. Whereas SA uses thermal fluctuations to avoid local minima, QA uses quantum fluctuations. Quantum annealing can find the ground states of the Ising spin systems through the simulation of a quantum system that is governed by the Schrödinger equation. The Hamiltonian of the system consists of two parts: problem part and driver part. The problem part corresponds to the cost function. The driver part must not commute with the problem part, and induces quantum fluctuations into the system. Furthermore, let us assume that the system initially has an unique easy-to-prepare state. The method starts in the unique state, and the total Hamiltonian gradually changes from the driver part to the problem part. The adiabatic theorem of quantum mechanics [13] ensures that the success probability to get the global minimum of the problem part of the Hamiltonian is close to unity as long as the running time is much longer than inverse square of the minimum energy gap between the ground state and the first excited state during the time evolution.

Quantum phase transition is closely related to the efficiency of QA. According to the finite-size scaling theory, systems that undergo a second-order quantum phase transition have a minimum energy gap that decays polynomially in the vicinity of the phase transition point [14,15]. Since the running time of QA increases at most polynomially, QA is efficient for the problem. On the other hand, systems with a first-order phase transition typically have a minimum gap that decays exponentially [16–19] except an anomalous case [20]. Hence, QA fails to find the ground state in a reasonable time except special cases. We can thus estimate the efficiency of QA by analyzing the degree of quantum phase transition of the system. An central issue of QA is reduction in running time for hard problems. For this purpose, avoiding first-order quantum phase transitions is an important challenge to

be addressed for QA.

An advantage of QA against SA is that QA has flexibility in type of quantum fluctuations. Although many studies adopt the transverse-field term as a driver part of the Hamiltonian, there is no restriction to use the term. The present thesis shows that first-order quantum phase transitions can be avoided by using the advantage.

1.4. Purpose of the thesis

The purpose of the present thesis is to explore a way to improve the efficiency of QA by using the advantage described above. The strategies discussed in the present thesis are (1) to use antiferromagnetic transverse interactions in addition to a transverse field and (2) to adjust order of degeneracy of energy levels. To reveal the way to improve QA contributes to research for quantum computation where its computational ability is still unclear.

1.5. Overview

The present thesis investigates quantum phase transitions in order to explore the way to improve the efficiency of QA. As mentioned above, QA has a potential to avoid the difficulty by using the degree of freedom in choosing the type of quantum fluctuations. We focus on mean-field models because of its facility of analysis. Although the mean-field models seem not to be realistic, the models are most simplified models involving the difficulty for QA. Moreover, combinatorial optimization problems are closely related to mean-field models. Since the cost functions of the combinatorial optimization problems are constructed artificially, the cost function is not necessarily expressed by a Hamiltonian of nearest neighbor interactions. For example, the cost function of the traveling salesman problem given by Hopfield and Tank includes long range interactions [21]. Accordingly, the analysis of the mean-field models is of significance.

We first overview the basics of QA in Chap. 2. Quantum annealing is originally developed as a natural extension of SA. The process of QA is explained in Sec. 2.1. We then introduce an important computation model, quantum adiabatic computation, which is a restricted version of QA in Sec. 2.2. The development of quantum adiabatic computation gives criteria of the required running time of QA. We next introduce some examples that show the advantage of QA over classical algorithms, especially over SA in Sec. 2.3. Finally, the physics implementation of QA is described in Sec. 2.4.

Chapter 3 is devoted to the analysis of the ferromagnetic p-spin model. The model is just a ferromagnetic model, and its ground state is the trivial spin-aligned state. Hence, we deal with the model as an example that exhibits the difficulty of QA, that is quantum first-order phase transitions, rather than a combinatorial optimization problem. Since the ferromagnetic p-spin model is the most simplified model that tends to undergo the first-order phase transition owing to the its mean-field nature, the model is suitable for the first step to study the way to avoid the difficulty. First, we describe a principal proposition of the present thesis, which is an extension of QA using antiferromagnetic transverse interactions in Sec. 3.1. Next, Sec. 3.2 describes the framework of the analysis used in the present thesis. Section 3.3.1 shows that antiferromagnetic transverse interactions change the first-order phase transition to the second-order phase transition. Furthermore, we calculate the energy gap to estimate the running time of QA in Sec. 3.3.2. It is possible to calculate the energy gap for relatively large size systems because of a symmetry of

the model. The resulting minimum energy gap scales polynomially in the vicinity of the second-order phase transition point, which is consistent with the result of the phase diagram. Section 3.4 is devoted to discussion for the large p limit. In this limit, the ferromagnetic p-spin model reduces to the Grover problem that is known to be intractable both for classical algorithms and quantum algorithms.

Chapter 4 analyzes the Hopfield model. The main purpose of this chapter is to check if the antiferromagnetic transverse interactions are also effective for random spin systems. The model is regarded as a model that covers a wide range of mean-field random spin systems. The model exhibits various type of phase transitions by adjusting a parameter called the number of embedded patterns of memory. In addition, the model is interesting since the phase diagram of the classical Hopfield model and that of quantum Hopfield model with the transverse-field term are almost the same [22]. The fact suggests that SA and QA with the transverse-field term has the same efficiency for the model. The question here is: Is it possible to improve the efficiency of QA by using the degree of freedom? The analysis of the phase diagram of the model answers the question. We first define the quantum Hopfield model in Sec. 4.1. We then analyze the system with a finite number of patterns embedded in Sec. 4.2.1. The resulting phase diagram shows that the first-order phase transition can be avoided in a similar way as the ferromagnetic p-spin model. However, in Sec. 4.3, it turns out that the antiferromagnetic term does not help the process of QA in the case where the number of embedded patterns is proportional to the system size. In this case, a phase called spin-glass phase hampers the process. The many patterns are not a direct cause of the difficulty. We show a case where many patterns are embedded, and the process of QA for the model does not undergo first-order phase transitions in Sec. 4.4.

Chapter 5 studies the nature of quantum phase transitions in the Wajnflasz-Pick model. The definition of the Wajnflasz-Pick model is given in Sec. 5.1 First, Sec. 5.2 investigates the effect of the macroscopic degeneracy of the ground state of the antiferromagnetic term, which can be considered as a nature that provides exponential speed-up in the ferromagnetic p-spin model. Next, we explore an alternative way to avoid first-order quantum phase transitions in Sec. 5.3. The classical Wajnflasz-Pick model is known to exhibits different phase transitions depending on certain parameters of the model. We check whether a similar phenomena occurs or not in a quantum case.

We summarize our findings and conclude the thesis in Chap. 6.

Chapter 2.

Quantum annealing

In this chapter, we introduce the fundamentals of quantum annealing [1–3,6] and quantum adiabatic computation (QAC) [23] , which are quantum computation model to obtain an approximate solution for combinatorial optimization problems. In addition, a physics implementation of QA is described.

2.1. Quantum annealing

This section describes the principle of QA explicitly. Let us consider the problem of finding the ground state of a Hamiltonian $\hat{H}_0$ represented in terms of the z components of the Pauli matrices $\hat{\sigma}_i^z$ $(i = 1, \ldots, N)$. In this dissertation, we call $\hat{H}_0$ the target Hamiltonian. For the purpose of introducing quantum fluctuations, an operator $\hat{V}$ is added to the target Hamiltonian. The operator $\hat{V}$ must satisfy the following two conditions: (i) it does not commute with the target Hamiltonian, $[\hat{H}_0, \hat{V}] \neq 0$, and (ii) it has a unique trivial ground state. This noncommutativity introduces quantum fluctuations into the system, causing state transitions. Hence, let us call this operator the driver Hamiltonian. A typical example of the driver Hamiltonian is the transverse-field operator $\hat{V}_{\mathrm{TF}} \equiv -\sum_{i=1}^{N} \hat{\sigma}_i^x$, where the $\hat{\sigma}_i^x$ $(i = 1, \ldots, N)$ are the x components of the Pauli matrix. Thus the total Hamiltonian is represented by

$$\hat{H}(t) = \hat{H}_0 + \Gamma(t)\hat{V}, \tag{2.1}$$

where $\Gamma(t)$ is the time-dependent control parameter which tunes the strength of quantum fluctuations. We slowly reduce Γ from a high value to zero. A quantum state $|\Psi(t)\rangle$ follows the Schrödinger equation

$$i\frac{d}{dt}|\Psi(t)\rangle = \hat{H}(t)|\Psi(t)\rangle, \tag{2.2}$$

where we set $\hbar = 1$. If the quantum fluctuations are controlled ingeniously, the quantum state finally reaches the ground state of $\hat{H}_0$ with a high probability.

Similarly to SA, a convergence condition of QA has been found. Morita and Nishimori have shown that, when the transverse field is adopted as the driver Hamiltonian, the power-law annealing schedule

$$\Gamma(t) = a(\delta t + b)^{-1/(2N-1)} \tag{2.3}$$

guarantees the success of QA in the infinite-time limit [5]. Here, a and b are constants of the order of N^0, and δ is a small parameter. This power law decreases much faster than the inverse-logarithmic law for the control parameter in SA. In this sense, QA outperforms SA.

2.2. Quantum adiabatic computation

We next introduce quantum adiabatic computation (QAC). The idea of QAC is essentially equivalent to QA at the point that both algorithms take advantage of tunneling effects induced by quantum fluctuations[1]. An important difference between the algorithms is that QAC puts an emphasis on the adiabatic evolution of quantum states.

To be more explicit, let us consider the following total Hamiltonian:

$$\hat{H}(t) = s(t)\hat{H}_0 + [1 - s(t)]\hat{V}. \tag{2.4}$$

The total Hamiltonian $\hat{H}_0$ and the operator $\hat{V}$ have already been defined in Sec. 2.1. The time-dependent control parameter $s(t)$ starts at zero and increases monotonically to unity. In other words, the total Hamiltonian varies smoothly from the driver Hamiltonian $\hat{V}$ to the target Hamiltonian $\hat{H}_0$. We assume $s(\tau) = 1$, that is, the running time of QAC is τ. For simplicity, the linear function $s(t) = t/\tau$ is adopted in most studies.

The basic idea of QAC is the following. We first prepare the initial state which is the trivial ground state of $\hat{V}$, and then simulate the time evolution of the state which obeys the Schrödinger equation. If the control parameter changes slowly ($\tau \gg 1$), the state will stay very close to the instantaneous ground state during the time evolution. Eventually, the system reaches the ground state of $\hat{H}_0$ at $t = \tau$, which is the desired optimal solution (Fig. 2.1).

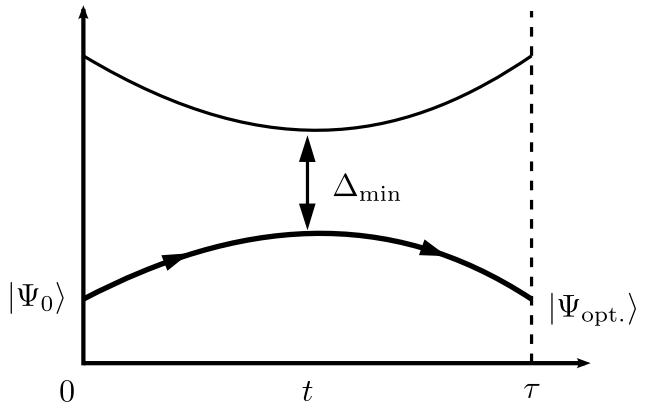

Figure 2.1.: A schematic view of quantum adiabatic computation. The bottom curve represents the instantaneous ground-state energy, and the top curve the first excited energy. The trivial initial ground state $|\Psi_0\rangle$ evolves adiabatically, and the system eventually reaches the optimal solution $|\Psi_{\text{opt.}}\rangle$ at $t = \tau$.

The condition for the system to stay close to the ground state is given by the adiabatic theorem [13]. In the following, we show the condition explicitly. Let us adopt the linear function as the control parameter. Remember that the total Hamiltonian depends on time only through the control parameter s. Hence, the kth instantaneous eigenstate and the corresponding eigenvalue of the total Hamiltonian are also functions of s:

$$\hat{H}(s)|k(s)\rangle = E_k(s)|k(s)\rangle. \tag{2.5}$$

[1] In other sections of this dissertation, we refer to QAC as QA.

We define $\Delta(s) \equiv E_1(s) - E_0(s)$, the instantaneous energy gap between the ground state and the first excited state. From the adiabatic theorem, the condition

$$\tau > \frac{1}{\epsilon} \frac{|\langle 1(s)| \frac{d\hat{H}(s)}{ds} |0(s)\rangle|}{[\Delta(s)]^2}, \quad \forall s \in [0,1] \tag{2.6}$$

ensures that, at the end of the evolution, the probability to find the system out of the ground state will be of the order of ϵ^2. Note that the matrix elements of $d\hat{H}(s)/ds$ are of the order of N. Thus, Eq. (2.6) can be simplified as

$$\tau \gg N\Delta_{\min}^{-2}, \tag{2.7}$$

where $\Delta_{\min}$ denotes the minimum energy gap during the evolution.

Equation (2.7) implies that the efficiency of QAC is governed largely by the minimum energy gap. In the case where the minimum energy gap decays polynomially in N, QAC is an efficient algorithm. On the other hand, if the minimum energy gap decays exponentially, QAC costs exponentially long time to solve the problem.

The difficulty of QAC has a relation to a statistical-mechanical property of spin systems. It is well known that the energy gap $\Delta(s)$ vanishes at a quantum phase transition point in the thermodynamic limit $N \to \infty$ [24]. Hence, the size scaling of the gap in the vicinity of the transition point determines the efficiency of QAC. If a system undergoes a first-order phase transition, the gap usually decays exponentially at the transition point [16–19]. In contrast, second-order phase transitions are associated with polynomially vanishing gaps [14,15]. Therefore the analysis of the phase diagram is useful to estimate the efficiency of QAC.

A simple example of such hard problems is to find the ground state of the ferromagnetic p-spin model for $p > 2$ using the transverse-field operator. The target Hamiltonian of the model is given by

$$\hat{H}_0 = -N\Big(\frac{1}{N}\sum_{i=1}^{N} \hat{\sigma}_i^z\Big)^p, \tag{2.8}$$

where $\hat{\sigma}_i^z$ denotes the z-component of the Pauli matrix at site i. Jörg *et al.* have shown that the system undergoes a quantum first-order transition, and the minimum energy gap decays exponentially at the transition point [18]. This model is a good benchmark because we can easily study the model both analytically and numerically. In particular, it is possible to numerically calculate the energy gap for a relatively large N. That is, we can learn the scaling of the energy gap probably independently of finite size effects. We will discuss the model closely in Chap. 3.

The difficulty of the first-order quantum phase transition is due to a precipitous transition of the ground state. To understand this, let us consider the following simplified Hamiltonian:

$$\hat{H}(t) = -|\uparrow\cdots\uparrow\rangle\langle\uparrow\cdots\uparrow| - \Gamma(t)|\rightarrow\cdots\rightarrow\rangle\langle\rightarrow\cdots\rightarrow| \tag{2.9}$$

Here $\Gamma(t)$ is a time-dependent coefficient corresponding to the transverse field. The quantum state $|\uparrow\cdots\uparrow\rangle$ represents the all-spin-up state, and $|\rightarrow\cdots\rightarrow\rangle$ the state that all spins points at $+x$ direction. Actually, the Hamiltonian describes the ferromagnetic p-spin model with the transverse-field term near the phase transition point [18]. The state $|\rightarrow\cdots\rightarrow\rangle$

corresponds to the ground state before the phase transition, and the all-spin-up state to the ground state after the transition. Since the Hamiltonian (2.9) is just a two-level system, we can easily diagonalize the Hamiltonian, then obtain the minimum energy gap. The resulting minimum energy gap is

$$\Delta_{\min} = 4 \times 2^{-N/2}, \tag{2.10}$$

indicating the failure of QA. The exponential factor in the above minimum energy gap comes from the exponentially small overlap between the ground states before the phase transition and after the transition.

2.3. Advantage of QA

In this section, we introduce studies that show advantages of QA over classical algorithms. We first review studies that have shown the advantage of QA against SA. Next, we show a problem that can be solved efficiently by QA, whereas the problem is intractable for classical algorithms.

As mentioned above, QA outperforms SA in a sense that the sufficiently slow annealing schedule of QA (2.3) converses to zero faster than that of SA. In addition, Morita and Nishimori have shown the sufficiently slow annealing schedule of QA with transverse ferromagnetic interactions instead of the transverse field [5]. Quantum annealing has degree of freedom that we can choose the driver Hamiltonian so that QA can find the ground state efficiently. Morita and Nishimori investigate the annealing schedule of the model described by the following Hamiltonian:

$$\hat{H}(t) = \hat{H}_{\text{Ising}} - \Gamma(t) \prod_i (1 + \hat{\sigma}_i^x), \tag{2.11}$$

where $\hat{H}_{\text{Ising}}$ represents a Hamiltonian of any classical Ising spin system. The driver Hamiltonian denotes transverse ferromagnetic interactions. The sufficient slow annealing schedule for the Hamiltonian (2.11) is given by

$$\Gamma(t) \propto \frac{2^{N-2}}{\delta' t}. \tag{2.12}$$

Here, δ' is a small parameter. In order to compare the annealing schedules (2.3) and (2.12), we calculate the time at which the transverse field decreases to a small value ϵ. The system is expected to be close to the optimal solution for sufficiently small ϵ. The time estimated from Eq. (2.3) is

$$\tau \approx \frac{1}{\delta} \left(\frac{1}{\epsilon} \right)^{2N-1}, \tag{2.13}$$

where we have neglected some constants. On the other hand, the time estimated from Eq. (2.12) is

$$\tau \approx \frac{2^{N-2}}{\delta' \epsilon}. \tag{2.14}$$

Considering that we are interested in relatively large size systems, we can find that the time for the latter case is smaller than the former case for sufficiently small ϵ. The result

suggests that we can achieve speed-up of QA by using the degree of freedom of the driver Hamiltonian.

Another study showing an advantage of QA over SA is given in Ref. [25]. The authors of the paper have established a mapping from the transition matrix of classical Markovian dynamics of the Ising model to quantum Hamiltonian and vice versa in a context of quantum annealing. Such a mapping has already been given by the Suzuki-Trotter decomposition of the Boltzmann factor, which is the path-integral formulation of quantum mechanics. The difference of the mapping from the decomposition is that the mapping given in Ref. [25] does not change the spatial dimension. The mapping thus provide a fair comparison between SA and QA. The paper has shown that the efficiency of QA is at least comparable to that of SA in a sense that problems expressed in terms of a short-range Ising model that is easy for SA can be solved efficiently by using QA. Furthermore, the authors has pointed that Schrödinger dynamics of the quantum Hamiltonian including transverse antiferromagnetic interactions introduced in the subsequent chapter of the present thesis cannot be expressed by Markovian dynamics using the mapping. The result suggests that QA with the antiferromagnetic term has a potential to solve problems efficiently that are intractable for classical algorithms.

Finally, we introduce an problem that can be solved efficiently by QA whereas exponential time is required for any classical algorithm. Somma *et al.* have studied QA on two binary trees glued randomly [26]. The task of the problem is to transfer a quantum state initially localized at one root of the binary graph to the other root. Since the number of vertices of the graph increases exponentially, classical algorithms take exponentially long time to reach the goal. Surprisingly, QA can solve the problem efficiently even though the system undergoes first-order quantum phase transitions. The key point is that the first-order quantum phase transitions occur twice. Somma *et al.* have calculated overlap of the evolved state with the instantaneous ground state and the first-excited state. The result has shown that the quantum state that initially follows the instantaneous ground state transits to the first-excited state at the first phase transition point, and goes back to the ground state at the second transition point. Although the problem is a special case, it is of great importance that the paper have shown a specific example of the advantage of QA over classical algorithms.

2.4. Physics implementation of QA

Simulation of QA is quite hard for today's computers. Since the number of the matrix elements of the Hamiltonian grows exponentially in N as 2^{2N}, classical computers cannot simulate the dynamics of systems with a large number of spins. For this reason, the realization of QA relies on quantum computer, which is a powerful simulator of quantum systems. Simulations executed on quantum computers are called quantum computation [27].

In this section, we present how to simulate quantum annealing procedures. To this end, we first describe the basic model of quantum computation called the quantum circuit model. Next, we show that QA reduces to a quantum circuit model with an arbitrary precision and with a polynomial overhead.

2.4.1. Quantum circuit model

First, let us introduce a qubit (quantum bit), the unit of quantum information. A qubit is the quantum mechanical analog of a bit. Corresponding to a bit taking two values (namely, 0 and 1), a qubit is a quantum two-state system such as spin-1/2. Without loss of generality, we adopt the eigenstates of the z component of Pauli matrix as such states:

$$|\sigma^z = 1\rangle \equiv |\uparrow\rangle, \quad |\sigma^z = -1\rangle \equiv |\downarrow\rangle. \tag{2.15}$$

The important difference between a qubit and a bit is that a qubit can take a quantum superposition state:

$$|\psi\rangle = \alpha|\uparrow\rangle + \beta|\downarrow\rangle, \tag{2.16}$$

where α and β are complex numbers.

Quantum computations are executed with a number of qubits. We now define some notations. Let N be the number of spins. A quantum state of the whole system is denoted by the tensor product of each spin state:

$$|\Psi\rangle = \bigotimes_{i=1}^{N} |\psi_i\rangle \equiv |\psi_1, \ldots, \psi_N\rangle. \tag{2.17}$$

Similarly, the fundamental basis states of the whole system are given by

$$|\{\sigma_i^z\}\rangle = \bigotimes_{i=1}^{N} |\sigma_i^z\rangle \equiv |\sigma_1^z, \ldots, \sigma_N^z\rangle, \tag{2.18}$$

where $\{\sigma_i^z\}$ denotes a spin configuration $(\sigma_1^z, \ldots, \sigma_N^z)$, and $|\sigma_i^z\rangle$ the eigenstate of $\hat{\sigma}_i^z$ with the eigenvalue σ_i^z. Each basis is called a computational basis or the z basis. Using the computational basis, a state of the whole system is rewritten as

$$|\Psi\rangle = \sum_{\{\sigma_i^z\}} c_{\{\sigma_i^z\}} |\{\sigma_i^z\}\rangle, \tag{2.19}$$

where $\sum_{\{\sigma_i^z\}}$ denotes the summation over all possible spin configurations, and $c_{\{\sigma_i^z\}}$ a complex number.

We next introduce fundamental units of quantum circuits. Quantum computations are defined as unitary transformations of a quantum state of the whole system, $|\Psi\rangle \to \hat{U}|\Psi\rangle$. It is known that any unitary operator can be approximated with an arbitrary precision by three fundamental unitary operators called gates [27]; namely the Hadamard gate $\hat{H}$ [2], the $\pi/8$ gate $\hat{T}$, and the controlled NOT (CNOT) gate $\hat{C}$. In order to define these gates, it is sufficient to define each action on the computational basis. First, the Hadamard gate acts on a qubit as follows:

$$\hat{H}|\uparrow\rangle = \frac{1}{\sqrt{2}}(|\uparrow\rangle + |\downarrow\rangle), \quad \hat{H}|\downarrow\rangle = \frac{1}{\sqrt{2}}(|\uparrow\rangle - |\downarrow\rangle). \tag{2.20}$$

Second, the $\pi/8$ gate also acts on a qubit as

$$\hat{T}|\uparrow\rangle = |\uparrow\rangle, \quad \hat{T}|\downarrow\rangle = e^{i\pi/4}|\downarrow\rangle. \tag{2.21}$$

[2] The symbol $\hat{H}$ denotes the Hadamard gate only in this section 2.4.1.

Finally, the CNOT gate acts on two qubits (the control qubit σ_i^z and the target qubit σ_j^z):

$$\hat{C}_{ij}|\sigma_i^z, \sigma_j^z\rangle = |\sigma_i^z, \sigma_i^z\sigma_j^z\rangle. \tag{2.22}$$

In other words, the CNOT gate flips the target qubit if and only if the control qubit is $|\downarrow\rangle$. Quantum circuits are a sequence of the fundamental gates.

It is convenient to show a quantum circuit as Fig. 2.2. The transverse lines represent qubits, and the open boxes are single-spin operators. When an open box is on a line, it means that the qubit is submitted to the operator represented by the box. The connected circles mean the CNOT gate. The filled and open circle represent the control qubit and the target qubit, respectively.

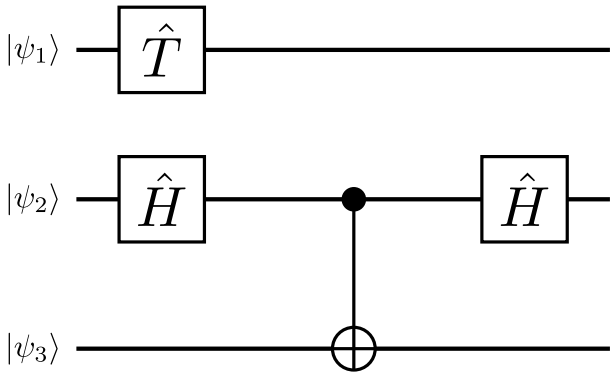

Figure 2.2.: An example of quantum circuits. The transverse lines represents qubits, and the open boxes single-spin operators. The two circles connected by a line represent a CNOT gate; the qubit on the open circle is the target, and the other is the control qubit.

The above explanation does not mean that any unitary operator can be translated to the fundamental unitary operators efficiently. The term efficiently means that the number of required fundamental gates is upper bounded by a polynomial in N. It is known that unitary operators which act on a single qubit can be approximated by the fundamental gates efficiently [27]. However, in general, unitary operators act on many qubits. Therefore it is necessary to check that a unitary operator can be surely approximated in an efficient way.

Fortunately, the following two operators can be approximated efficiently:

$$\hat{U}^z_{i_1,\ldots,i_l} \equiv \exp(\alpha\hat{\sigma}^z_{i_1}\cdots\hat{\sigma}^z_{i_l}), \quad \hat{U}^x_{l_1,\ldots,i_l} \equiv \exp(\alpha\hat{\sigma}^x_{i_1}\cdots\hat{\sigma}^x_{i_l}), \tag{2.23}$$

where α is a pure imaginary number, and $i_1, \ldots, i_l$ are site indices. The above operators are important because quantum annealing procedures are represented by the operators as we will see in Sec. 2.4.2. In the following, we show quantum circuits of the operators.

We describe the quantum circuit of $\hat{U}^z_{i_1,\ldots,i_l}$. For example, a quantum circuit of $\hat{U}^z_{1,2}$ is expressed as Fig. 2.3. Generalization is easy. The circuit of $\hat{U}^z_{i_1,\ldots,i_l}$ consists of N qubits included in the total Hamiltonian and one auxiliary qubit initialized as $|\uparrow\rangle$. Note that the operator $\hat{U}^z_{i_1,\ldots,i_l}$ causes a phase shift $e^{+\alpha}$ or $e^{-\alpha}$ determined by the parity $\sigma^z_{i_1}\cdots\sigma^z_{i_l}$, although it does not cause state transitions:

$$\hat{U}^z_{i_1,\ldots,i_l}|\sigma^z_i, \ldots, \sigma^z_N\rangle = \exp(\alpha\sigma^z_{i_1}\cdots\sigma^z_{i_l})|\sigma^z_i, \ldots, \sigma^z_N\rangle. \tag{2.24}$$

First, l CNOT gates register the parity in the auxiliary qubit. Next, a single-qubit gate, $\exp(\alpha\hat{\sigma}^z_{N+1})$, causes the phase shift. Finally, l CNOT gates initialize the auxiliary qubit again. As described above, the unitary operator $\hat{U}^z_{i_1,\ldots,i_l}$ can be expressed by quantum circuit efficiently.

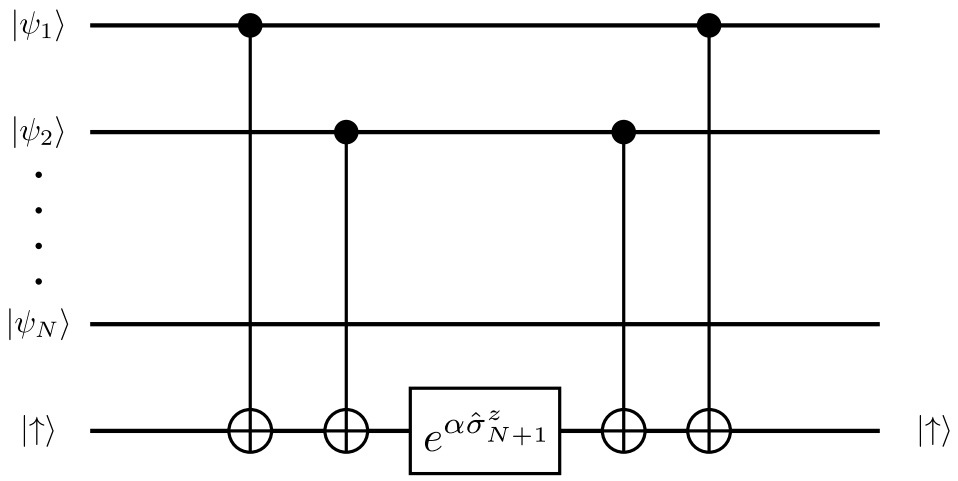

Figure 2.3.: A quantum circuit of $\hat{U}^z_{1,2}$. The circuit consists of N qubits and one auxiliary qubit. First, the two CNOT gates register the parity $\sigma^z_1\sigma^z_2$ to the auxiliary qubit, $|\sigma^z_{N+1} = +1\rangle \to |\sigma^z_{N+1} = \sigma^z_1\sigma^z_2\rangle$. Next, the single-spin gate causes a phase shift $e^{\alpha\sigma^z_1\sigma^z_2}$. Finally, the two CNOT gates initialize the auxiliary qubit. We can find that the effect of the circuit on the computational basis is the same as that of the operator $\hat{U}^z_{1,2}$.

We next present the quantum circuit of $\hat{U}^x_{i_1,\ldots,i_l}$. This quantum circuit is readily derived from the result of $\hat{U}^z_{i_1,\ldots,i_l}$ using the fact that

$$\hat{H}_i\hat{\sigma}^z_i\hat{H}_i = \hat{\sigma}^x_i, \quad \text{and} \quad \hat{H}^2_i = \hat{1}_i, \tag{2.25}$$

for any i $(= 1, \ldots, N)$. Here, $\hat{H}_i$ denotes the Hadamard gate which acts on the ith spin. From these equations, the unitary operator $\hat{U}^x_{i_1,\ldots,i_l}$ is rewritten as

$$\begin{aligned}\hat{U}^x_{i_1,\ldots,i_l} &= \hat{H}_{i_1}\cdots\hat{H}_{i_l}\hat{U}^z_{i_1,\ldots,i_l}\hat{H}_{i_l}\cdots\hat{H}_{i_1} \\ &= \left(\bigotimes_{i=1}^{N}\hat{H}_i\right)\hat{U}^z_{i_1,\ldots,i_l}\left(\bigotimes_{i=1}^{N}\hat{H}_i\right).\end{aligned} \tag{2.26}$$

Figure 2.4 shows the quantum circuit of $\hat{U}^x_{1,2}$.

2.4.2. Equivalence between quantum circuit model and quantum annealing

Quantum annealing procedures are equivalent to quantum computations described above. First, the direction from quantum circuit model to QA has been proved by Aharonov *et al.* [28]. To prove it, they have used a target Hamiltonian whose ground state has a positive overlap with the output of a quantum circuit. In addition, they have shown that the minimum gap of the converted quantum annealing procedure is polynomially small

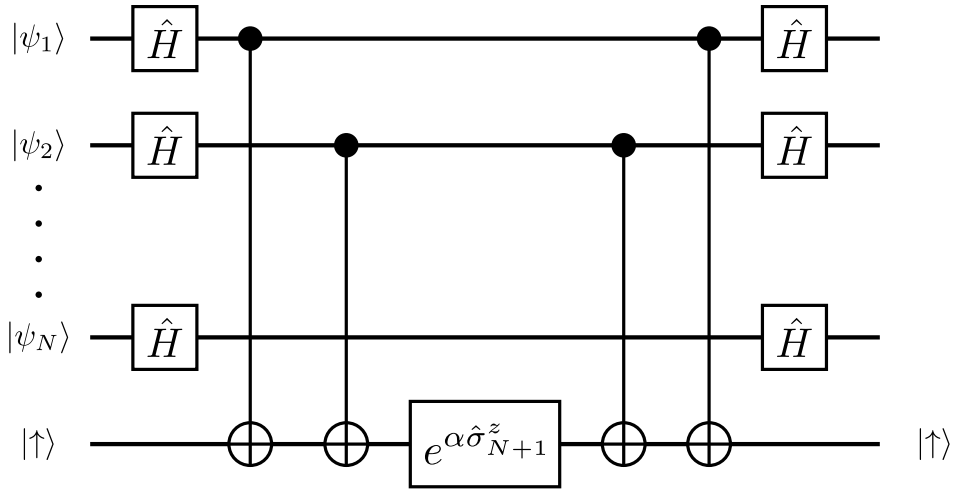

Figure 2.4.: A quantum circuit of $\hat{U}^x_{1,2}$. The difference for the operator $\hat{U}^z_{1,2}$ is that the Hadamard gates act on the N qubits.

in the number of gates of the quantum circuit; that is, problems solved efficiently with quantum circuits are easy also for QA.

The reverse direction has been discussed closely by Dam *et al.* [29]. They have approximated a quantum annealing procedure by a quantum circuit. The approximation has been established in two steps as follows.

The first step is a discretization of continuous time evolution. Since quantum circuits consist of a finite number of quantum gates, quantum circuits cannot represent quantum annealing procedures precisely. To resolve this, we discretize the continuous change of the total Hamiltonian from $\hat{V}$ to $\hat{H}_0$ by a finite sequence of Hamiltonians $\hat{H}'_1, \hat{H}'_2, \ldots, \hat{H}'_r$, where $\hat{H}'_j \equiv (j/r)\hat{H}_0 + (1 - j/r)\hat{V}$. Hence, the approximated time evolution operator is given by

$$\hat{U}' = e^{-i(\tau/r)\hat{H}'_r} \cdots e^{-i(\tau/r)\hat{H}'_1}. \tag{2.27}$$

The next step is to approximate $\hat{U}'_j$ defined by

$$\hat{U}'_j \equiv e^{-i(\tau/r)\hat{H}'_j} = e^{-i(\tau/r)(j/r)\hat{H}_0 - i(\tau/r)(1-j/r)\hat{V}} \tag{2.28}$$

so that the resulting unitary operator can be implemented by quantum gates efficiently. Here, we naively divide it into two parts as follows:

$$\hat{U}''_j \equiv e^{-i(\tau/r)(j/r)\hat{H}_0} e^{-i(\tau/r)(1-j/r)\hat{V}}. \tag{2.29}$$

Since $\hat{H}_0$ consists only of the z components of Pauli matrices, and $\hat{V}$ consists of the x components, the exponential operators can be readily expressed by quantum gates as shown in Sec. 2.4.1.

The key issue is the error resulting from the approximations. Here, the error of the approximate operator is measured by the operator norm defined by

$$\|\hat{A}\| \equiv \max_{\langle\Psi|\Psi\rangle=1} \|\hat{A}|\Psi\rangle\|. \tag{2.30}$$

Dam *et al.* have shown that if $r = \mathrm{O}(\tau^2 N^2)$, then the order of the error is unity; that is

$$\left\| \hat{U} - \prod_{j=1}^{r} \hat{U}_j'' \right\| = \mathrm{O}(\tau^2 N^2 / r), \tag{2.31}$$

where $\hat{U}$ denotes the time evolution operator before the approximations. Quantum computer therefore can perform quantum annealing procedures efficiently unless the annealing time is exponentially long in N.

Chapter 3.

Quantum annealing with antiferromagnetic transverse interactions for the Ferromagnetic p-spin model

As described in the previous chapter, the conventional QA using transverse field cannot solve the simple problem, the ferromagnetic p-spin model. Nevertheless, this result does not necessarily suggest a complete failure of QA for this problem. The reason is that only the transverse field is used as the driver Hamiltonian. Another driver Hamiltonian may lead to improved performance. This type of degree of freedom is an advantage of QA. In this chapter, we introduce a new approach of QA, and discuss the efficiency of the approach for the ferromagnetic p-spin model whose Hamiltonian is given by Eq. (2.8). We show that the approach enables us to avoid the difficulty of the conventional QA [30].

First, Sec. 3.1 describes QA with antiferromagnetic transverse interactions. In this section, we discuss annealing paths that are convenient to understand the concept of the new approach. Second, Sec. 3.2 is devoted to analytical computations. We will calculate the partition function of the system, and derive self-consistent equations in the low-temperature limit. Section 3.3 shows numerical results for the phase diagram and the minimum energy gap as a function of N. Next, Sec. 3.4 analyzes the phase diagram in the large p limit in . Finally, we conclude and make discussions in Sec. 3.5.

3.1. Quantum annealing with antiferromagnetic transverse interactions

The unique point different from the conventional QA is an introduction of the following antiferromagnetic interaction

$$\hat{V}_{\rm AF} = +N\Big(\frac{1}{N}\sum_{i=1}^{N}\hat{\sigma}_i^x\Big)^2 \tag{3.1}$$

in addition to the conventional transverse-field term $\hat{V}_{\rm TF}$. Here $\hat{\sigma}_i^x$ denotes the x-component of the Pauli matrix at site i. The total Hamiltonian is therefore

$$\hat{H}(s,\lambda) = s\{\lambda\hat{H}_0 + (1-\lambda)\hat{V}_{\rm AF}\} + (1-s)\hat{V}_{\rm TF}, \tag{3.2}$$

where the control parameters s and λ should be changed appropriately as functions of time. The initial Hamiltonian has $s = 0$ and any λ, and the final Hamiltonian has $s = \lambda = 1$. Intermediate values of (s, λ) should be chosen according to the prescription given in the subsequent sections.

It is convenient to consider the quantum annealing procedure on the s-λ plane. A line $\{(s(t), \lambda(t)) \mid 0 \leq t \leq \tau\}$ is called an annealing path. For example, the line $\lambda = 1$ corresponds to the conventional QA since the antiferromagnetic term $\hat{V}_{\mathrm{AF}}$ completely vanishes. On this annealing path, the ferromagnetic p-spin model undergoes a first-order phase transition. The problem we are concerned with is whether or not we can avoid the first order phase transition by taking another annealing path.

We must not take the line $\lambda = 0$ as an annealing path. The total Hamiltonian is diagonalized in the x basis on this line:

$$\hat{H}(s) = s\hat{V}_{\mathrm{AF}} + (1-s)\hat{V}_{\mathrm{TF}} = sN\Big(\frac{1}{N}\sum_{i=1}^{N}\hat{\sigma}_i^x\Big)^2 - (1-s)\sum_{i=1}^{N}\hat{\sigma}_i^x. \tag{3.3}$$

Thus, quantum fluctuations completely disappear, and quantum state transitions do not occur. This means that the system does not perform quantum annealing processes.

3.2. Analytical computation

3.2.1. Partition function

We first calculate the partition function of the system at finite temperature. The partition function is expressed as

$$Z = \mathrm{Tr}\, e^{-\beta\hat{H}(s,\lambda)}, \tag{3.4}$$

where β is the inverse temperature, and the total Hamiltonian is given by

$$\begin{aligned}\hat{H}(s,\lambda) &= s\{\lambda\hat{H}_0 + (1-\lambda)\hat{V}_{\mathrm{AFF}}\} + (1-s)\hat{V}_{\mathrm{TF}} \\ &= -s\lambda N\Big(\frac{1}{N}\sum_{i=1}^{N}\hat{\sigma}_i^z\Big)^p + s(1-\lambda)N\Big(\frac{1}{N}\sum_{i=1}^{N}\hat{\sigma}_i^x\Big)^2 - (1-s)\sum_{i=1}^{N}\hat{\sigma}_i^x.\end{aligned} \tag{3.5}$$

For such a quantum system, the Suzuki-Trotter formula [31] is used in order to calculate the partition function. The first step of the formula is to divide the exponential operator into two parts using the Trotter decomposition:

$$e^{\hat{A}+\hat{B}} = \lim_{M\to\infty}(e^{\hat{A}/M}e^{\hat{B}/M})^M, \tag{3.6}$$

where $\hat{A}$ and $\hat{B}$ are quantum operators which do not commute with each other generally, and M is an integer called the Trotter number. The validity of the decomposition is easily checked by expanding the exponential operators into the Taylor series, and then neglecting the higher order $\mathrm{O}(1/M^2)$, which does not contribute to the result in $M \to \infty$ limit. Using the decomposition, we have

$$\begin{aligned}Z &= \lim_{M\to\infty} Z_M \\ &\equiv \lim_{M\to\infty} \mathrm{Tr}\big(e^{-\frac{\beta}{M}s\lambda\hat{H}_0}e^{-\frac{\beta}{M}\{s(1-\lambda)\hat{V}_{\mathrm{AFF}}+(1-s)\hat{V}_{\mathrm{TF}}\}}\big)^M \\ &= \lim_{M\to\infty}\sum_{\{\sigma_i^z\}}\langle\{\sigma_i^z\}|\Big(\exp\Big[\frac{\beta s\lambda N}{M}\Big(\frac{1}{N}\sum_{i=1}^{N}\hat{\sigma}_i^z\Big)^p\Big] \\ &\quad\times\exp\Big[-\frac{\beta s(1-\lambda)N}{M}\Big(\frac{1}{N}\sum_{i=1}^{N}\hat{\sigma}_i^x\Big)^2 + \frac{\beta(1-s)}{M}\sum_{i=1}^{N}\hat{\sigma}_i^x\Big]\Big)^M|\{\sigma_i^z\}\rangle.\end{aligned} \tag{3.7}$$

Here $|\{\sigma_i^z\}\rangle$ denotes an orthonormal basis that diagonalizes the z-component of the Pauli matrices, and the summation is taken over all the possible basis.

Next, we introduce the following M closure relations:

$$\begin{aligned}\hat{1}(\alpha) \equiv & \sum_{\{\sigma_i^z(\alpha)\}} |\{\sigma_i^z(\alpha)\}\rangle\langle\{\sigma_i^z(\alpha)\}| \\ & \times \sum_{\{\sigma_i^x(\alpha)\}} |\{\sigma_i^x(\alpha)\}\rangle\langle\{\sigma_i^x(\alpha)\}|, \end{aligned} \tag{3.8}$$

where $\alpha = 1, \ldots, M$, and the summation $\sum_{\{\sigma_i^x(\alpha)\}}$ and $|\{\sigma_i^x(\alpha)\}\rangle$ are defined similarly to the z basis. Inserting $\hat{1}(\alpha)$ just before the αth exponential operator involving $\hat{\sigma}_i^x$ in Eq. (3.7), we have

$$\begin{aligned} Z_M = & \sum_{\{\sigma_i^z(\alpha)\}} \sum_{\{\sigma_i^x(\alpha)\}} \prod_{\alpha=1}^{M} \exp\Big[\frac{\beta s\lambda N}{M}\Big(\frac{1}{N}\sum_{i=1}^{N}\sigma_i^z(\alpha)\Big)^p \\ & - \frac{\beta s(1-\lambda)N}{M}\Big(\frac{1}{N}\sum_{i=1}^{N}\sigma_i^x(\alpha)\Big)^2 + \frac{\beta(1-s)}{M}\sum_{i=1}^{N}\sigma_i^x(\alpha)\Big] \\ & \times \prod_{i=1}^{N}\langle\sigma_i^z(\alpha)|\sigma_i^x(\alpha)\rangle\langle\sigma_i^x(\alpha)|\sigma_i^z(\alpha+1)\rangle \end{aligned} \tag{3.9}$$

with periodic boundary conditions such that $\sigma_i^z(1) = \sigma_i^z(M+1)$ for $i = 1, \ldots, N$.

To simplify the spin product terms $[\sum_{i=1}^{N}\sigma_i^z(\alpha)/N]^p$ and $[\sum_{i=1}^{N}\sigma_i^x(\alpha)/N]^2$, we introduce the following integral representation of the delta function:

$$\delta\Big(Nm - \sum_{i=1}^{N}\sigma_i\Big) = \int d\tilde{m}\exp\Big[-\tilde{m}\Big(Nm - \sum_{i=1}^{N}\sigma_i\Big)\Big], \tag{3.10}$$

where m denotes the magnetization (order parameter), and $\tilde{m}$ is the conjugate variable. Using Eq. (3.10), we can rewrite Z_M as

$$\begin{aligned} Z_M = & \sum_{\{\sigma_i^z(\alpha)\}} \sum_{\{\sigma_i^x(\alpha)\}} \prod_{\alpha=1}^{M} \int\cdots\int dm^z(\alpha)\, d\tilde{m}^z(\alpha)\, dm^x(\alpha)\, d\tilde{m}^x(\alpha) \\ & \times \exp\Big[N\Big(s\lambda\frac{\beta}{M}\big(m^z(\alpha)\big)^p - \tilde{m}^z(\alpha)m^z(\alpha)\Big)\Big] \\ & \times \exp\Big[N\Big(-s(1-\lambda)\frac{\beta}{M}\big(m^x(\alpha)\big)^2 + (1-s)\frac{\beta}{M}m^x(\alpha) - \tilde{m}^x(\alpha)m^x(\alpha)\Big)\Big] \\ & \times \prod_{i=1}^{N}\exp[\tilde{m}^z(\alpha)\sigma_i^z(\alpha) + \tilde{m}^x(\alpha)\sigma_i^x(\alpha)]\langle\sigma_i^z(\alpha)|\sigma_i^x(\alpha)\rangle\langle\sigma_i^x(\alpha)|\sigma_i^z(\alpha+1)\rangle. \end{aligned} \tag{3.11}$$

Here, we have neglected a few irrelevant constants. Since the spin product terms have disappeared, we can perform the summation over all spin configurations independently at

each site. Then, we obtain

$$
\begin{aligned}
Z_M = \int \cdots \int \prod_{\alpha=1}^{M} & dm^z(\alpha)\, d\tilde{m}^z(\alpha)\, dm^x(\alpha)\, d\tilde{m}^x(\alpha) \\
& \times \exp\Big[N \sum_{\alpha=1}^{M} \Big(s\lambda \frac{\beta}{M} \big(m^z(\alpha)\big)^p - \tilde{m}^z(\alpha) m^z(\alpha) \Big) \Big] \\
& \times \exp\Big[N \sum_{\alpha=1}^{M} \Big(-s(1-\lambda) \frac{\beta}{M} \big(m^x(\alpha)\big)^2 + (1-s) \frac{\beta}{M} m^x(\alpha) - \tilde{m}^x(\alpha) m^x(\alpha) \Big) \Big] \\
& \times \exp\Big[N \ln \mathrm{Tr} \prod_{\alpha=1}^{M} \exp[\tilde{m}^z(\alpha)\sigma^z(\alpha) + \tilde{m}^x(\alpha)\sigma^x(\alpha)] \\
& \qquad \times \langle \sigma^z(\alpha) | \sigma^x(\alpha) \rangle \langle \sigma^x(\alpha) | \sigma^z(\alpha+1) \rangle \Big],
\end{aligned} \tag{3.12}
$$

where the trace means the summation over the spin variables, $\sigma^z(\alpha)$ and $\sigma^x(\alpha)$ ($\alpha = 1, \ldots, M$).

Note that the exponent in Eq. (3.12) is proportional to N. Thus, the integrals over the variables are evaluated by the saddle-point method, which is to take the maximum value of the integrand as the result of integral (see, e.g., Appendix A.1 of [32]). The saddle-point conditions for $m^z(\alpha)$ and $m^x(\alpha)$ lead to

$$
\tilde{m}^z(\alpha) = \frac{\beta}{M} ps\lambda \big(m^z(\alpha)\big)^{p-1}, \tag{3.13}
$$

$$
\tilde{m}^x(\alpha) = \frac{\beta}{M} \{(1-s) - 2s(1-\lambda) m^x(\alpha)\}. \tag{3.14}
$$

We now use the static approximation, which removes all the α dependence of the parameters. We will check the validity of the approximation in Sec. 3.3.2. After this approximation, we can easily take trace in Eq. (3.12) by the inverse operation of the Trotter decomposition. Then, using Eqs. (3.13) and (3.14), we finally obtain

$$
Z = \iint dm^z\, dm^x\, \exp[-N\beta f(\beta, s, \lambda; m^z, m^x)], \tag{3.15}
$$

where $f(\beta, s, \lambda; m^z, m^x)$ is the pseudo free energy defined as follows:

$$
\begin{aligned}
f(\beta, s, \lambda; m^z, m^x) = & (p-1) s\lambda (m^z)^p - s(1-\lambda)(m^x)^2 \\
& - \frac{1}{\beta} \ln 2 \cosh \beta \sqrt{\big\{ ps\lambda (m^z)^{p-1} \big\}^2 + \big\{ 1 - s - 2s(1-\lambda) m^x \big\}^2}.
\end{aligned} \tag{3.16}
$$

The saddle-point equations are thus

$$
\begin{aligned}
m^z = & \frac{ps\lambda (m^z)^{p-1}}{\sqrt{\big\{ ps\lambda (m^z)^{p-1} \big\}^2 + \big\{ 1 - s - 2s(1-\lambda) m^x \big\}^2}} \\
& \times \tanh \beta \sqrt{\big\{ ps\lambda (m^z)^{p-1} \big\}^2 + \big\{ 1 - s - 2s(1-\lambda) m^x \big\}^2},
\end{aligned} \tag{3.17}
$$

$$
\begin{aligned}
m^x = & \frac{1 - s - 2s(1-\lambda) m^x}{\sqrt{\big\{ ps\lambda (m^z)^{p-1} \big\}^2 + \big\{ 1 - s - 2s(1-\lambda) m^x \big\}^2}} \\
& \times \tanh \beta \sqrt{\big\{ ps\lambda (m^z)^{p-1} \big\}^2 + \big\{ 1 - s - 2s(1-\lambda) m^x \big\}^2}.
\end{aligned} \tag{3.18}
$$

3.2.2. Low-temperature limit

We next derive self-consistent equations in the low temperature limit to examine quantum phase transitions. Since the start of the QA process belongs to the paramagnetic phase and the goal is the ferromagnetic phase, a quantum phase transition inevitably occurs in the course of time evolution.

It is useful to consider two possibilities separately depending on whether the argument of the square root in Eqs. (3.17) and (3.18) vanishes or not. We start our discussion from the latter case.

When the square root in Eqs. (3.17) and (3.18) assumes a finite value, the hyperbolic tangent tends to unity in the $\beta \to \infty$ limit. Then, we have

$$m^z = \frac{ps\lambda(m^z)^{p-1}}{\sqrt{\left\{ps\lambda(m^z)^{p-1}\right\}^2 + \left\{1-s-2s(1-\lambda)m^x\right\}^2}}, \tag{3.19}$$

$$m^x = \frac{1-s-2s(1-\lambda)m^x}{\sqrt{\left\{ps\lambda(m^z)^{p-1}\right\}^2 + \left\{1-s-2s(1-\lambda)m^x\right\}^2}}. \tag{3.20}$$

The pseudo free energy (3.16) becomes

$$f(s,\lambda;m^z,m^x) = (p-1)s\lambda(m^z)^p - s(1-\lambda)(m^x)^2 - \sqrt{\left\{ps\lambda(m^z)^{p-1}\right\}^2 + \left\{1-s-2s(1-\lambda)m^x\right\}^2}. \tag{3.21}$$

Equations (3.19) and (3.20) have a ferromagnetic (F) solution with $m^z > 0$ and a quantum paramagnetic (QP) solution satisfying $m^z = 0$ and $m^x \neq 0$. Substitution of $m^z = 0$ into Eq. (3.20) yields

$$m^x = \frac{1-s-2s(1-\lambda)m^x}{|1-s-2s(1-\lambda)m^x|}, \tag{3.22}$$

i.e., m^x can be ± 1. However, $m^x = -1$ is not a proper solution since, with $m^x = -1$, $1-s-2s(1-\lambda)m^x = 1-s+2s(1-\lambda) \geq 0$ for $0 \leq s \leq 1$, $0 \leq \lambda \leq 1$, which leads to $m^x = 1$ according to Eq. (3.22). The other possibility $m^x = 1$ satisfies Eq. (3.22) when $s < 1/(3-2\lambda)$. Therefore the QP phase can exist in the region $0 \leq s < 1/(3-2\lambda)$, and its free energy is

$$f_{\rm QP}(s,\lambda) = -s\lambda + 2s - 1, \tag{3.23}$$

which is independent of p.

The free energy of the F phase cannot be obtained analytically for general p. However, we can evaluate it in the $p \to \infty$ limit as follows: In this limit, Eq. (3.19) reads $m^z = 0$ or $m^z = 1$. The latter solution corresponds to the F phase. The magnetization in the x direction is zero since Eqs. (3.19) and (3.20) satisfy $(m^z)^2 + (m^x)^2 = 1$. Substituting the values of magnetization into Eq. (3.21) and taking the limit $p \to \infty$, we find

$$f_{\rm F}(s,\lambda)|_{p\to\infty} = -s\lambda. \tag{3.24}$$

Let us next consider the case where the argument of the square root in Eqs. (3.17) and (3.18) vanishes. We then assume that m^z and m^x tend to the following values as $\beta \to \infty$:

$$m^z \to 0, \quad m^x \to \frac{1-s}{2s(1-\lambda)} \tag{3.25}$$

such that the argument of hyperbolic tangent approaches a finite constant:

$$\beta\sqrt{\left\{ps\lambda(m^z)^{p-1}\right\}^2+\left\{1-s-2s(1-\lambda)m^x\right\}^2}\to c. \tag{3.26}$$

In order to find a non-trivial solution, it is also necessary to assume the following relation:

$$\frac{ps\lambda(m^z)^{p-1}}{1-s-2s(1-\lambda)m^x}\to 0. \tag{3.27}$$

Under these assumptions, Eqs. (3.17) and (3.18) read $m^z = 0$ and $m^x = \tanh c$. These equations satisfy the condition (3.25) if we choose c such that $\tanh c = (1-s)/2s(1-\lambda)$.

Unless $s = 1$, the magnetizations (3.25) satisfy the condition of QP solution. We then call this phase QP2 in order to distinguish it from the QP phase described before. The free energy of the QP2 phase is obtained in the limit (3.25) and $\beta \to \infty$ under the assumption (3.26):

$$f_{\mathrm{QP2}}(s,\lambda) = -\frac{(1-s)^2}{4s(1-\lambda)}. \tag{3.28}$$

The domain of applicability of the free energy (3.28) is restricted by $1/(3-2\lambda) \le s < 1$ since $|(1-s)/2s(1-\lambda)| = |\tanh c| \le 1$ and $s \neq 1$. This region of s will be called the QP2 domain hereafter.

3.3. Numerical results

3.3.1. Phase diagram

Let us next analyze numerically the phase diagram on the s-λ plane for finite values of p. We construct the phase diagram as follows. We first solve numerically the self-consistent equations (3.19) and (3.20) for a given value of p and at a point (s,λ) in the phase diagram and then evaluate the corresponding free energy. By comparing all possible solutions and their free energies including f_{QP2}, we identify the stable solution having the smallest value of the free energy.

It is useful to show the dependence of the free energy on s for some values of p and λ as in Fig. 3.1. We have confirmed numerically that the free energy lies below f_{QP2} in the QP2 domain, and the QP2 phase is completely suppressed by the other phases. This system thus undergoes a quantum phase transition from the QP phase for small s to the F phase for large s.

To determine whether the transition is first order or second order, we show the behavior of the magnetization m^x in Fig. 3.2. The parameters of the figure correspond to those in Fig. 3.1. When $\lambda = 0.1$, the magnetization m^x for $p = 3$ has a small jump at $s = 0.3544(1)$, and m^x for $p \ge 5$ decreases continuously from unity to our numerical precision. This means that m^z for $p \ge 5$ increases continuously from zero to a finite value. Therefore a second-order transition occurs for $p \ge 5$ at $\lambda = 0.1$. The same is true for $\lambda = 0.3$ in the sense that there exists a second-order transition at the boundary of the QP2 phase for $p \ge 5$.

A remarkable fact is that the magnetization for some parameters (e.g., $\lambda = 0.3$, $p = 11$) in Fig. 3.2 jumps within the F phase. This discontinuity results in an exponential decrease of the energy gap as N increases. There exists a first-order transition within the F phase. However, this unusual behavior disappears for smaller values of λ for any finite p, excluding

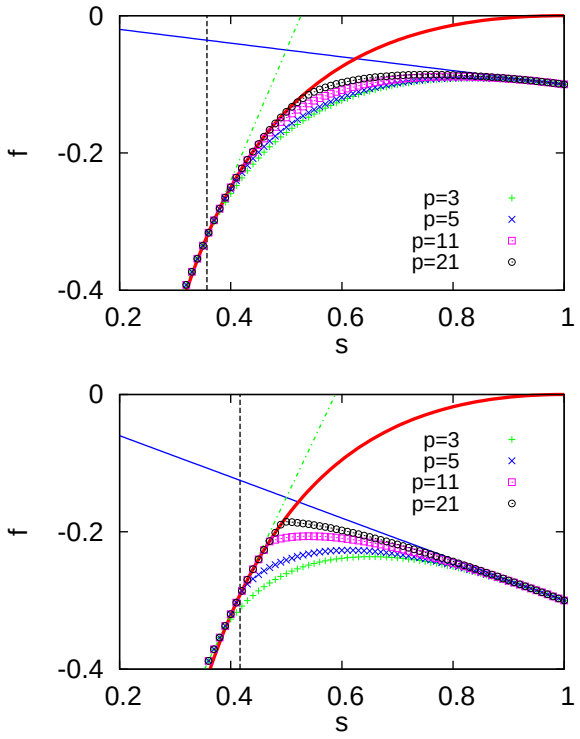

Figure 3.1.: Free energy vs. s for some values of p. The parameter λ is 0.1 (top), and 0.3 (bottom). The dash-dotted line in light green represents the free energy of the QP phase, Eq. (3.23), the thin solid line in blue is for the F phase, Eq. (3.24), and the thick solid line in red for the QP2 phase, Eq. (3.28). The vertical dashed line denotes the lower limit of the QP2 domain ($s = 1/(3 - 2\lambda)$). Although it is difficult to discern in the present scale, all the data for finite p we studied have lower values than that of f_{QP2} in the QP2 domain.

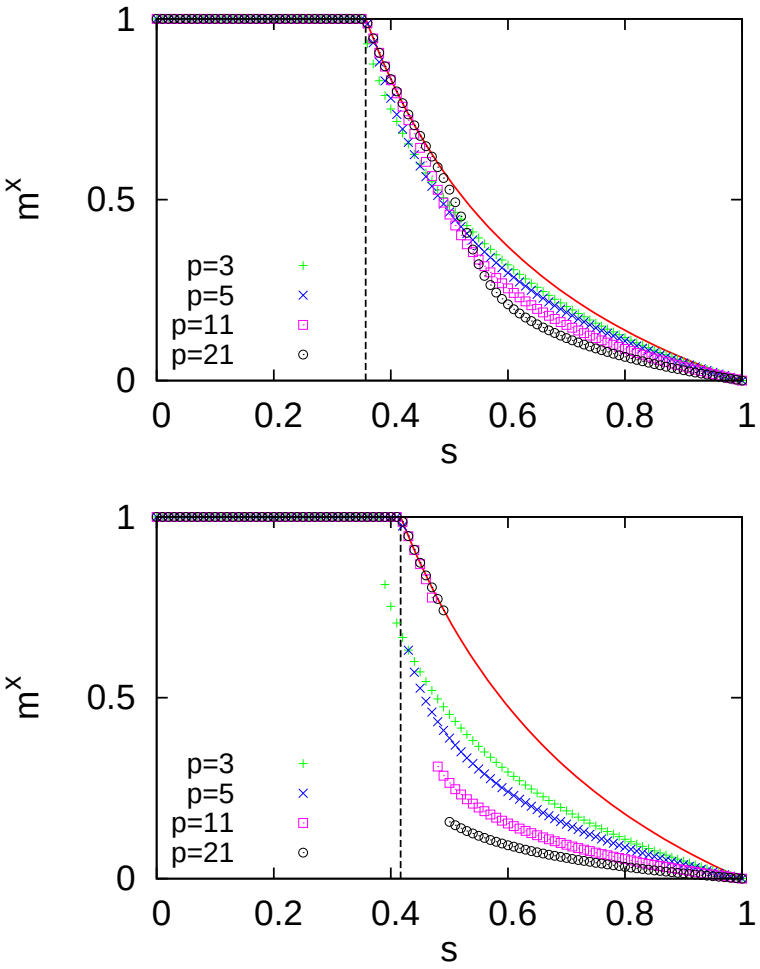

Figure 3.2.: Magnetization m^x corresponding to Fig. 3.1. The solid line represents the x component of magnetization of the QP2 phase (3.25), and the vertical dashed lines are the same as those in Fig. 3.1. For $\lambda = 0.1$ (top panel) and $p \geq 5$, a second-order transition occurs at the boundary of the QP2 domain; The magnetization decreases continuously from unity to zero. In contrast, the magnetization for $\lambda = 0.3$ (bottom panel) has a jump.

$p = 3$, that we checked. Thus for smaller λ, only a second-order transition takes place as we increase s from zero to a value close to unity.

The resulting phase diagrams are shown in Fig. 3.3 for $p = 3, 5$, and 11. We see that a boundary of second-order transition exists for small λ and $p \geq 5$. It is observed that one can reach the F phase from the QP phase by choosing a path that avoids a first-order transition as long as the first-order F-F boundary does not reach the $\lambda = 0$ axis, which happens probably only in the limit $p \to \infty$ as we shall discuss below.

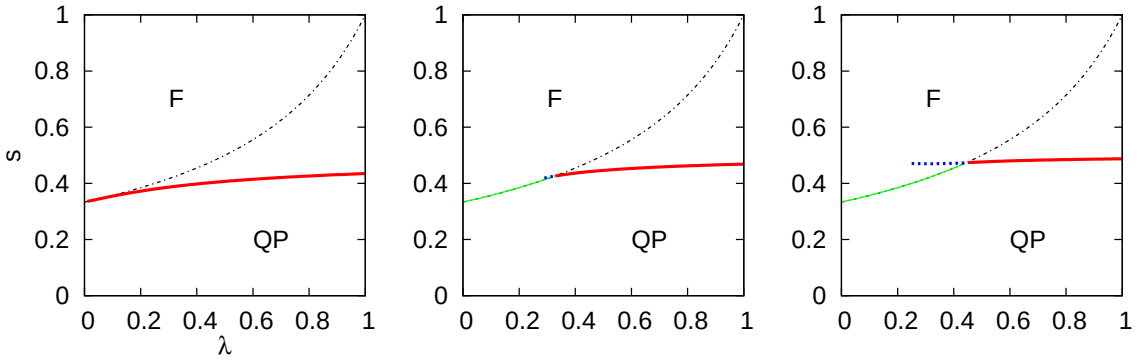

Figure 3.3.: Phase diagrams on the s-λ plane for $p = 3$ (left), $p = 5$ (middle), and $p = 11$ (right). The dash-dotted line represents the boundary of the QP2 domain ($s = 1/(3-2\lambda)$), where a transition takes place between the QP and F phases. For large λ, the QP and F phases are separated by the horizontal phase boundary (QP-F boundary). The thick solid line in red represents the first-order transition, and the thin solid line in light green is for the second-order transition. For $p = 5$ and 11, the magnetization jumps on the dashed line in blue (F-F boundary) within the F phase.

3.3.2. Energy gap

We next study the behavior of the energy gap across the phase transitions found in the previous section.

To calculate the energy gap for large N, we adopt the method used in [18]. The Hamiltonian under consideration is expressed by the components of total spin operator $\hat{S}^{x,z}$, thus commuting with the total spin $\hat{\boldsymbol{S}}$. Since the total angular momentum is conserved during the time evolution, we have to pay attention only to the subspace that has the maximum angular momentum $S = N/2$. The dimension of this subspace is $N + 1$, which greatly enhances the possible system size to $N \sim 100$. Still the size is restricted by computer resources. However, there is an alternative approach to calculate the energy gap in the thermodynamic limit. We will introduce the approach in Appendix A.

It is useful to first verify the validity of the static approximation. Figure 3.4 shows a representative energy gap with a second-order phase transition: As one sees in the enlarged view shown in the bottom panel, the gap shows wiggly behavior for a finite range. The wiggly behavior starts at $s \simeq 0.4184$ for $\lambda = 0.3$, which corresponds to the left end of the QP2 domain and also to the second-order transition point between the QP and F phases. The same behavior terminates at $s \simeq 0.4676$ for $\lambda = 0.3$, corresponding to the first-order F-F boundary. These two transition points evaluated analytically using the

static approximation, Eqs. (3.19) and (3.20), are shown in dashed vertical lines in Fig. 3.4 and agree fairly satisfactorily with the numerical results, as N increases, for the interval where the gap is very small.

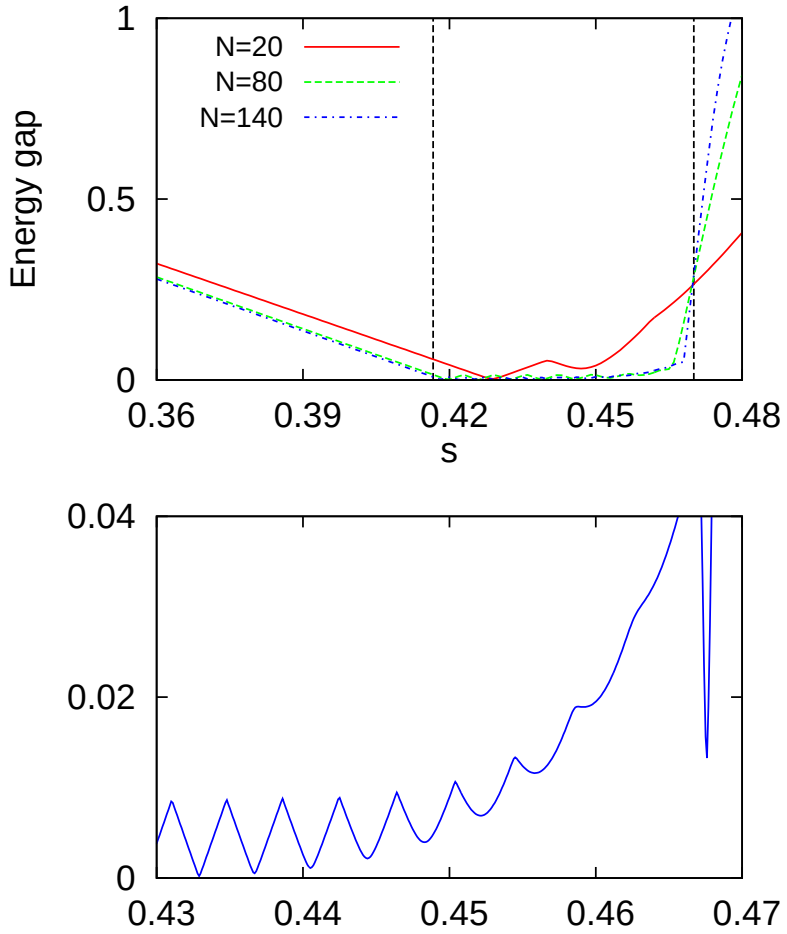

Figure 3.4.: Top panel: Energy gap vs. s for $p = 11$ and $\lambda = 0.3$. The vertical dashed lines represent the boundary of the QP2 domain at $s \simeq 0.4167$ and the F-F boundary at $s \simeq 0.4701$. The bottom panel is the enlarged view of the top panel for $N = 140$.

The rightmost local minimum of the energy gap in Fig. 3.4 behaves differently from other local minima and decays exponentially as N increases as shown in Fig. 3.5. This is expected from the jump in the magnetization shown in Fig. 3.2 because a jump implies a first-order transition though the system is ferromagnetic in both sides of the transition point. Although this is not the global minimum, it will affect the efficiency of QA for much larger systems where the rightmost one will become the global minimum since the other local minima decay only polynomially as shown below.

Figure 3.6 shows the size dependence of local minima of the energy gap for $p = 5$ and $\lambda = 0.1$. All minima shown here decay polynomially. In Fig. 3.7 the global minimum of energy gap for selected p is depicted as a function of N at $\lambda = 0.1$. For any value of p,

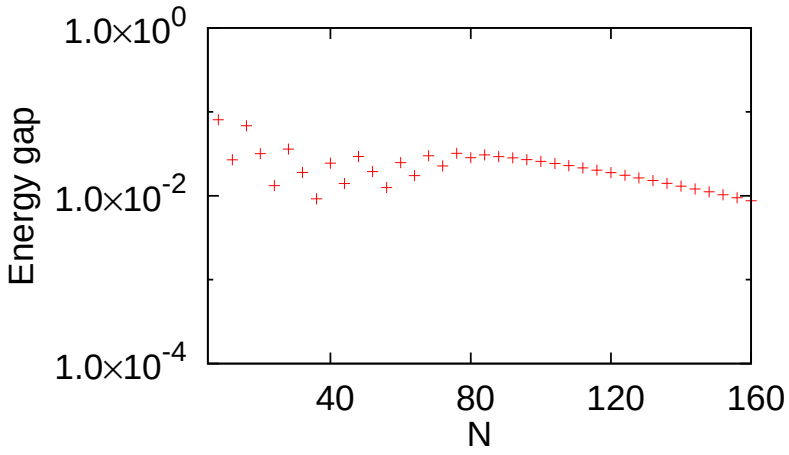

Figure 3.5.: The rightmost local minimum of the energy gap as a function of N for $p = 11$ and $\lambda = 0.3$ on a semi-log scale. The gap closes exponentially with N.

the gap closes polynomially at least up to the system size we studied, $N = 160$.

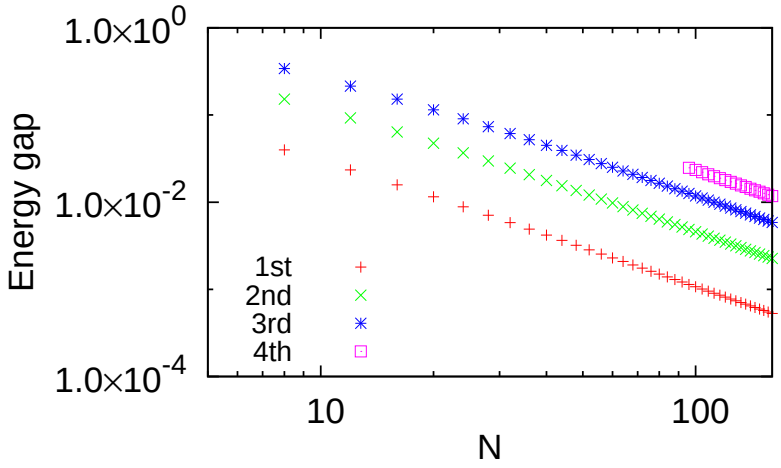

Figure 3.6.: Energy gap vs. N at local minima for $p = 5, \lambda = 0.1$ on a log-log scale. We number the minima from left to right. No gaps vanish exponentially up to the size studied here.

The above results suggest that first-order transitions will be able to be avoided if we choose a path around $\lambda = 0.1$ when we reach the F phase from the QP phase by increasing s as long as p is not too small and not too large, $5 \leq p \leq 21$. It is then interesting to see what happens in the limit of large p.

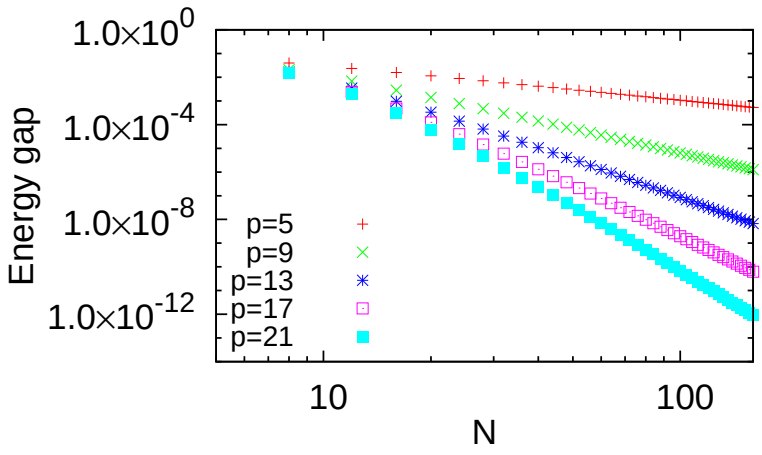

Figure 3.7.: Minimum gap vs. N for some values of p on a log-log scale for $\lambda = 0.1$. Each data scales polynomially.

3.4. Phase diagram for large p

The ferromagnetic p-spin model reduces to the Grover problem in the $p \to \infty$ limit [18]. In the limit $p \to \infty$, the target Hamiltonian reads

$$\hat{H}_0 = -N|\uparrow\cdots\uparrow\rangle\langle\uparrow\cdots\uparrow|. \tag{3.29}$$

In other words, only the all-up state $|\uparrow\cdots\uparrow\rangle$ has the lowest energy $-N$, and the other states have the same energy 0. The energy landscape of Eq. (3.29) is exactly that of the Grover problem.

Farhi *et al.* have proposed a QA version of Grover's algorithm [33], which adopts the transverse field as a driver Hamiltonian. Unfortunately, the time complexity is the same as that of classical algorithms. However, Roland and Cerf have improved the efficiency of QA by adjusting the evolution rate $s(t)$, then reproducing the quadratic speed-up, and they have proved that their algorithm is optimal [34]. This result indicates that our approach cannot avoid jumps of magnetization in the $p \to \infty$ limit. It is therefore interesting to study how this difficulty appears in our method.

To this end, it is instructive to study the behavior of the free energy and magnetization for large but finite values of p. The free energy in Fig. 3.1 is seen to approach the asymptotic values in Eqs. (3.24) and (3.28) from below. Hence, the QP2 phase does not appear for any finite p. From Fig. 3.2, we observe that the magnetization in the x direction is close to the QP2 phase magnetization (3.25), shown in red solid lines, in the region where the free energy approaches f_{QP2}. The magnetization in the z direction is

$$m^z = \sqrt{1 - \left(\frac{1-s}{2s(1-\lambda)}\right)^2} \not\equiv 0 \tag{3.30}$$

since the QP2 phase does not appear.

We extrapolate these results to the case of $p \to \infty$. That is, while the free energies are described by Eqs. (3.23), (3.24), and (3.28), the magnetization in the QP2 phase is given by Eq. (3.30). To be precise, this is not the QP2 phase since the magnetization in

the z direction is nonzero. With a caution on the domain of QP and QP2 in mind, we compare the values of the free energy of the three phases and obtain the phase diagram as in Fig. 3.8. The F phase and the QP phase are separated by a horizontal phase boundary. The boundary of second-order transition is given by $s = 1/(3 - 2\lambda)$ $(\lambda \leq 1/2)$, and the first-order F-QP transition boundary is $s = 1/2$ $(\lambda > 1/2)$. Solving $f_{\mathrm{F}}|_{p\to\infty} = f_{\mathrm{QP2}}$, we get the F-F boundary as

$$s = \frac{1 - 2\sqrt{\lambda - \lambda^2}}{(2\lambda - 1)^2}. \tag{3.31}$$

The figure shows that an abrupt change of magnetization, a first-order transition, is inevitable in the limit $p \to \infty$.

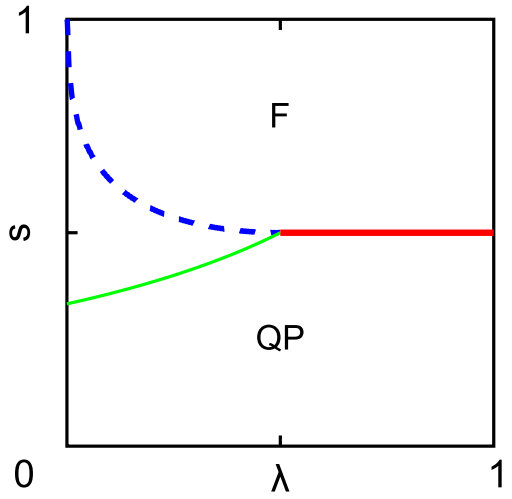

Figure 3.8.: Phase diagram in the limit $p \to \infty$. Three lines represent the same phase boundary as those in Fig. 3.3. The QP phase has the magnetization $m^z = 0$. The F phase above the F-F boundary, shown dashed in blue, has the magnetization $m^z = 1$ and the phase below the F-F boundary has $0 < m^z < 1$.

3.5. Summary and discussion

In this section, we have introduced the transverse antiferromagnetic interactions in addition to the traditional transverse-field term to the QA process. Through the mean-field analysis of the phase diagrams and the numerical analysis of the minimum energy gap, we have found that the first-order phase transition can be avoided and the computational time of QA can be reduced to a polynomial of the number of spins. What the result mean is that QA holds a potential to accomplish exponential speed-up by taking advantage of the degree of freedom in the way to introduce quantum fluctuations.

The question we have to ask here is what nature of the antiferromagnetic term does improve QA. A characteristic feature of the antiferromagnetic term is its macroscopic degeneracy of the ground states: Whereas the transverse-field term has the unique ground state, almost all eigenstates of the antiferromagnetic term, whose number is close to 2^N, are the ground states. One may infer that the macroscopic degeneracy is a key for the sig-

nificant speed-up. Nevertheless, this inference turns out to be wrong through the analysis of the Wajnflasz-Pick model in Chap. 5.

Another inference is that the large overlap between the desired ground state of the target Hamiltonian and the ground state of the antiferromagnetic term shortens the computational time significantly. In contrast to the exponentially small overlap in N between the ground state of the transverse-field term and the final state, the overlap between ground state of the antiferromagnetic term and the final state scales as $N^{-1/4}$. This feature indicates that the antiferromagnetic term is effective only for limited cases such as a problem of the ferromagnetic p-spin model. However, we will obtain results indicating the effectiveness of the antiferromagnetic term for random spin systems in the next chapter.

Chapter 4.

Quantum annealing with antiferromagnetic transverse interactions for the Hopfield model

The main purpose of this chapter is to reveal whether the antiferromagnetic transverse interactions are able to make first-order quantum phase transitions to second-order for random spin systems. We adopt the Hopfield model as a random spin system because the model is expected to cover a wide range of randomness. First, the model is introduced in Sec. 4.1. Next, we analyze the phase diagram for the model with many-body interactions and a finite number of patterns embedded in Sec. 4.2, the model with two-body interactions and many patterns embedded in Sec. 4.3, and the model with many-body interactions and many patterns embedded in Sec. 4.4. Finally, Sec. 4.5 is devoted to summary and discussion.

4.1. The model

The Hamiltonian of the Hopfield model with many-body interactions is given as

$$\hat{H}_0 = -\sum_{i_1<\cdots<i_k} J_{i_1,\ldots,i_k}\hat{\sigma}^z_{i_1}\cdots\hat{\sigma}^z_{i_k} \tag{4.1}$$

with

$$J_{i_1,\ldots,i_k} = \frac{1}{N^{k-1}}\sum_{\mu=1}^{p}\xi^\mu_{i_1}\cdots\xi^\mu_{i_k}. \tag{4.2}$$

Here, k is an integer denoting the degree of interactions, and ξ^μ_i takes ± 1 at random. The number of embedded patterns p is an integer denoting the number of embedded patterns. The total Hamiltonian is given as

$$\hat{H}(s,\lambda) = -s\lambda N\sum_{\mu=1}^{p}\Big(\frac{1}{N}\sum_{i=1}^{N}\xi^\mu_i\hat{\sigma}^z_i\Big)^k + s(1-\lambda)N\Big(\frac{1}{N}\sum_{i=1}^{N}\hat{\sigma}^x_i\Big)^2 - (1-s)\sum_{i=1}^{N}\hat{\sigma}^x_i. \tag{4.3}$$

The Hopfield model was proposed as a model for associative memory [35]. Memories expressed by spin configurations are embedded in the quenched random couplings. The Hopfield model exhibits different behaviors depending on the number of embedded memory patterns. If only a single pattern is embedded, the Hopfield model is equivalent to the Mattis model, in which there is no frustration. This means that the Hopfield model has the same statistical-mechanical properties as the fully connected ferromagnetic model. In

the other extreme limit where the number of embedded patterns is very large, the coupling constants tend to Gaussian variables with zero mean. This is very similar to the Sherrington-Kirkpatrick (SK) model, although there are still correlations among coupling constants. We expect that the case with finite patterns greater than one to be an interpolation between the Mattis model and the SK model. In this sense, the Hopfield model covers a wide range of random spin systems. The statistical-mechanical property of the Hopfield model with finite patterns has been investigated by Amit *et al.* [36]. The case of many patterns has been studied in Ref. [37]. Nishimori and Nonomura have developed a full statistical-mechanical analysis of the quantum Hopfield model, i.e., the Hopfield model in a transverse field [22]. The statistical-mechanical property of the Hopfield model with many-body interactions has been studied by Gardner [38]. Ma and Gong have shown the phase diagram of the Hopfield model with many-body interactions in a transverse field in the limit of infinite degree of interactions [39].

4.2. Hopfield model with finite patterns embedded

4.2.1. Analysis

We give self-consistent equations for the Hopfield model with finite patterns embedded. It is known that the quantum Hopfield model that has two-body interactions exhibits a second-order transition [22]. We deal with the case of $k > 2$ to check whether antiferromagnetic transverse interactions enable us to avoid a first-order transition.

The analysis is quite similar to that for the ferromagnetic p-spin model (see Appendix B for detailed calculations). The order parameters of the Hopfield model are the overlaps with embedded patterns m_μ ($\mu = 1, \dots p$). In the low-temperature limit $\beta \to \infty$, the pseudo free energy and the self-consistent equations are

$$f(s,\lambda;\{m_\mu\},m^x) = (k-1)s\lambda\sum_\mu (m_\mu)^k - s(1-\lambda)(m^x)^2 - \left[\sqrt{\{ks\lambda\textstyle\sum_\mu (m_\mu)^{k-1}\xi^\mu\}^2 + \{1-s-2s(1-\lambda)m^x\}^2}\right], \tag{4.4}$$

and

$$(m_\mu)^{k-1} = \left[\frac{ks\lambda\left(\sum_\mu (m_\mu)^{k-1}\xi^\mu\right)(m_\mu)^{k-2}\xi^\mu}{\sqrt{\{ks\lambda\sum_\mu (m_\mu)^{k-1}\xi^\mu\}^2 + \{1-s-2s(1-\lambda)m^x\}^2}}\right], \tag{4.5}$$

$$m^x = \left[\frac{1-s-2s(1-\lambda)m^x}{\sqrt{\{ks\lambda\sum_\mu (m_\mu)^{k-1}\xi^\mu\}^2 + \{1-s-2s(1-\lambda)m^x\}^2}}\right]. \tag{4.6}$$

Here, m^x denotes the magnetization along the x direction, and the brackets $[\dots]$ are for the average over the randomness of the embedded patterns.

The self-consistent equations (4.5) and (4.6) have the quantum paramagnetic (QP) solution in the region $0 \le s \le 1/(3-2\lambda)$. The order parameters in the QP phase satisfy $m_\mu = 0$ for all μ and $m^x = 1$. The free energy in the QP phase is

$$f_{\rm QP}(s,\lambda) = -s\lambda + 2s - 1. \tag{4.7}$$

Let us consider the solutions for nonzero m_μ's. According to the experience in the classical case [36], we expect that the overlaps that give the lowest value of the free energy are symmetric, i.e., $m^\mu = m$ for $\mu \leq l$ with a given integer l, and the others are zero. The pseudo free energy and self-consistent equations for such symmetric solutions are

$$f_l(s,\lambda;m,m^x) = (k-1)s\lambda l m^k - s(1-\lambda)(m^x)^2 - \left[\sqrt{\{ks\lambda m^{k-1}z_l\}^2 + \{1-s-2s(1-\lambda)m^x\}^2}\right], \tag{4.8}$$

and

$$m = \left[\frac{ks\lambda m^{k-1}(z_l)^2/l}{\sqrt{\{ks\lambda m^{k-1}z_l\}^2 + \{1-s-2s(1-\lambda)m^x\}^2}}\right], \tag{4.9}$$

$$m^x = \left[\frac{1-s-2s(1-\lambda)m^x}{\sqrt{\{ks\lambda m^{k-1}z_l\}^2 + \{1-s-2s(1-\lambda)m^x\}^2}}\right], \tag{4.10}$$

where we defined the random variable $z_l \equiv \sum_{\mu=1}^{l} \xi^\mu$. In particular, for $l = 1$, the pseudo free energy f_1 and the self-consistent equations are identical with those of the many-body interacting ferromagnetic model in the ferromagnetic phase. This assures us that the phase diagram of the Hopfield model with finite patterns is the same as that of the many-body interacting ferromagnetic model if f_1 has the lowest value in the symmetric solutions. The phase for $l = 1$ is referred to as the retrieval (R) phase. The state in the R phase correlates with one of the embedded patterns.

4.2.2. Numerical results

We compared the free energies for symmetric order parameters (4.8), finding that the free energy for the R phase has the lowest value in the free energies among f_1, f_2, f_3, and f_4, at least for $3 \leq k \leq 21$ and odd k. We show an example for $k = 5$ in Fig. 4.1. From this result, we conclude that the R phase is the most stable one among the phases having a symmetric order parameter.

This result indicates that antiferromagnetic transverse interactions greatly improve the process of QA for the generalized Hopfield model with finite patterns. Since the pseudo free energy and the self-consistent equations for $l = 1$ are identical with those of the ferromagnetic model with many-body interactions, the phase diagrams for the generalized Hopfield model with finite patterns are the same as those of the many-body interacting ferromagnetic model shown in Sec. 3.3.1 except that the ferromagnetic phase is replaced by the R phase. We have shown in Sec. 3.3.1 that, whereas the phase transition from the QP phase to the ferromagnetic phase is of first order in the case of three-body interactions, the first-order transition disappears in a range of low λ for $5 \leq k \leq 21$ and odd k. The conventional QA with a transverse field undergoes a first-order quantum phase transition from the QP phase to the R phase. Antiferromagnetic transverse interactions have thus shown to enable us to avoid the difficulty of QA coming from the first-order phase transitions for $5 \leq k \leq 21$ and odd k, even in the presence of randomness.

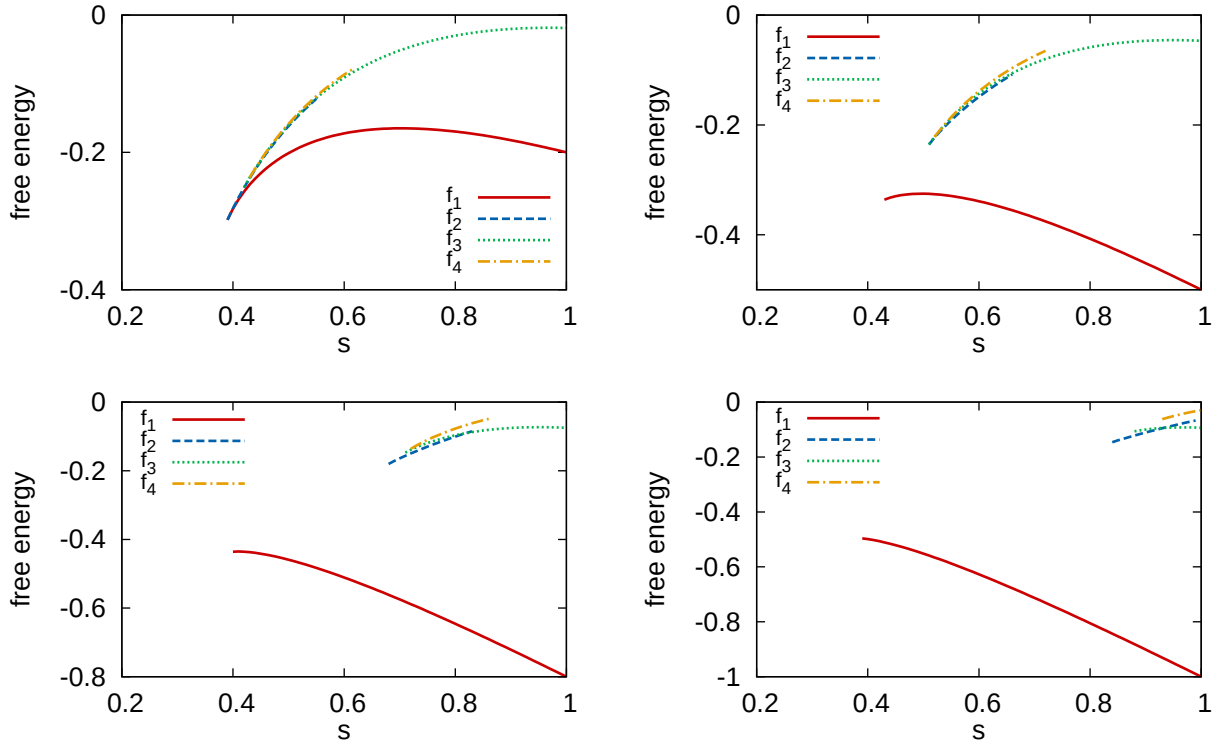

Figure 4.1.: The free energies for symmetric order parameters with $k = 5$, f_1, f_2, f_3, and f_4, for $\lambda = 0.2$ (top left), 0.5 (top right), 0.8 (bottom left), and 1 (bottom right). The free energy f_1 always has the lowest value among the free energies compared.

4.3. Hopfield model with two-body interactions and with many patterns embedded

Let us next consider the case of many patterns, i.e., the number of patterns increases as N increases. Unlike the case of finite patterns, the quantum Hopfield model with $k = 2$ exhibits a first-order phase transition between the spin-glass (SG) phase and the R phase. Hence, we also deal with the $k = 2$ case. First, we analyze the $k = 2$ case, and next the case of $k > 2$.

4.3.1. Self-consistent equations

The target Hamiltonian is

$$\hat{H}_0 = -\frac{1}{2}\sum_{ij} J_{ij}\hat{\sigma}_i^z\hat{\sigma}_j^z, \tag{4.11}$$

where J_{ij} is given as

$$J_{ij} = \frac{1}{N}\sum_{\mu=1}^{p}\xi_i^\mu\xi_j^\mu. \tag{4.12}$$

The number of patterns must be proportional to the number of spins $p = \alpha N$ so that the free energy is extensive, as explained in Appendix C.

To obtain the self-consistent equations, we closely follow Chap. 10 of Ref. [40]. Detailed calculations are described in Appendix C. We assume that the system has a non-vanishing overlap with only one embedded pattern. Then we have the following self-consistent equations in the low-temperature limit:

$$m = \int Dz \frac{s\lambda m + \sqrt{\alpha\tilde{q}}z}{\sqrt{(s\lambda m + \sqrt{\alpha\tilde{q}}z)^2 + (1 - s - 2s(1-\lambda)m^x)^2}}, \tag{4.13}$$

$$m^x = \int Dz \frac{1 - s - 2s(1-\lambda)m^x}{\sqrt{(s\lambda m + \sqrt{\alpha\tilde{q}}z)^2 + (1 - s - 2s(1-\lambda)m^x)^2}}, \tag{4.14}$$

$$q = \int Dz \frac{(s\lambda m + \sqrt{\alpha\tilde{q}}z)^2}{(s\lambda m + \sqrt{\alpha\tilde{q}}z)^2 + (1 - s - 2s(1-\lambda)m^x)^2}, \tag{4.15}$$

where m denotes the overlap, m^x the magnetization along the x direction, and q the spin-glass order parameter. We defined the Gaussian measure as $Dz \equiv dz \exp(-z^2/2)/\sqrt{2\pi}$. The variable $\tilde{q}$ satisfies

$$\tilde{q} = \frac{(s\lambda)^2 q}{(1 - s\lambda C)^2} \tag{4.16}$$

with

$$C = \int Dz \frac{\{1 - s - 2s(1-\lambda)m^x\}^2}{\{(s\lambda m + \sqrt{\alpha\tilde{q}}z)^2 + (1 - s - 2s(1-\lambda)m^x)^2\}^{3/2}}. \tag{4.17}$$

The pseudo free energy is written as

$$f = \frac{1}{2}s\lambda m^2 - s(1-\lambda)(m^x)^2 - \frac{\alpha}{2}s\lambda + \frac{\alpha}{2}\tilde{q}C - \int Dz \sqrt{(s\lambda m + \sqrt{\alpha\tilde{q}})^2 + (1 - s - 2s(1-\lambda)m^x)^2}. \tag{4.18}$$

4.3.2. Phase diagram

We compared the free energies for three phases: The first is the R phase, $m > 0$, the second is the SG phase, $m = 0$ and $q > 0$, and the last is the QP phase, $m = q = 0$. The phase diagram for the case of $p = 0.04N$ is given in Fig. 4.2. Although the phase transition from the QP phase to the SG phase is of second order, the phase transition from the SG phase to the R phase is always of first order. Therefore, even the method using antiferromagnetic transverse interactions requires an exponentially long time to find the ground state.

The second-order boundary can be obtained analytically. Expanding Eq. (4.15) in powers of q, we have

$$q = \alpha\Big(\frac{s\lambda}{1 - s(3-\lambda)}\Big)^2 q + \mathrm{O}(q^2). \tag{4.19}$$

Hence, the phase boundary is

$$s = \frac{1}{3 - \lambda(1 - \sqrt{\alpha})} \tag{4.20}$$

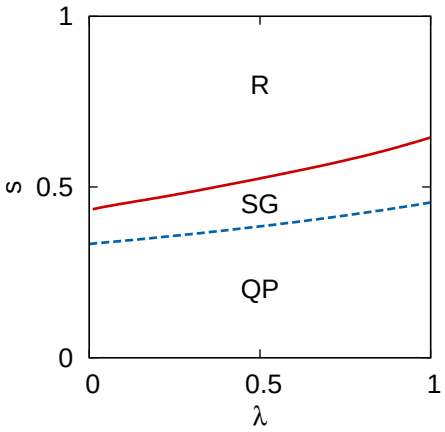

Figure 4.2.: The phase diagram of the Hopfield model with $k = 2$ and with many patterns $p = 0.04N$. The red solid line represents the first-order phase boundary, and the blue dashed line the second-order boundary. The first-order phase transition is inevitable for the QA process.

or

$$s = \frac{1}{3 - \lambda(1 + \sqrt{\alpha})}. \tag{4.21}$$

Since the boundary (4.20) lies below the other (4.21), Eq. (4.20) gives the true thermodynamic phase boundary between the QP phase and the SG phase.

4.4. Hopfield model with many-body interactions and with many patterns embedded

4.4.1. Self-consistent equations

Let us next consider the case of $k > 2$. The Hamiltonian is given by Eqs. (4.1) and (4.2). The number of patterns must be $p = \alpha N^{k-1}$ so that the free energy is extensive. We consider the case where the system has a non-zero overlap with a single pattern only. We closely follow the calculation in Ref. [38] to derive the self-consistent equations (see Appendix D for detailed calculations). The self-consistent equations in the low-temperature limit are

$$m = \int Dz \frac{s\lambda(km^{k-1} + \sqrt{\alpha k q^{k-1}}z)}{\sqrt{(s\lambda[km^{k-1} + \sqrt{\alpha k q^{k-1}}z])^2 + (1 - s - 2s(1-\lambda)m^x)^2}}, \tag{4.22}$$

$$m^x = \int Dz \frac{1 - s - 2s(1-\lambda)m^x}{\sqrt{(s\lambda[km^{k-1} + \sqrt{\alpha k q^{k-1}}z])^2 + (1 - s - 2s(1-\lambda)m^x)^2}}, \tag{4.23}$$

$$q = \int Dz \frac{(s\lambda[km^{k-1} + \sqrt{\alpha k q^{k-1}}z])^2}{(s\lambda[km^{k-1} + \sqrt{\alpha k q^{k-1}}z])^2 + (1 - s - 2s(1-\lambda)m^x)^2}. \tag{4.24}$$

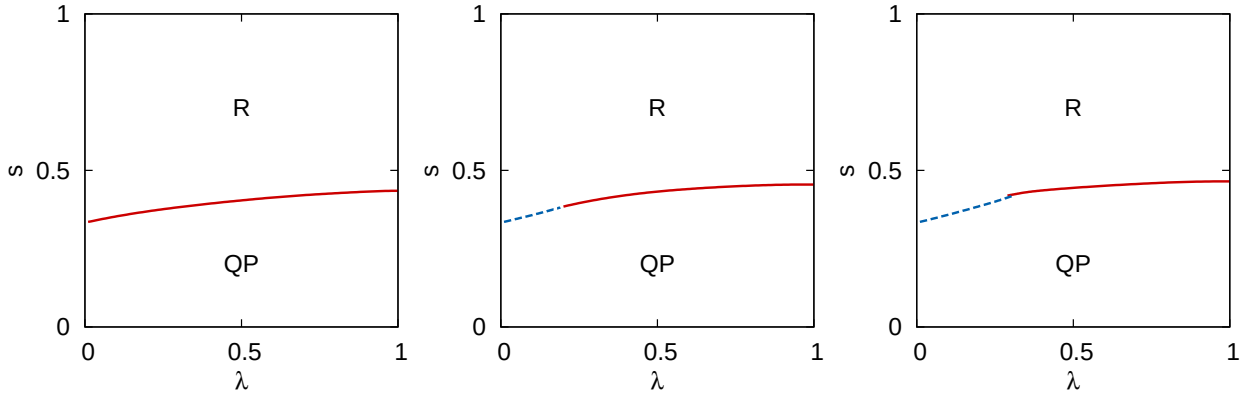

Figure 4.3.: The phase diagram of the generalized Hopfield model with many patterns $p = 0.04N^{k-1}$ for $k = 3$ (left), $k = 4$ (center), $k = 5$ (right). The red solid line represents the first-order phase boundary, and the blue dashed line the second-order boundary. In contrast to the previous case of $k = 2$, the SG phase does not appear. Whereas the first-order transition is inevitable for $k = 3$, we can avoid the first-order transition for $k = 4$ and 5.

The pseudo free energy is

$$f = s\lambda(k-1)m^k - s(1-\lambda)(m^x)^2 + \frac{\alpha}{2}k(k-1)(s\lambda)^2 C q^{k-1} - \int Dz \sqrt{(s\lambda[km^{k-1} + \sqrt{\alpha k q^{k-1}}z])^2 + (1-s-2s(1-\lambda)m^x)^2}, \tag{4.25}$$

where

$$C = \int Dz \frac{\{1-s-2s(1-\lambda)m^x\}^2}{\{(s\lambda[km^{k-1} + \sqrt{\alpha k q^{k-1}}z])^2 + (1-s-2s(1-\lambda)m^x)^2\}^{3/2}}. \tag{4.26}$$

4.4.2. Phase diagram

We now describe the phase diagram of the generalized Hopfield model with $k = 3$, 4, and 5 and many patterns $p = 0.04N^{k-1}$. In the same way as in Sec. 4.3.2, the free energies for the three phases were compared. Figure 4.3 shows the resulting phase diagram. The SG phase does not appear, since the free energy for the SG phase has a higher value than the other free energies for the R phase and the QP phase. The first-order boundary vanishes for $k = 4$ and 5, and there exist annealing paths to avoid the first-order transition.

4.5. Summary and discussion

In this chapter, we have investigated the statistical-mechanical property of the Hopfield model with the antiferromagnetic transverse interactions subjected to a transverse field. The model shows different behaviors depending on the number of patterns embedded.

First, we have considered the generalized Hopfield model with k-body interactions and a finite number of patterns embedded. The Suzuki-Trotter decomposition and the mean-field analysis have given the self-consistent equations and the pseudo free energy. We have

concluded that the phase diagram is the same as the many-body interacting ferromagnetic model at least for $3 \leq k \leq 21$ and odd k. Considering the result in Sec. 3.3.1 (see also [41]), the present result indicates that antiferromagnetic transverse interactions greatly improve the QA process for the model except for the case of $k = 3$. We conclude that antiferromagnetic transverse interactions are effective also for the random spin system.

Second, the Hopfield model with two-body interactions and extensively many patterns has been analyzed. The difference from the previous case is that the SG phase appears owing to the many unretrieved patterns. The spins in the SG phase tend to align in the $\pm z$ direction, but do not correlate with any embedded patterns. We have used the Suzuki-Trotter decomposition, the mean-field analysis, the replica trick, and the static ansatz to study the phase diagram. The analysis within the RS solution has derived the phase diagram including three phases: the QP phase, the SG phase, and the R phase. Although the phase boundary between the QP phase and the SG phase is of second order, the boundary between the SG phase and the R phase stays always of first order. This result indicates difficulties for QA with antiferromagnetic transverse interactions. Once the system is trapped in a basin in the SG phase, it is hard to escape there to reach the true ground state.

Finally, we have investigated the generalized Hopfield model with many-body interactions and extensively many patterns. The resulting phase diagram consists of the QP and R phases. Although the SG solution exists, it has a higher free energy than the other states. We have confirmed that the first-order phase boundary vanishes at certain values of λ for $k = 4$ and $k = 5$. Hence, it is possible to avoid the difficulty of exponentially long running time of QA that results from a first-order phase transition.

Chapter 5.

Quantum annealing in the Wajnflasz-Pick model

The subjects of this chapter are twofold: One is to check the effect of macroscopic degeneracy against the efficiency of QA. As mentioned in Sec. 3.5, the antiferromagnetic term has the feature that the ground states are exponentially degenerate, which is not the case with the transverse-field term. The other subject is to find an alternative way to control the order of quantum phase transitions other than the method using the antiferromagnetic term. First, the model is defined in Sec. 5.1. Sec. 5.2 then investigates the effect of the macroscopic degeneracy. Next, in Sec. 5.3, the alternative way is explored. Finally, Sec. 5.4 is devoted to summary and discussion.

5.1. The model

5.1.1. Classical Wajnflasz-Pick model

Before moving onto the explanation for the quantum Wajnflasz-Pick model, let us introduce the classical counterpart. The Wajnflasz-Pick model [42] is considered as a generalization of the Ising model: The model is composed of two level variables like an Ising spin, but each level can be degenerate. The Hamiltonian is defined as

$$H = -\frac{1}{N}\sum_{ij}\tau_i\tau_j - h\sum_i \tau_i, \tag{5.1}$$

where N represents the number of sites and h a longitudinal field. The summation $\sum_{ij}$ is taken over all possible pairs of sites. The variable τ takes ± 1. The state of $\tau = +1$ is referred to as an upper state, and the state $\tau = -1$ as a lower state. The order of degeneracy of the upper states is denoted by g_{p}, and that of lower sates is denoted by g_{m}.

Let us consider phase transitions of the model (5.1) for a fixed h. The model can be reduced to the following Ising spin system [43]:

$$H' = -\frac{1}{N}\sum_{ij}\sigma_i\sigma_j - \left(h + \frac{T}{2}\ln\frac{g_{\mathrm{p}}}{g_{\mathrm{m}}}\right)\sum_i \sigma_i, \tag{5.2}$$

where σ denotes an Ising spin. This Hamiltonian yields the same partition function as that of the system (5.1) at temperature T. Hence, the phase diagram is obtained through the knowledge of the usual Ising model. The difference from the usual Ising model is that the effective longitudinal field

$$h' \equiv h + \frac{T}{2}\ln\frac{g_{\mathrm{p}}}{g_{\mathrm{m}}} \tag{5.3}$$

can vary with temperature. Let T_c be the critical temperature of the usual Ising model. Since the system (5.2) is completely equivalent to the usual Ising spin model if $g_p = g_m$, the system (5.1) undergoes the second-order phase transition as temperature decreases when h is fixed at zero, and there is no phase transition for a finite h fixed. In the imbalanced case $g_p \neq g_m$, We can find that the first-order phase transition occurs when $g_p/g_m > \exp(2h/T_c) \equiv g^*$, the second-order phase transition occurs when $g_p/g_m = g^*$, and no phase transition when $g_p/g_m < g^*$. Thus, the order of phase transition of the classical Wajnflasz-Pick model is controllable by adjusting the ratio of the orders of degeneracy.

5.1.2. Quantum Wajnflasz-Pick model

We generalize the classical Wajnflasz-Pick model to a quantum model in a similar way as Refs. [44, 45]. The Hamiltonian of the quantum Wajnflasz-Pick model with a term corresponding to the transverse field is defined as

$$\hat{H}(s) = s\left[-\frac{1}{N}\sum_{i,j=1}^{N}\hat{\tau}_i^z\hat{\tau}_j^z - h\sum_{i=1}^{N}\hat{\tau}_i^z\right] - (1-s)\sum_{i=1}^{N}\hat{\tau}_i^x, \tag{5.4}$$

where $s \in [0,1]$ denotes the dimensionless time, and h a longitudinal field. The operator $\hat{\tau}^z$ represents a degenerate two-level system:

$$\hat{\tau}^z \equiv \mathrm{diag}(\underbrace{+1,\ldots,+1}_{g_p},\underbrace{-1,\ldots,-1}_{g_m}). \tag{5.5}$$

The last term in Eq. (5.4) is a driver part that induces quantum fluctuations into the system. We define the operator $\hat{\tau}^x$ as follows:

$$\hat{\tau}^x \equiv \begin{pmatrix} \boldsymbol{A}(g_p) & \mathbf{1}(g_p,g_m) \\ \mathbf{1}(g_m,g_p) & \boldsymbol{A}(g_m) \end{pmatrix}, \tag{5.6}$$

where the matrix $\boldsymbol{A}(l)$ is a square matrix of order l whose diagonal elements are zero, and upper (lower) triangular elements are ω ($\overline{\omega}$):

$$\boldsymbol{A}(l) \equiv \begin{pmatrix} 0 & \omega & \cdots & \omega \\ \overline{\omega} & 0 & \ddots & \vdots \\ \vdots & \ddots & \ddots & \omega \\ \overline{\omega} & \cdots & \overline{\omega} & 0 \end{pmatrix}. \tag{5.7}$$

Here, ω is a complex variable, and its complex conjugate is $\overline{\omega}$. The other matrix $\mathbf{1}(l,m)$ is an $l \times m$ matrix with ones. The off-diagonal block matrix $\mathbf{1}$ represents spin flips, and $\boldsymbol{A}$ the transition between degenerate states. This is a simple way to introduce quantum fluctuations into the system.

5.2. Effect of macroscopic degeneracy for QA

This section investigates how macroscopic degeneracy affects the efficiency of QA. As a result, we will find that the existence of exponentially degenerate ground states of the antiferromagnetic term is not sufficient to achieve the exponential speed-up of QA.

5.2.1. How to induce quantum fluctuations

We consider the quantum Wajnflasz-Pick model with $g_{\rm p} = 2$ and $g_{\rm m} = 1$, and with two types of operators that induce quantum fluctuations:

$$\hat{\tau}^{x,1} \equiv \begin{pmatrix} 0 & 1 & 1 \\ 1 & 0 & 1 \\ 1 & 1 & 0 \end{pmatrix}, \qquad \hat{\tau}^{x,2} \equiv \begin{pmatrix} 0 & 0 & 1 \\ 0 & 0 & 1 \\ 1 & 1 & 0 \end{pmatrix}. \tag{5.8}$$

The former operator causes state transitions between the generate states, whereas the latter does not cause such transitions. Let us calculate the degeneracy of the ground state of the term $+\big(\sum_i \hat{\tau}_i^{x,2}\big)^2$. Since the eigenvalues of the operator are -1, 0, and $+1$, the number of the ground state is evaluated as

$$\sum_{n=0}^{N/2} \binom{N}{2n} \binom{N-2n}{N/2-n} > \binom{N}{N/3} \binom{2N/3}{N/3} \simeq {\rm Poly}(1/N)\, 3^N, \tag{5.9}$$

leading to the degeneracy comparable to the number of all configurations. The factor ${\rm Poly}(1/N)$ denotes a polynomial of $1/N$. Here, we have assumed that N is a multiple of six for simplicity.

The remaining issue is which term should be used for a transverse field. In order to check the effect of the macroscopic degeneracy, we have to select a model that undergoes first-order phase transitions when quantum fluctuations are induced only by a transverse field. As mentioned later, the Wajnflasz-Pick model with a transverse-field term consisting of $\tau^{x,2}$ does not undergoes a first-order quantum phase transition. In contrast, the model with $\tau^{x,1}$ occurs a first-order phase transition. Therefore the total Hamiltonian to be studied is

$$\hat{H}(s,\lambda) = -s\lambda N \left(\frac{1}{N} \sum_i \hat{\tau}_i^z \right)^2 + s(1-\lambda) N \left(\frac{1}{N} \sum_i \hat{\tau}_i^{x,2} \right)^2 - (1-s) \sum_i \hat{\tau}_i^{x,1}. \tag{5.10}$$

5.2.2. Partition function and self-consistent equation

The analysis is similar to that of the ferromagnetic p-spin model except that we have to use three types of closures in order to convert the model to a classical model. After some calculations (see Appendix E), we have the following pseudo free energy:

$$f = s\lambda \big(m^z\big)^2 - s(1-\lambda)\big(m^x\big)^2 - \frac{1}{\beta} \ln {\rm Tr} \exp \beta \big(\tilde{m}^z \hat{\sigma}^z + \tilde{m}^x \hat{\tau}^{x,2} + (1-s)\hat{\tau}^{x,1} \big), \tag{5.11}$$

where

$$\tilde{m}^z \equiv s\lambda(2m^z + h), \tag{5.12}$$

$$\tilde{m}^x \equiv -2s(1-\lambda)m^x. \tag{5.13}$$

Let us consider the low-temperature limit to study quantum phase transitions. In this limit, the maximum eigenvalue of the operator in Eq. (5.11) contributes to the free energy. The eigenvalues are

$$\begin{aligned} \lambda_1 &\equiv \tilde{m}^x - 1 + s, \\ \lambda_2 &\equiv \frac{1-s}{2} - \sqrt{(\tilde{m}^z + (1-s)/2)^2 + 2(\tilde{m}^x + (1-s))^2}, \\ \lambda_3 &\equiv \frac{1-s}{2} + \sqrt{(\tilde{m}^z + (1-s)/2)^2 + 2(\tilde{m}^x + (1-s))^2}. \end{aligned}$$

We can easily check that λ_3 is the maximum eigenvalue. Hence, the pseudo free energy in the low-temperature limit is written as

$$f = s\lambda\left(m^z\right)^2 - s(1-\lambda)\left(m^x\right)^2 - \frac{1-s}{2} - \sqrt{(\tilde{m}^z + (1-s)/2)^2 + 2(\tilde{m}^x + (1-s))^2}. \tag{5.14}$$

From the saddle-point condition, the self-consistent equations are

$$m^z = \frac{\tilde{m}^z + (1-s)/2}{\sqrt{(\tilde{m}^z + (1-s)/2)^2 + 2(\tilde{m}^x + (1-s))^2}}, \tag{5.15}$$

$$m^x = \frac{2(\tilde{m}^x + (1-s))}{\sqrt{(\tilde{m}^z + (1-s)/2)^2 + 2(\tilde{m}^x + (1-s))^2}}. \tag{5.16}$$

5.2.3. Numerical results

Let us show the solutions of the self-consistent equations (5.15) and (5.16) for certain fixed values of h. First, Fig. 5.1 shows m^z as a function of s for $\lambda = 0.2$, 0.4, 0.6, 0.8, and 1.0. The magnetization has a nonzero value for the following reason. The ground state of the transverse-field term is the equally weighted superposition of all possible eigenstates in the z basis. Since the number of the upper states is larger than that of the lower states, the system has a positive magnetization. The magnetization eventually equals -1 in consequence of the longitudinal field. We can find that all data except for $h = -1.0$ have jumps. The width of the jump reduces as the magnitude of h increases. It is natural that the system has no phase transition for large h. Focusing on the dependency of λ, we can find that the jump of the magnetization reduces as λ increases. The results indicate that the antiferromagnetic term negatively affects the efficiency of QA.

Next, Fig. 5.2 shows m^x as a function of s for the same values as those of Fig. 5.1. Unlike the previous results, we cannot find jumps. Since the magnetization becomes smoother as λ decreases, we can estimate that the antiferromagnetic term has an effect to suppress rapid change of m^x.

5.3. Control of order of quantum phase transition

This section explores an alternative way to control the order of quantum phase transitions. We investigate that how the order of degeneracy, g_{p} and g_{m}, and the transition between the degenerate states expressed by ω affect the nature of the quantum phase transition of the quantum Wajnflasz-Pick model. To this end, we study the statistical-mechanical propeties of the quantum Wajnflasz-Pick model by using the mean-field analysis. To reveal the effect of the transitions, we analyze the dependency of an order parameter of the model on a strength of quantum fluctuations under various transition rates ω.

5.3.1. Mean-Field Analysis

In what follows, we derive the pseudo free energy to investigate an order parameter of the system. First, the partition function of the quantum system is transformed to a corresponding classical system by using the Trotter decomposition. Next, we use the mean-field analysis, and introduce an order parameter similar to magnetization. Applying

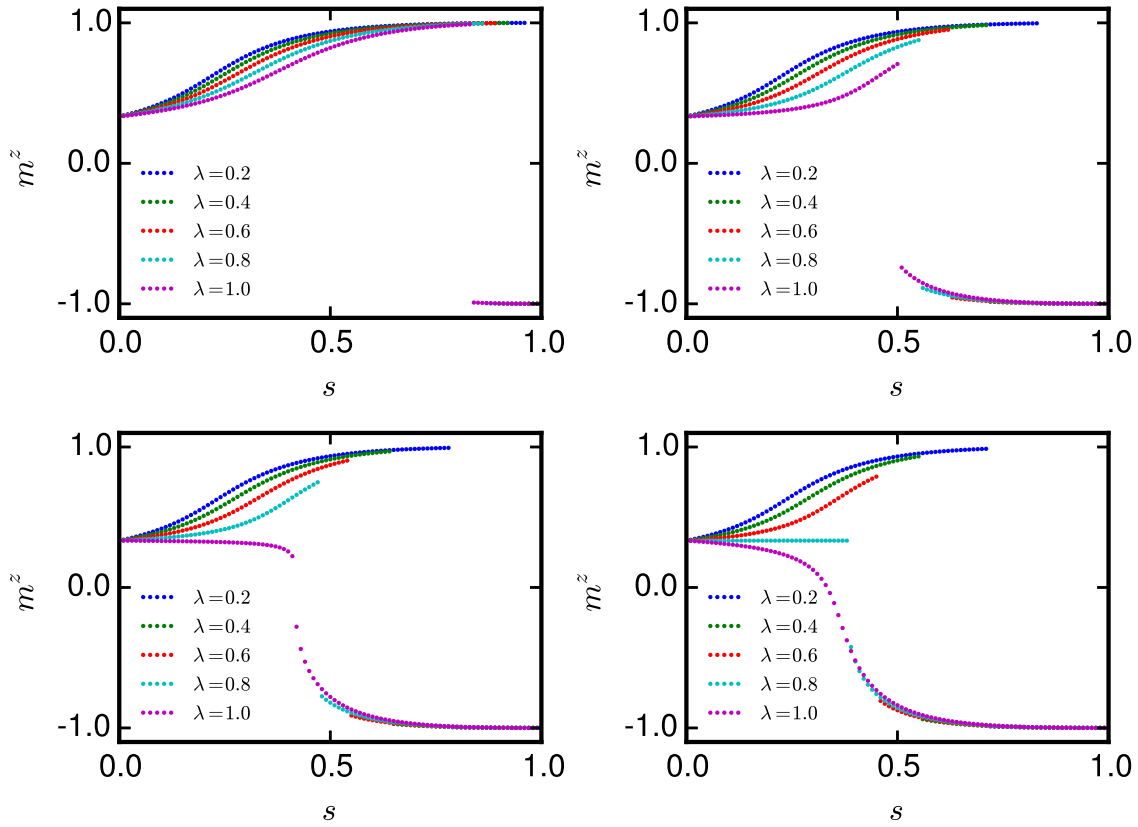

Figure 5.1.: The magnetization m^z as a function of s. The values of the longitudinal field are $h = -0.1$ (upper left), -0.5 (upper right), -0.7 (lower left), and -1.0 (lower right).

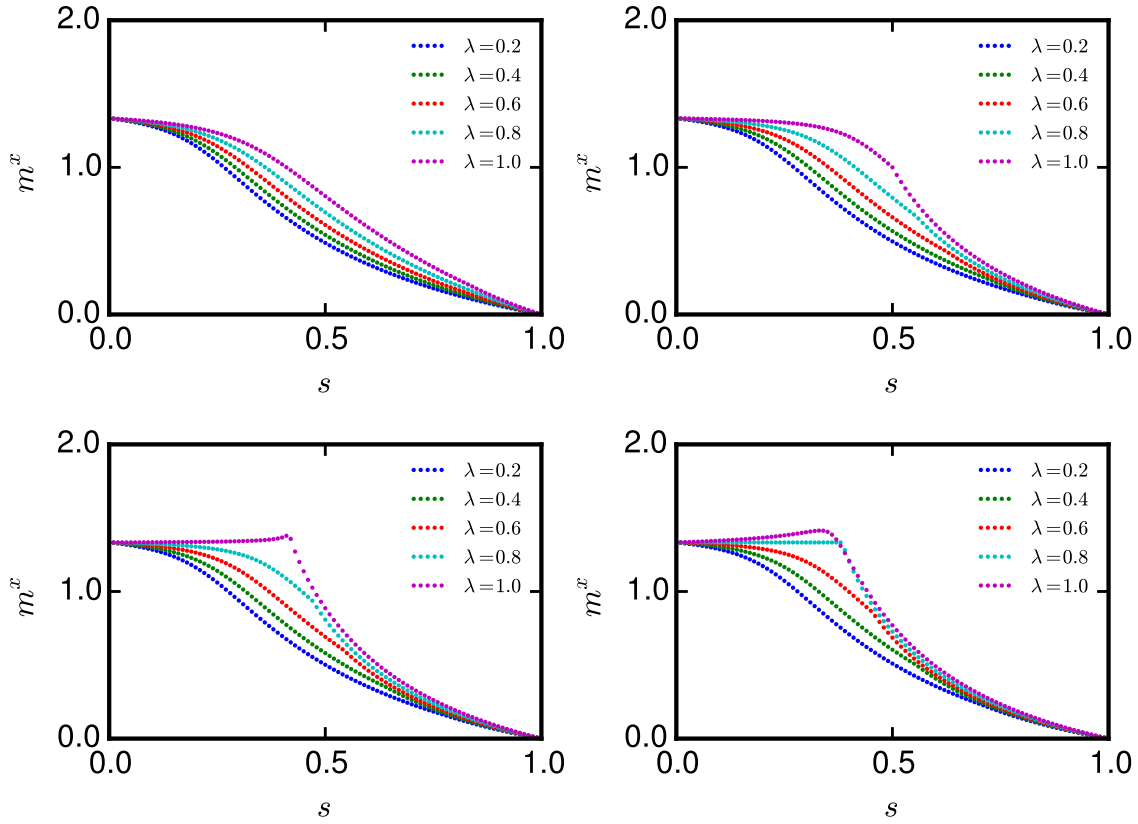

Figure 5.2.: The magnetization m^x as a function of s. The values of the longitudinal field are $h = -0.1$ (upper left), -0.5 (upper right), -0.7 (lower left), and -1.0 (lower right).

the static ansatz, we can get the pseudo-free energy. Since focusing on the quantum phase transitions in the model, we take the low-temperature limit.

Let us consider the Hamiltonian given by Eq. (5.4). We can reuse the results of the analysis for the ferromagnetic p-spin model. Although the analysis was for spin-1/2 systems, Eqs. (3.12)-(3.14) hold for any discrete level system whose Hamiltonian is given in a similar way as Eq. (3.5). Since the Hamiltonian of the quantum Wajnflasz-Pick model consists of the target part and the transverse-field term, λ is equal to unity. Consequently, we have the partition function

$$\begin{aligned} Z_M = \int \cdots \int \prod_\alpha dm(\alpha) d\tilde{m}(\alpha) \exp\left\{ \frac{\beta N}{M} \left(s\{[m(\alpha)]^2 + hm(\alpha)\} - \tilde{m}(\alpha) m(\alpha) \right) \right\} \\ \times \exp\left\{ N \ln \sum_{\{\tau^z\}} \sum_{\{\tau^x\}} \prod_\alpha \exp\left\{ \frac{\beta}{M} (\tilde{m}(\alpha)\tau^z(\alpha) + (1-s)\tau^x(\alpha)) \right\} \right. \\ \left. \times \langle \tau^z(\alpha) | \tau^x(\alpha) \rangle \langle \tau^x(\alpha) | \tau^z(\alpha+1) \rangle \right\}, \end{aligned} \tag{5.17}$$

and the conjugate variable at the saddle point

$$\tilde{m}(\alpha) = s(2m(\alpha) + h). \tag{5.18}$$

Using the static ansatz and the inverse operation of the Trotter decomposition, we obtain the pseudo free energy

$$f = sm^2 - \frac{1}{\beta} \ln \mathrm{Tr} \exp \beta(\tilde{m}\hat{\tau}^z + (1-s)\hat{\tau}^x). \tag{5.19}$$

Here $\tilde{m} = s(2m + h)$.

If ω is a positive real value, the trace in Eq. (5.19) is evaluated as follows. The Perron-Frobenius theorem ensures that the ground state of the operator $\tilde{m}\hat{\tau}^z + (1-s)\hat{\tau}^x$ is unique and the elements of the eigenvector are positive. Taking the symmetry of the operator with regards to basis transformation into account, the eigenvector can be expressed as

$$\boldsymbol{v} = (\underbrace{v_\mathrm{p}, \ldots, v_\mathrm{p}}_{g_\mathrm{p}}, \underbrace{v_\mathrm{m}, \ldots, v_\mathrm{m}}_{g_\mathrm{m}})^\mathrm{T}, \tag{5.20}$$

where v_p and v_m are real and positive. Hence, the characteristic equation for the eigenvalue is reduced to equations with two unknowns v_p and v_m. Solving the equations, we have the maximum eigenvalue of the operator:

$$\lambda_\mathrm{max} = \frac{1}{2} \left\{ (g_\mathrm{p} + g_\mathrm{m} - 2)(1-s)\omega + \sqrt{\{(g_\mathrm{p} - g_\mathrm{m})(1-s)\omega + 2\tilde{m}\}^2 + 4g_\mathrm{p} g_\mathrm{m} (1-s)^2} \right\}. \tag{5.21}$$

Consequently, the pseudo free energy in the low-temperature limit is given as

$$f = sm^2 - \lambda_\mathrm{max}, \tag{5.22}$$

and the self-consistent equation is

$$m = \frac{2\tilde{m} + (g_\mathrm{p} - g_\mathrm{m})(1-s)\omega}{\sqrt{\{(g_\mathrm{p} - g_\mathrm{m})(1-s)\omega + 2\tilde{m}\}^2 + 4g_\mathrm{p} g_\mathrm{m} (1-s)^2}}. \tag{5.23}$$

The Perron-Frobenius theorem is not applicable to the case of negative ω or complex ω. In such cases, the stable solution is obtained by checking all eigenvalues of the operator.

5.3.2. Results for positive ω

This section shows the following results:

1. If the order of degeneracy is the same $g_{\rm p} = g_{\rm m} \equiv g$, the model is equivalent to the spin-1/2 system
2. If there is no transition between degenerate states $\omega = 0$, the model is equivalent to the spin-1/2 system
3. For nonzero ω fixed, the model tends to undergo a first-order quantum phase transition as the difference between $g_{\rm p}$ and $g_{\rm m}$ gets larger.
4. For fixed $g_{\rm p}$ and $g_{\rm m}$ ($g_{\rm p} \neq g_{\rm m}$), the model tends to undergo a first-order quantum phase transition as ω gets larger.

First, let us show the result 1. The pseudo free energy is rewritten as

$$f = sm^2 - (g-1)(1-s)\omega - \sqrt{\{s(2m+h)\}^2 + \{g(1-s)\}^2}. \tag{5.24}$$

On the other hand, the pseudo free energy of a spin-1/2 system whose Hamiltonian is given by

$$\hat{H} = s\left\{-\frac{1}{N}\left(\sum_{ij}\hat{\sigma}_i^z\hat{\sigma}_j^z\right)^2 - h\sum_i \hat{\sigma}_i^z\right\} - g(1-s)\sum_i \hat{\sigma}_i^x \tag{5.25}$$

is

$$f = sm^2 - \sqrt{\{s(2m+h)\}^2 + \{g(1-s)\}^2}. \tag{5.26}$$

The difference between the two pseudo free energies is the second term on the right-hand side of Eq. (5.24). The term, however, just shift the pseudo free energy as a function of m. Hence, the stable solution is the same for both models. Since the Wajnflasz-Pick model is equivalent to the spin-1/2 system (5.25), the system undergoes the second-order phase transition in the absent of a longitudinal field. The transition point is $s^\star = 1/(1+(2/g))$, and the magnetization is

$$m = \begin{cases} 0 & (s \leq s^\star), \\ \pm\sqrt{1+\left\{\dfrac{g(1-s)}{2s}\right\}^2} & (s^\star < s). \end{cases} \tag{5.27}$$

There is no phase transition in the present of the field.

Next, the result 2 is obtained as follows. The pseudo free energy is

$$f = sm^2 - \sqrt{s^2(2m+h)^2 + g_{\rm p}g_{\rm m}(1-s)^2}. \tag{5.28}$$

This pseudo free energy is the same as that of the spin-1/2 system whose Hamiltonian is

$$\hat{H} = s\left\{-\frac{1}{N}\left(\sum_{ij}\hat{\sigma}_i^z\hat{\sigma}_j^z\right)^2 - h\sum_i \hat{\sigma}_i^z\right\} - \sqrt{g_{\rm p}g_{\rm m}}(1-s)\sum_i \hat{\sigma}_i^x. \tag{5.29}$$

Hence, we can find that, if $h = 0$, the transition point is $s^\star = 1/(1 + 2/\sqrt{g_\mathrm{p} g_\mathrm{m}})$, and the magnetization is

$$m = \begin{cases} 0 & (s \leq s^\star), \\ \pm\sqrt{1 + \left\{\dfrac{\sqrt{g_\mathrm{p} g_\mathrm{m}}(1-s)}{2s}\right\}^2} & (s^\star < s). \end{cases} \tag{5.30}$$

Let us show the third result. We solve the self-consistent equation (5.23) numerically, then obtain the stable solution by comparing the values of free energies for the solutions. Figure 5.3 shows the stable magnetization for the cases of $(g_\mathrm{p}, g_\mathrm{m}) = (2, 1)$, $(3, 1)$, and $(4, 1)$. We can find that the magnetization jumps for nonzero longitudinal field. We also find the model tends to undergo the first-order phase transition as the difference between the order of degeneracy become large. Figure 5.4 shows the phase diagram of the model.

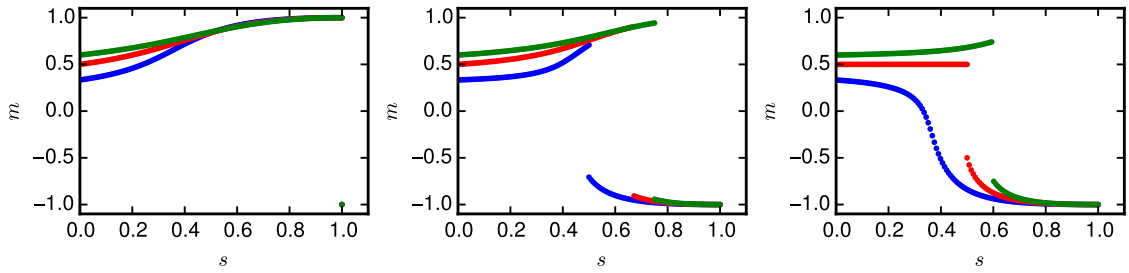

Figure 5.3.: The magnetization m as a function of s for $\omega = 1$. The values of longitudinal field are $h = 0$ (left), $h = -0.5$ (middle), and $h = -1$ (right). The blue dots represent the magnetization for $(g_\mathrm{p}, g_\mathrm{m}) = (2, 1)$, the red dots for $(3, 1)$, and the green for $(4, 1)$.

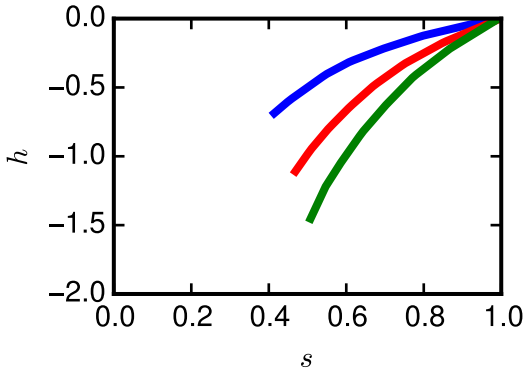

Figure 5.4.: The phase diagram for $\omega = 1$ on s-h plane. The blue solid line represents the first-order phase boundary for $(g_\mathrm{p}, g_\mathrm{m}) = (2, 1)$, the red solid line for $(3, 1)$, and the green for $(4, 1)$.

Finally, the result 4 is obtained in the same manner as the previous analysis. Fig. 5.5 shows the magnetization for $(g_\mathrm{p}, g_\mathrm{m}) = (2, 1)$ for $\omega = 0.16$, 0.47, and 1.0. It turns out that the first-order phase transition tends to occur as ω increases. The phase diagram on s-h plane is shown in Fig 5.6.

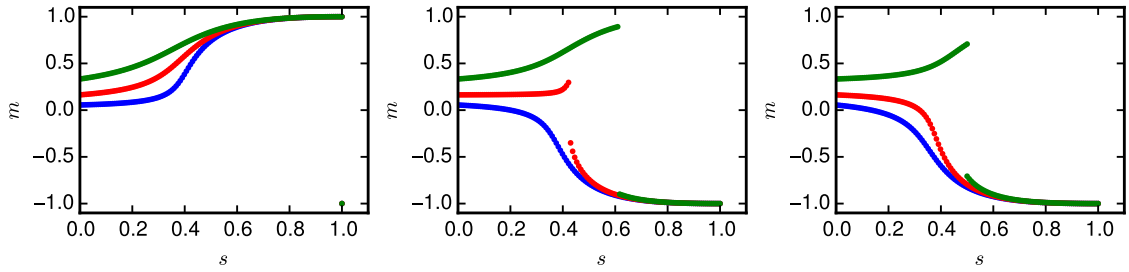

Figure 5.5.: The magnetization m as a function of s for $(g_{\mathrm{p}}, g_{\mathrm{m}}) = (2, 1)$. The values of longitudinal field are $h = 0$ (left), $h \simeq -0.3$ (middle), and $h \simeq -0.5$ (right). The blue dots represent the magnetization for $\omega = 0.16$, the red dots for 0.47, and the green for 1.

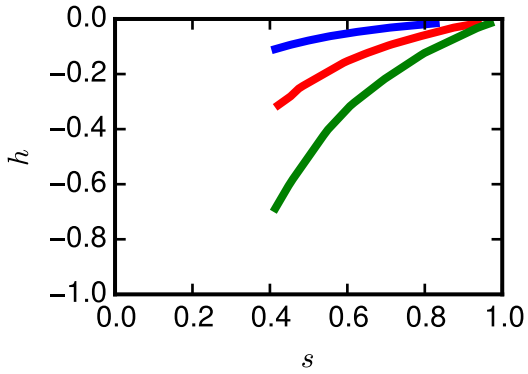

Figure 5.6.: The phase diagram for $(g_{\mathrm{p}}, g_{\mathrm{m}}) = (2, 1)$ on s-h plane. The blue solid line represents the first-order phase boundary for $\omega \simeq 0.16$, the red solid line for 0.47, and the green for 1.

5.4. Summary and discussion

In this chapter, we have studied the statistical-mechanical property of the quantum Wajnflasz-Pick model. First, the effect of macroscopic degeneracy of the ground states of the antiferromagnetic term has been discussed. In contrast to the results in the previous chapters, the antiferromagnetic term would rather cause the first-order phase transition. Thus, we conclude that macroscopic degeneracy is not a sufficient condition to avoid first-order phase transitions.

Next, we have checked whether the first-order quantum phase transition is avoidable by adjusting the order of degeneracy of the upper state and the lower state. As a result, we have found that the model does not undergo the first-order quantum phase transition if the orders of degeneracy are the same, $g_{\mathrm{p}} = g_{\mathrm{m}}$, or there is no transition between degenerate states, $\omega = 0$. Furthermore, in those cases, the model turns out to be equivalent to the usual spin-1/2 system. In contrast, if the transitions exist, $\omega \neq 0$, in the model with imbalanced degeneracies $g_{\mathrm{p}} \neq g_{\mathrm{m}}$, the model undergoes the first-order quantum phase transition. The results indicate that we have to pay attention to the transition and the order of degeneracy when QA is executed by using qudits.

Chapter 6.

Conclusion

We have investigated the phase diagram of the mean-field models in order to explore the way to avoid the problematic first-order quantum phase transition. We have analyzed three mean-field models, namely the ferromagnetic p-spin model, the Hopfield model, and the Wajnflasz-Pick model.

Chapter 3 has investigated the ferromagnetic p-spin model. The main proposition of the chapter is that the antiferromagnetic transverse interactions improves the efficiency of QA significantly. The Suzuki-Trotter decomposition has been used to calculate the partition function of the model. In addition, we have used the static ansatz to reduce the system to a single spin system, and the saddle-point method to derive the self-consistent equations. The self-consistent equations have been solved numerically to obtain the phase diagram. The resulting phase diagram has shown that the first-order quantum phase transition for intermediate values of p can be avoidable thanks to the antiferromagnetic term. Since the model conserves the total angular momentum during the Schrödinger dynamics, the Hilbert space that is needed to calculate the energy gap reduces to the subspace whose dimension is $(N+1) \times (N+1)$. We can thus diagonalize the Hamiltonian for relatively large size systems, then calculate the minimum energy gap. As a result, the diagonalization has revealed that the energy gap decreases polynomially in the vicinity of the second-order quantum phase transition point. Hence, we have concluded that we can achieve exponential speed-up by using the antiferromagnetic term. Another result to notice is that the magnetization of the system jumps within the ferromagnetic phase. Although the order parameter that characterizes the jump of the magnetization is unclear, the energy gap at the point of the jump decays exponentially. Accordingly, the jump of the magnetization also negatively affects the efficiency of QA. We have also analyze the model in the infinite p limit. In this limit, the model is equivalent to the Grover problem, which is a hard problem for both classical algorithms and quantum algorithms. The phase diagram in this limit shows that the first-order phase transition is inevitable, which is consistent with the fact that QA must require exponentially long time to solve the Grover problem.

Chapter 4 has analyzed the phase diagram of the Hopfield model. Through the analysis of the model, we have revealed the effect of the antiferromagnetic term for random spin systems. The analysis is almost the same as that of the ferromagnetic p-spin model except that we have used the replica method to take the configurational average. The model displays different behavior according to the number of patterns embedded. When the number of patterns are finite, the phase diagram is equivalent to the ferromagnetic p-spin model. This result indicates that the antiferromagnetic term is effective not only for the ferromagnetic model but also for the random spin system. However, if the number of patterns is proportional to N, QA with the antiferromagnetic term requires exponentially long time to follow the instantaneous ground state owing to the existence of the spin-

glass phase. The spin-glass phase is considered to be a feature of difficulty of QA. We have confirmed that even if many patterns are embedded, the first-order quantum phase transition can be avoided unless the spin-glass phase appears.

In Chap. 5, we have studied the statistical-mechanical property of the Wajnflasz-Pick model. First, the effect of the macroscopic degeneracy of the antiferromagnetic term has been investigated. The result has shown that the efficiency of QA gets worse owing to the antiferromagnetic term in the model. Hence, we have concluded that the macroscopic degeneracy is not a sufficient condition for the exponential speed-up of QA. Next, we have studied phase diagram of the model by adjusting the order of degeneracy of the upper state and the lower state and the transitions between the degenerate states. The results have shown that the second-order quantum phase transition can turn to the first-order transition depending on the order of degeneracy and the transitions between the degenerate states. The lessons we have learnt from the analysis is that we must be careful about the order of degeneracy and the transitions between the degenerate states when such a system (5.8) is used as a physics bit in QA.

We have shed light on the way to improve the efficiency of QA by taking advantage of the degree of freedom in the type of quantum fluctuations through the statistical-mechanical analysis of the mean-field models. However, we just have revealed the effect of the antiferromagnetic term for some models. We need a guiding principle to derive a driver Hamiltonian that improves the efficiency of QA for a given problem. In addition, it is insufficient to avoid first-order quantum phase transitions to improve the efficiency of QA. It has been reported that another difficulty related to the Anderson localization phenomena appears in the spin-glass phase [46]. Further studies are needed to bring out the potential of QA. It is my hope that the present study can contribute to the development of QA.

Appendix A.

Analysis with the Holstein-Primakoff transformation

We introduce an approach to calculate the energy gap alternative to the one in Sec. 3.3.2. The size of the Hamiltonian which we can analyze numerically is restricted by computer resources. The approach introduced below, however, enables us to analyze the energy gap in the thermodynamic limit by consideration of quantum fluctuations around a classical ground state of the total Hamiltonian (3.5). Through the analysis, it has been found that the wiggly behavior of the energy gap shown in Sec. 3.3.2 is a finite size effect.

This section is devoted to the explanation of the approach discussed in Ref. [41]. In Sec. A.1, we first discuss a classical ground state of the Hamiltonian. In Sec. A.2, we introduce an approach to calculate the energy gap in the thermodynamic limit.

A.1. Classical ground state

First, we show that the total Hamiltonian (3.5) is represented with classical variables in the thermodynamic limit. As mentioned in Sec. 3.3.2, we can rewrite the total Hamiltonian by using the total spin operator as follows:

$$\hat{H}(s,\lambda) = -s\lambda N\left(\frac{\hat{S}^z}{S}\right)^2 + s(1-\lambda)N\left(\frac{\hat{S}^x}{S}\right)^2 - (1-s)N\frac{\hat{S}^x}{S}, \tag{A.1}$$

where $S = N/2$ denotes the angular momentum. We define magnetization operators as $\hat{m}^\alpha \equiv \hat{S}^\alpha/S$ with $\alpha = x$, y, and z. The magnetization operators satisfy the following commutation relation:

$$[\hat{m}^x, \hat{m}^y] = i\frac{2}{N}\hat{m}^z \tag{A.2}$$

and its cyclic permutations. Considering that the expectation value of the magnetization operators lies in the interval $[-1, 1]$, we find that the operators commute with each other in the thermodynamic limit. Hence, the system is regarded as the classical system whose energy per spin is given as

$$e(s,\lambda; m^z, m^x) = -s\lambda(m^z)^p + s(1-\lambda)(m^x)^2 - (1-s)m^x, \tag{A.3}$$

where m^x and m^z denote the x and z components of the magnetization vector $\boldsymbol{m}$, respectively. Remember that, during the time evolution, the state always belongs to the subspace which has the maximum angular momentum $S = N/2$. This means that $\boldsymbol{m}$ is a unit vector. For further calculations, we express the magnetization vector as $\boldsymbol{m} = (\cos\theta, \sin\theta\sin\varphi, \sin\theta\cos\varphi)$, where θ denotes the polar angle measured from the x

direction, and φ the azimuthal angle from the z direction. Substituting the magnetization vector $\boldsymbol{m}$ described with the angles θ, φ into Eq. (A.3), we have

$$e(s,\lambda;\theta,\varphi) = -s\lambda(\sin\theta\cos\varphi)^p + s(1-\lambda)\cos^2\theta - (1-s)\cos\theta. \tag{A.4}$$

The direction of the magnetization vector $\boldsymbol{m}$ of the ground state is determined by the minimum condition for the energy function (A.4). Since p is odd, the minimum lies on the plane with $\varphi = 0$. The energy on the plane is

$$e(s,\lambda;\theta) = -s\lambda\sin^p\theta + s(1-\lambda)\cos^2\theta - (1-s)\cos\theta. \tag{A.5}$$

The direction of magnetization vector depends only on the angle θ. The angle θ has to satisfy

$$\frac{de(s,\lambda;\theta)}{d\theta} = ps\lambda\sin^{p-1}\theta\cos\theta - 2s(1-\lambda)\sin\theta\cos\theta + (1-s)\sin\theta = 0. \tag{A.6}$$

Equation (A.6) has more than one solutions. Comparing energies for all possible solutions, we get the ground state energy. In the following, we discuss the possible types of solutions. First, Eq. (A.6) has trivial solutions, $\theta = 0$ and $\theta = \pi$. However, the solution $\theta = \pi$ gives the local maximum. We thus consider only the other solution. The energy for the solution $\theta = 0$ is

$$e(s,\lambda) = -s\lambda + 2s - 1. \tag{A.7}$$

In addition, the magnetization vector for the solution is $\boldsymbol{m} = (1,0,0)$. Hence, the solution $\theta = 0$ corresponds to the QP solution. Other solutions corresponding to the F solutions, $\theta > 0$, satisfy

$$ps\lambda\sin^{p-2}\theta\cos\theta + 2s(1-\lambda)\cos\theta - 1 + s = 0. \tag{A.8}$$

Solving Eq. (A.8) numerically, we obtain the F solutions.

A.2. Energy gap

If we regard the system (A.1) as a completely classical system, the energy gap between the ground state and the first excited state vanishes. The classical magnetization vector can changes continuously. Hence, the energy of the system (A.4) takes continuous values.

However, small quantum fluctuations are crucial for the energy gap of the system (A.1). Low-order terms are relevant for the energy gap as shown below.

We first express the Hamiltonian (A.1) by a boson annihilation operator. It is convenient to rotate the system so that the magnetization vector of the classical ground state is in the z direction. Thus, we define the total spin operator of the rotated system, $\hat{S}^{\alpha'}$ with $\alpha' = x'$, y', and z', as

$$\begin{pmatrix} \hat{S}^x \\ \hat{S}^y \\ \hat{S}^z \end{pmatrix} = \begin{pmatrix} -\sin\theta_0 & 0 & \cos\theta_0 \\ 0 & 1 & 0 \\ \cos\theta_0 & 0 & \sin\theta_0 \end{pmatrix} \begin{pmatrix} \hat{S}^{x\prime} \\ \hat{S}^{y\prime} \\ \hat{S}^{z\prime} \end{pmatrix}, \tag{A.9}$$

where θ_0 denotes the polar angle of the classical ground state. The magnetization vector slightly fluctuates around the z' direction. To express the small fluctuations, we use the Holstein-Primakoff transformation:

$$\hat{S}^{z\prime} = \frac{N}{2} - \hat{a}^\dagger \hat{a}, \qquad \hat{S}'_+ = (N - \hat{a}^\dagger \hat{a})^{1/2} \hat{a} = (\hat{S}'_-)^\dagger, \tag{A.10}$$

where $\hat{a}$ denotes a boson annihilation operator which satisfies $[\hat{a}, \hat{a}^\dagger] = 1$. Note that we now consider sufficiently large systems. Thus, quantum fluctuations are small relative to the classical state, $N \gg \langle \hat{a}^\dagger \hat{a} \rangle$. Thus we have

$$\hat{S}^{x\prime} \approx \frac{\sqrt{N}}{2}(\hat{a} + \hat{a}^\dagger). \tag{A.11}$$

Using the transformations, we rewrite the Hamiltonian (A.1) as

$$\begin{aligned} \hat{H}(s,\lambda) = &-s\lambda N\Big[\sin\theta_0 - \frac{1}{\sqrt{N}}\cos\theta_0(\hat{a}+\hat{a}^\dagger) + \frac{2}{N}\sin\theta_0 \hat{a}^\dagger\hat{a}\Big]^p \\ &+ s(1-\lambda)N\Big[\cos\theta_0 - \frac{1}{\sqrt{N}}\sin\theta_0(\hat{a}+\hat{a}^\dagger) - \frac{2}{N}\cos\theta_0\hat{a}^\dagger\hat{a}\Big]^2 \\ &- (1-s)\Big[\cos\theta_0 - \frac{1}{\sqrt{N}}\sin\theta_0(\hat{a}+\hat{a}^\dagger) - \frac{2}{N}\cos\theta_0\hat{a}^\dagger\hat{a}\Big]. \end{aligned} \tag{A.12}$$

We next expand the Hamiltonian (A.12), and leave terms whose order is greater than N^0. Using the fact that the angle θ_0 satisfies Eq. (A.6), we find that the term of the order of $\sqrt{N}$ vanishes. Eventually, we obtain

$$\hat{H}(s,\lambda) = Ne(s,\lambda;\theta_0) + \gamma(s,\lambda;\theta_0) + \gamma(s,\lambda;\theta_0)[(\hat{a}^\dagger)^2 + (\hat{a})^2] + \delta(s,\lambda;\theta_0)\hat{a}^\dagger\hat{a}, \tag{A.13}$$

where $e(s,\lambda;\theta_0)$ is the energy of the classical ground state (A.5). The functions δ and γ are defined as

$$\begin{aligned} \delta \equiv &-s\lambda[p(p-1)\sin^{p-2}\theta_0\cos^2\theta_0 - 2p\sin^p\theta_0] \\ &+ s(1-\lambda)[2\sin^2\theta_0 - 4\cos^2\theta_0] + 2(1-s)\cos\theta_0, \end{aligned} \tag{A.14}$$

and

$$\gamma \equiv -\frac{s\lambda p(p-1)}{2}\sin^{p-2}\theta_0\cos^2\theta_0 + s(1-\lambda)\sin^2\theta_0. \tag{A.15}$$

We can calculate the energy gap by using the Bogoliubov transformation:

$$\hat{a} = \cosh\frac{\Theta}{2}\,\hat{b} + \sinh\frac{\Theta}{2}\,\hat{b}^\dagger, \qquad \hat{a}^\dagger = \cosh\frac{\Theta}{2}\,\hat{b}^\dagger + \sinh\frac{\Theta}{2}\,\hat{b}, \tag{A.16}$$

where $\hat{b}$ is another annihilation operator which satisfies $[\hat{b}, \hat{b}^\dagger] = 1$. Choosing the angle Θ as

$$\tanh\Theta = -\frac{2\gamma}{\delta} \equiv \epsilon, \tag{A.17}$$

we have

$$\hat{H} = Ne + \gamma + \frac{\delta}{2}\big(\sqrt{1-\epsilon^2} - 1\big) + \Delta\hat{b}^\dagger\hat{b} \tag{A.18}$$

with

$$\Delta = \delta\sqrt{1-\epsilon^2}. \tag{A.19}$$

Therefore the energy gap in the thermodynamic limit is given by Δ.

Appendix B.

Self-consistent equations for the Hopfield model with many-body interactions and finite patterns embedded

We derive the self-consistent equations (4.5) and (4.6) by mean-field analyses. The Suzuki-Trotter formula and the static ansatz enable us to obtain the partition function. Then, using a saddle-point condition, we obtain the self-consistent equations.

Let us calculate the partition function. We first translate the quantum system into a classical system using the Suzuki-Trotter formula [31]. The Hamiltonian is given as

$$\begin{aligned}\hat{H}(s,\lambda) &= s\{\lambda\hat{H}_0 + (1-\lambda)\hat{V}_{\rm AFF}\} + (1-s)\hat{V}_{\rm TF} \\ &= -s\lambda N\sum_{\mu=1}^{p}\Big(\frac{1}{N}\sum_{i=1}^{N}\xi_i^\mu\hat{\sigma}_i^z\Big)^k + s(1-\lambda)N\Big(\frac{1}{N}\sum_{i=1}^{N}\hat{\sigma}_i^x\Big)^2 - (1-s)\sum_{i=1}^{N}\hat{\sigma}_i^x, \quad \text{(B.1)}\end{aligned}$$

where k denotes an integer for the degree of interactions, and ξ's the random variables. The variable p is an integer independent of N. Using the Trotter decomposition, and introducing M closure relations, we have the following expression of the partition function for a finite Trotter number M,

$$\begin{aligned}Z_M = {\rm Tr}\prod_{\alpha=1}^{M}\exp\Big\{&\frac{\beta s\lambda N}{M}\sum_{\mu=1}^{p}\Big(\frac{1}{N}\sum_{i=1}^{N}\xi_i^\mu\sigma_i^z(\alpha)\Big)^k - \frac{\beta s(1-\lambda)N}{M}\Big(\frac{1}{N}\sum_{i=1}^{N}\sigma_i^x(\alpha)\Big)^2 \\ &+ \frac{\beta(1-s)}{M}\sum_{i=1}^{N}\sigma_i^x(\alpha)\Big\}\prod_{i=1}^{N}\prod_{\alpha=1}^{M}\langle\sigma_i^z(\alpha)|\sigma_i^x(\alpha)\rangle\langle\sigma_i^x(\alpha)|\sigma_i^z(\alpha+1)\rangle. \quad \text{(B.2)}\end{aligned}$$

Here, Tr denotes the summation over all possible spin configurations of $\{\sigma_i^z\}$ and $\{\sigma_i^x\}$ satisfying periodic boundary conditions, $\sigma_i^z(1) = \sigma_i^z(M+1)$ for all i. We next linearize the spin-product terms by using delta functions,

$$\delta\Big(Nm_\mu(\alpha) - \sum_i \xi_i^\mu\sigma_i^z\Big) = \int d\tilde{m}_\mu(\alpha)\,\exp\Big\{-\tilde{m}_\mu(\alpha)\frac{\beta}{M}\Big(Nm_\mu(\alpha) - \sum_i\xi_i^\mu\sigma_i^z(\alpha)\Big)\Big\}, \quad \text{(B.3)}$$

and

$$\delta\Big(Nm^x(\alpha) - \sum_i \sigma_i^x\Big) = \int d\tilde{m}^x(\alpha)\,\exp\Big\{-\tilde{m}^x(\alpha)\frac{\beta}{M}\Big(Nm^x(\alpha) - \sum_i\sigma_i^x(\alpha)\Big)\Big\}. \quad \text{(B.4)}$$

Then, Eq. (B.2) reads

$$
\begin{aligned}
Z_M = \int \prod_{\alpha,\mu} & dm_\mu(\alpha)\, d\tilde{m}_\mu(\alpha)\, dm^x(\alpha)\, d\tilde{m}^x(\alpha) \\
& \times \exp\Bigg\{ N \frac{\beta}{M} \sum_\alpha \Bigg(s\lambda \sum_\mu \big(m_\mu(\alpha)\big)^k - \sum_\mu \tilde{m}_\mu(\alpha) m_\mu(\alpha) \\
& \qquad - s(1-\lambda)\big(m^x(\alpha)\big)^2 + (1-s)m^x(\alpha) - \tilde{m}^x(\alpha) m^x(\alpha) \Bigg) \Bigg\} \\
& \times \exp\Bigg\{ \sum_i \ln\Bigg(\mathrm{Tr} \exp \frac{\beta}{M} \Big\{ \sum_{\alpha,\mu} \tilde{m}_\mu(\alpha) \xi_i^\mu \sigma_i^z(\alpha) + \sum_\alpha \tilde{m}^x(\alpha) \sigma_i^x(\alpha) \Big\} \\
& \qquad \times \prod_\alpha \langle \sigma_i^z(\alpha) | \sigma_i^x(\alpha) \rangle \langle \sigma_i^x(\alpha) | \sigma_i^z(\alpha+1) \rangle \Bigg) \Bigg\}. \qquad \text{(B.5)}
\end{aligned}
$$

In the thermodynamic limit $N \to \infty$, according to the law of large numbers, the summation over the site index i becomes the average over the randomness of the embedded patterns. We refer to this average as the configurational average. Furthermore, the integrals are evaluated by the saddle-point method. The saddle-point conditions for $m_\mu(\alpha)$ and $m^x(\alpha)$ lead to

$$
\tilde{m}_\mu(\alpha) = s\lambda k \big(m_\mu(\alpha)\big)^{k-1} \qquad \text{(B.6)}
$$

and

$$
\tilde{m}^x(\alpha) = 1 - s - 2s(1-\lambda) m^x(\alpha), \qquad \text{(B.7)}
$$

respectively. Using the static ansatz, i.e., neglecting the α-dependence of the order parameters, we can take the trace in Eq. (B.5) with the inverse operation of the Trotter decomposition. We thus obtain the following partition function:

$$
\begin{aligned}
Z = \int \cdots \int \prod_\mu dm_\mu\, dm^x \exp\Big\{ -N\beta \Big(& (k-1) s\lambda \sum_\mu (m_\mu)^k - s(1-\lambda)(m^x)^2 \\
& - \frac{1}{\beta} \Big[\ln 2\cosh \beta \sqrt{\{ks\lambda \textstyle\sum_\mu (m_\mu)^{k-1} \xi^\mu\}^2 + \{1 - s - 2s(1-\lambda) m^x\}^2} \Big] \Big) \Big\}, \qquad \text{(B.8)}
\end{aligned}
$$

where the brackets $[\ldots]$ denote the configurational average. Therefore the pseudo free energy is

$$
\begin{aligned}
& f(\beta, s, \lambda; \{m_\mu\}, m^x) \\
& = (k-1) s\lambda \sum_\mu (m_\mu)^k - s(1-\lambda)(m^x)^2 \\
& \quad - \frac{1}{\beta} \Big[\ln 2\cosh \beta \sqrt{\{ks\lambda \textstyle\sum_\mu (m_\mu)^{k-1} \xi^\mu\}^2 + \{1 - s - 2s(1-\lambda) m^x\}^2} \Big], \qquad \text{(B.9)}
\end{aligned}
$$

and the self-consistent equations are

$$
\begin{aligned}
(m_\mu)^{k-1} = \Bigg[& \frac{ks\lambda \big(\sum_\mu (m_\mu)^{k-1} \xi^\mu\big) (m_\mu)^{k-2} \xi^\mu}{\sqrt{\{ks\lambda \sum_\mu (m_\mu)^{k-1} \xi^\mu\}^2 + \{1 - s - 2s(1-\lambda) m^x\}^2}} \\
& \times \tanh \beta \sqrt{\{ks\lambda \textstyle\sum_\mu (m_\mu)^{k-1} \xi^\mu\}^2 + \{1 - s - 2s(1-\lambda) m^x\}^2} \Bigg], \qquad \text{(B.10)}
\end{aligned}
$$

and

$$m^x = \left[\frac{1-s-2s(1-\lambda)m^x}{\sqrt{\{ks\lambda \sum_\mu (m_\mu)^{k-1}\xi^\mu\}^2 + \{1-s-2s(1-\lambda)m^x\}^2}} \right.$$
$$\left. \times \tanh \beta \sqrt{\{ks\lambda \sum\nolimits_\mu (m_\mu)^{k-1}\xi^\mu\}^2 + \{1-s-2s(1-\lambda)m^x\}^2} \right]. \tag{B.11}$$

In the low-temperature limit $\beta \to \infty$, the pseudo free energy and the self-consistent equations become

$$f(s,\lambda;\{m_\mu\},m^x) = (k-1)s\lambda \sum_\mu (m_\mu)^k - s(1-\lambda)(m^x)^2$$
$$- \left[\sqrt{\{ks\lambda \sum\nolimits_\mu (m_\mu)^{k-1}\xi^\mu\}^2 + \{1-s-2s(1-\lambda)m^x\}^2} \right] \tag{B.12}$$

and

$$(m_\mu)^{k-1} = \left[\frac{ks\lambda \big(\sum_\mu (m_\mu)^{k-1}\xi^\mu\big)(m_\mu)^{k-2}\xi^\mu}{\sqrt{\{ks\lambda \sum_\mu (m_\mu)^{k-1}\xi^\mu\}^2 + \{1-s-2s(1-\lambda)m^x\}^2}} \right], \tag{B.13}$$

$$m^x = \left[\frac{1-s-2s(1-\lambda)m^x}{\sqrt{\{ks\lambda \sum_\mu (m_\mu)^{k-1}\xi^\mu\}^2 + \{1-s-2s(1-\lambda)m^x\}^2}} \right]. \tag{B.14}$$

Appendix C.

Self-consistent equations for the Hopfield model with many patterns

We derive the self-consistent equations for the Hopfield model with an extensive number of patterns embedded (4.13)–(4.17). We closely follow Chap. 10 of Ref. [40] in the calculation. The calculation uses the replica trick for configurational average.

Let us calculate the partition function. In a similar way to the derivation of Eq. (B.5), the replicated partition function for a Trotter number M is written as

$$\begin{aligned}
[Z_M^n] = \int \prod_{\alpha,\mu,\rho} & dm_{\mu\rho}(\alpha)\, dm_\rho^x(\alpha)\, d\tilde{m}_\rho^x(\alpha) \\
& \times \mathrm{Tr} \exp -\frac{\beta}{M} \sum_{\alpha,\rho} \tilde{m}_\rho^x(\alpha) \Big\{ N m_\rho^x(\alpha) - \sum_i \sigma_{i\rho}^x(\alpha) \Big\} \\
& \times \exp -\frac{\beta s \lambda N}{2M} \sum_{\alpha,\mu,\rho} \big(m_{\mu\rho}(\alpha)\big)^2 \times \Big[\exp \frac{\beta s \lambda}{M} \sum_{\alpha,\mu,\rho,i} m_{\mu\rho}(\alpha) \xi_i^\mu \sigma_{i\rho}^z(\alpha) \Big] \\
& \times \exp \frac{\beta N}{M} \sum_{\alpha,\rho} \Big\{ -s(1-\lambda) \big(m_\rho^x(\alpha)\big)^2 + (1-s) m_\rho^x(\alpha) \Big\} \\
& \times \prod_{\alpha,\rho,i} \langle \sigma_{i\rho}^z(\alpha) | \sigma_{i\rho}^x(\alpha) \rangle \langle \sigma_{i\rho}^x(\alpha) | \sigma_{i\rho}^z(\alpha+1) \rangle, \qquad \text{(C.1)}
\end{aligned}$$

where α $(= 1, \ldots, M)$ represents the Trotter index, and ρ $(= 1, \ldots, n)$ the replica index. We have used a Gaussian integral, instead of the delta function, to linearize the spin-product term regarding $\sigma_{i\rho}^z(\alpha)$.

We consider the case where only a single pattern has a non-vanishing overlap with the state of the system: $m_{1\rho}(\alpha) \equiv m_\rho(\alpha) = \mathrm{O}(N^0)$. The overlap with the other patterns results from coincidental contributions, hence $m_{\mu\rho}(\alpha) = \mathrm{O}(1/\sqrt{N})$ for $\mu \geq 2$. Expanding the configurational average for $\mu \geq 2$ in $1/\sqrt{N}$, we have

$$\Big[\exp \frac{\beta s \lambda}{M} \sum_{\alpha,\rho,i} m_{\mu\rho}(\alpha) \xi_i^\mu \sigma_{i\rho}^z(\alpha) \Big] \simeq \exp \frac{\beta^2 s^2 \lambda^2}{2M^2} \sum_i \sum_{\alpha\rho,\alpha'\rho'} m_{\mu\rho}(\alpha) m_{\mu\rho'}(\alpha) \sigma_{i\rho}^z(\alpha) \sigma_{i\rho'}^z(\alpha'). \qquad \text{(C.2)}$$

Consequently, the term involving $m_{\mu\rho}(\alpha)$ for $\mu \geq 2$ in Eq. (C.1) is expressed as a quadratic form:

$$\prod_{\mu \geq 2} \exp -\frac{N \beta s \lambda}{2M} \sum_{\alpha\rho,\alpha'\rho'} \tilde{\Lambda}_{\alpha\rho,\alpha'\rho'} m_{\mu\rho}(\alpha) m_{\mu\rho'}(\alpha'), \qquad \text{(C.3)}$$

with a matrix $\tilde{\Lambda} = (\tilde{\Lambda}_{\alpha\rho,\alpha'\rho'})$,

$$\tilde{\Lambda}_{\alpha\rho,\alpha'\rho'} \equiv \delta_{\alpha\rho,\alpha'\rho'} - \frac{\beta s\lambda}{MN}\sum_i \sigma^z_{i\rho}(\alpha)\sigma^z_{i\rho'}(\alpha'). \tag{C.4}$$

The integral with regard to $m_{\mu\rho}(\alpha)$ for $\mu \geq 2$ yields

$$(\det\tilde{\Lambda})^{-(p-1)/2} \simeq (\det\tilde{\Lambda})^{-\alpha N/2} = \exp -\frac{\alpha N}{2}\ln\det\tilde{\Lambda} = \exp -\frac{\alpha N}{2}\sum_{\lambda\in\sigma(\tilde{\Lambda})}\ln\lambda, \tag{C.5}$$

where we have defined the set of eigenvalues of $\tilde{\Lambda}$ as $\sigma(\tilde{\Lambda})$. To linearize the spin-product term in $\tilde{\Lambda}$, we replace the matrix by

$$\Lambda_{\alpha\rho,\alpha'\rho'} \equiv \delta_{\alpha\rho,\alpha'\rho'} - \frac{\beta s\lambda}{M}q_{\rho\rho'}(\alpha,\alpha') - \delta_{\rho\rho'}\frac{\beta s\lambda}{M}R_\rho(\alpha,\alpha') \tag{C.6}$$

with the constraint

$$q_{\rho\rho'}(\alpha,\alpha') = \begin{cases} \dfrac{1}{N}\displaystyle\sum_i \sigma^z_{i\rho}(\alpha)\sigma^z_{i\rho'}(\alpha') & (\rho\neq\rho') \\ 0 & (\rho=\rho) \end{cases}, \tag{C.7}$$

$$R_\rho(\alpha,\alpha') = \frac{1}{N}\sum_i \sigma^z_{i\rho}(\alpha)\sigma^z_{i\rho}(\alpha'), \tag{C.8}$$

introduced by delta functions:

$$\begin{aligned}
&\delta\Big(Nq_{\rho\rho'}(\alpha,\alpha') - \sum_i \sigma^z_{i\rho}(\alpha)\sigma^z_{i\rho'}(\alpha')\Big) \\
&= \int d\tilde{q}_{\rho\rho'}(\alpha,\alpha')\exp\Big\{-\frac{\alpha\beta^2}{2M^2}\tilde{q}_{\rho\rho'}(\alpha,\alpha')\Big(Nq_{\rho\rho'}(\alpha,\alpha') - \sum_i \sigma^z_{i\rho}(\alpha)\sigma^z_{i\rho'}(\alpha')\Big)\Big\}, \qquad \text{(C.9)} \\
&\delta\Big(NR_\rho(\alpha,\alpha') - \sum_i \sigma^z_{i\rho}(\alpha)\sigma^z_{i\rho}(\alpha')\Big) \\
&= \int d\tilde{R}_\rho(\alpha,\alpha')\exp\Big\{-\frac{\alpha\beta^2}{2M^2}\tilde{R}_\rho(\alpha,\alpha')\Big(NR_\rho(\alpha,\alpha') - \sum_i \sigma^z_{i\rho}(\alpha)\sigma^z_{i\rho}(\alpha')\Big)\Big\}. \qquad \text{(C.10)}
\end{aligned}$$

Thus, we can rewrite Eq. (C.1) as

$$
\begin{aligned}
&[Z_M^n] \\
&= \int \prod_{\alpha\rho} dm_\rho(\alpha)\, dm_\rho^x(\alpha)\, d\tilde{m}_\rho^x(\alpha) \prod_{(\alpha\rho,\alpha'\rho')} dq_{\rho\rho'}(\alpha,\alpha')\, d\tilde{q}_{\rho\rho'}(\alpha,\alpha') \prod_{\alpha\alpha'\rho} dR_\rho(\alpha,\alpha')\, d\tilde{R}_\rho(\alpha,\alpha') \\
&\quad \times \exp\Bigg\{ -\frac{N\beta s\lambda}{2M} \sum_{\alpha\rho} \big(m_\rho(\alpha)\big)^2 - \frac{\alpha N}{2} \sum_{\lambda\in\sigma(\Lambda)} \ln\lambda \\
&\quad - \frac{N\beta s(1-\lambda)}{M} \sum_{\alpha\rho} \big(m_\rho^x(\alpha)\big)^2 + \frac{N\beta(1-s)}{M} \sum_{\alpha\rho} m_\rho^x(\alpha) - \frac{N\beta}{M} \sum_{\alpha\rho} \tilde{m}_\rho^x(\alpha) m_\rho^x(\alpha) \\
&\quad - \frac{N\alpha\beta^2}{2M^2} \sum_{(\alpha\rho,\alpha'\rho')} \tilde{q}_{\rho\rho'}(\alpha,\alpha') q_{\rho\rho'}(\alpha,\alpha') - \frac{N\alpha\beta^2}{2M^2} \sum_{\alpha\alpha'\rho} \tilde{R}_\rho(\alpha,\alpha') R_\rho(\alpha,\alpha') \Bigg\} \\
&\quad \times \Bigg[\mathrm{Tr} \exp\Bigg\{ \frac{\beta s\lambda}{M} \sum_{\alpha\rho} \sum_i m_\rho(\alpha)\xi_i \sigma_{i\rho}^z(\alpha) + \frac{\beta}{M} \sum_{\alpha\rho} \sum_i \tilde{m}_\rho^x(\alpha) \sigma_{i\rho}^x(\alpha) \\
&\quad + \frac{\alpha\beta^2}{2M^2} \sum_{(\alpha\rho,\alpha'\rho')} \sum_i \tilde{q}_{\rho\rho'}(\alpha,\alpha') \sigma_{i\rho}^z(\alpha) \sigma_{i\rho'}^z(\alpha') + \frac{\alpha\beta^2}{2M^2} \sum_{\alpha\alpha'\rho} \sum_i \tilde{R}_\rho(\alpha,\alpha') \sigma_{i\rho}^z(\alpha) \sigma_{i\rho}^z(\alpha') \Bigg\} \\
&\quad \times \prod_{\alpha\rho i} \langle \sigma_{i\rho}^z(\alpha) | \sigma_{i\rho}^x(\alpha) \rangle \langle \sigma_{i\rho}^x(\alpha) | \sigma_{i\rho}^z(\alpha+1) \rangle \Bigg]. \qquad \text{(C.11)}
\end{aligned}
$$

Here, ξ_i denotes ξ_i^1, and $(\alpha\rho, \alpha'\rho')$ all the possible combinations of α, α', ρ, and ρ' except for the case of $\rho = \rho'$.

We can take the trace in (C.11) independent of i. As a result, Eq. (C.11) reads $[Z_M^n] = \int \prod dm \ldots \exp(-N\beta\tilde{f})$, where

$$
\begin{aligned}
\tilde{f} &= \frac{s\lambda}{2M} \sum_{\alpha\rho} \big(m_\rho(\alpha)\big)^2 + \frac{\alpha}{2\beta} \sum_{\lambda\in\sigma(\Lambda)} \ln\lambda \\
&\quad + \frac{s(1-\lambda)}{M} \sum_{\alpha\rho} \big(m_\rho^x(\alpha)\big)^2 - \frac{1-s}{M} \sum_{\alpha\rho} m_\rho^x(\alpha) + \frac{1}{M} \sum_{\alpha\rho} \tilde{m}_\rho^x(\alpha) m_\rho^x(\alpha) \\
&\quad + \frac{\alpha\beta}{2M^2} \sum_{(\alpha\rho,\alpha'\rho')} \tilde{q}_{\rho\rho'}(\alpha,\alpha') q_{\rho\rho'}(\alpha,\alpha') + \frac{\alpha\beta}{2M^2} \sum_{\alpha\alpha'\rho} \tilde{R}_\rho(\alpha,\alpha') R_\rho(\alpha,\alpha') \\
&\quad - \frac{1}{\beta} \Bigg[\ln \mathrm{Tr} \exp\Big\{ \frac{\beta s\lambda}{M} \sum_{\alpha\rho} m_\rho(\alpha) \sigma_\rho^z(\alpha)\xi + \frac{\beta}{M} \sum_{\alpha\rho} \tilde{m}_\rho^x(\alpha) \sigma_\rho^x(\alpha) \\
&\quad + \frac{\alpha\beta^2}{2M^2} \sum_{(\alpha\rho,\alpha'\rho')} \tilde{q}_{\rho\rho'}(\alpha,\alpha') \sigma_\rho^z(\alpha) \sigma_{\rho'}^z(\alpha') + \frac{\alpha\beta^2}{2M^2} \sum_{\alpha\alpha'\rho} \tilde{R}_\rho(\alpha,\alpha') \sigma_\rho^z(\alpha) \sigma_\rho^z(\alpha') \Big\} \\
&\quad \times \prod_{\alpha\rho} \langle \sigma_\rho^z(\alpha) | \sigma_\rho^x(\alpha) \rangle \langle \sigma_\rho^x(\alpha) | \sigma_\rho^z(\alpha+1) \rangle \Bigg]. \qquad \text{(C.12)}
\end{aligned}
$$

The saddle-point conditions for $m_\rho(\alpha)$, $\tilde{m}_\rho^x(\alpha)$, $\tilde{q}_{\rho\rho'}(\alpha,\alpha')$, and $\tilde{R}_\rho(\alpha,\alpha')$ lead to the fol-

lowing self-consistent equations:

$$m_\rho(\alpha) = [\xi \langle \sigma_\rho^z(\alpha) \rangle], \tag{C.13}$$

$$m_\rho^x(\alpha) = [\langle \sigma_\rho^x(\alpha) \rangle], \tag{C.14}$$

$$q_{\rho\rho'}(\alpha, \alpha') = [\langle \sigma_\rho^z(\alpha) \sigma_{\rho'}^z(\alpha') \rangle], \tag{C.15}$$

$$R_\rho(\alpha, \alpha') = [\langle \sigma_\rho^z(\alpha) \sigma_\rho^z(\alpha') \rangle], \tag{C.16}$$

where the brackets $\langle \ldots \rangle$ mean the average with respect to the weight

$$\begin{aligned} &\exp\Big\{ \frac{\beta s \lambda}{M} \sum_{\alpha\rho} m_\rho(\alpha) \sigma_\rho^z(\alpha) \xi + \frac{\beta}{M} \sum_{\alpha\rho} \tilde{m}_\rho^x(\alpha) \sigma_\rho^x(\alpha) \\ &+ \frac{\alpha\beta^2}{2M^2} \sum_{(\alpha\rho, \alpha'\rho')} \tilde{q}_{\rho\rho'}(\alpha, \alpha') \sigma_\rho^z(\alpha) \sigma_{\rho'}^z(\alpha') + \frac{\alpha\beta^2}{2M^2} \sum_{\alpha\alpha'\rho} \tilde{R}_\rho(\alpha, \alpha') \sigma_\rho^z(\alpha) \sigma_\rho^z(\alpha') \Big\} \\ &\times \prod_{\alpha\rho} \langle \sigma_\rho^z(\alpha) | \sigma_\rho^x(\alpha) \rangle \langle \sigma_\rho^x(\alpha) | \sigma_\rho^z(\alpha + 1) \rangle. \end{aligned} \tag{C.17}$$

We look for the replica symmetric (RS) solution of Eqs. (C.13)–(C.16). Furthermore, we use the static ansatz, that is, we neglect the dependence of the order parameters on the Trotter number:

$$\begin{aligned} &m_\rho(\alpha) = m, \qquad m_\rho^x(\alpha) = m^x, \qquad \tilde{m}_\rho^x(\alpha) = \tilde{m}^x, \\ &q_{\rho\rho'}(\alpha, \alpha') = q, \quad R_\rho(\alpha, \alpha') = \begin{cases} R & (\alpha \neq \alpha') \\ 1 & (\alpha = \alpha) \end{cases}, \\ &\tilde{q}_{\rho\rho'}(\alpha, \alpha') = \tilde{q}, \quad \tilde{R}_\rho(\alpha, \alpha') = \tilde{R}. \end{aligned} \tag{C.18}$$

First, we evaluate the trace in Eq. (C.12). Linearizing the spin-product term by using a Gaussian integral, we can rewrite the term including trace as

$$\begin{aligned} &n \Big[\int Dz \, \ln \mathrm{Tr} \int Dw \prod_\alpha \exp\Big\{ \frac{\beta}{M} \Big(s\lambda\xi m + \sqrt{\alpha\tilde{q}} z + \sqrt{\alpha(\tilde{R} - \tilde{q})} w \Big) \sigma^z(\alpha) \Big\} \\ &\times \exp\Big\{ \frac{\beta}{M} \tilde{m}^x \sigma^x(\alpha) \Big\} \langle \sigma^z(\alpha) | \sigma^x(\alpha) \rangle \langle \sigma^x(\alpha) | \sigma^z(\alpha + 1) \rangle \Big] + \mathrm{O}(n^2), \end{aligned} \tag{C.19}$$

where Dz denotes the Gaussian measure $Dz \equiv dz \exp(-z^2/2)/\sqrt{2\pi}$, and Dw is defined similarly. Let us take the limit $M \to \infty$. Using the inverse operation of the Trotter decomposition, we have

$$n \Big[\int Dz \, \ln \int Dw \, 2 \cosh \beta \sqrt{\big(s\lambda m\xi + \sqrt{\alpha\tilde{q}} z + \sqrt{\alpha(\tilde{R} - \tilde{q})} w \big)^2 + \big(\tilde{m}^x \big)^2} \Big] + \mathrm{O}(n^2). \tag{C.20}$$

The values of the integral are the same for both cases $\xi = 1$ and $\xi = -1$, since the value is invariant under the variable transformation $z \to -z$ and $w \to -w$. Hence, Eq. (C.20) reads

$$n \int Dz \, \ln \int Dw \, 2 \cosh \beta \sqrt{\big(s\lambda m\xi + \sqrt{\alpha\tilde{q}} z + \sqrt{\alpha(\tilde{R} - \tilde{q})} w \big)^2 + \big(\tilde{m}^x \big)^2} + \mathrm{O}(n^2). \tag{C.21}$$

Next, we study the eigenvalues of Λ. The matrix has three types of elements:

$$\Lambda_{\alpha\rho,\alpha',\rho'} = \begin{cases} -\dfrac{\beta s\lambda}{M} q & \text{if } \rho \neq \rho' \\ -\dfrac{\beta s\lambda}{M} R & \text{if } \rho = \rho' \text{ and } \alpha \neq \alpha' \\ 1 - \dfrac{\beta s\lambda}{M} & \text{if } \rho = \rho' \text{ and } \alpha = \alpha' \end{cases}. \tag{C.22}$$

We can easily find that the matrix has the eigenvalues:

$$\lambda_1 = 1 - \beta s\lambda\Big(\frac{1}{M} + \frac{M-1}{M} R + (n-1)q\Big) \tag{C.23}$$

with degeneracy 1, and

$$\lambda_2 = 1 - \beta s\lambda\Big(\frac{1}{M} + \frac{M-1}{M} R - q\Big) \tag{C.24}$$

with degeneracy $n-1$, and

$$\lambda_3 = 1 - \frac{\beta s\lambda}{M}(1-R) \tag{C.25}$$

with degeneracy $n(M-1)$. Hence, the eigenvalue sum in Eq. (C.12) reads

$$n\left\{\ln(1 - \beta s\lambda R + \beta s\lambda q) - \frac{\beta s\lambda q}{1 - \beta s\lambda R + \beta s\lambda q} - \beta s\lambda(1-R)\right\} + \mathrm{O}(n^2) \tag{C.26}$$

The pseudo free energy is given by using the replica trick:

$$f = -\frac{1}{N\beta}[\log Z] = -\frac{1}{N\beta} \lim_{n\to 0} \frac{[Z^n] - 1}{n} = \lim_{n\to 0} \frac{\tilde{f}}{n}. \tag{C.27}$$

From the above results, we obtain

$$\begin{aligned} f = {} & \frac{s\lambda}{2} m^2 + s(1-\lambda)(m^x)^2 - (1-s)m^x + \tilde{m}^x m^x - \frac{\alpha\beta}{2}\tilde{q}q + \frac{\alpha\beta}{2}\tilde{R}R \\ & + \frac{\alpha}{2\beta}\left\{\ln(1 - \beta s\lambda R + \beta s\lambda q) - \frac{\beta s\lambda q}{1 - \beta s\lambda R + \beta s\lambda q} - \beta s\lambda(1-R)\right\} \\ & - \frac{1}{\beta}\int Dz \ln \int Dw\, 2\cosh\beta\sqrt{\big(s\lambda m + \sqrt{\alpha\tilde{q}}z + \sqrt{\alpha(\tilde{R}-\tilde{q})}w\big)^2 + \big(\tilde{m}^x\big)^2}. \end{aligned} \tag{C.28}$$

In what follows, we will derive self-consistent equations in the low-temperature limit. To simplify expressions shown later, we define the followings:

$$g \equiv s\lambda m + \sqrt{\alpha\tilde{q}}z + \sqrt{\alpha(\tilde{R}-\tilde{q})}w, \tag{C.29}$$

$$u \equiv \sqrt{g^2 + (\tilde{m}^x)^2}, \tag{C.30}$$

$$Y \equiv \int Dw \cosh\beta u. \tag{C.31}$$

The saddle-point conditions for the pseudo free energy (C.28) leads to the self-consistent equations

$$m = \int Dz\, Y^{-1} \int Dw\, \frac{g}{u} \sinh \beta u, \tag{C.32}$$

$$m^x = \int Dz\, Y^{-1} \int Dw\, \frac{\tilde{m}^x}{u} \sinh \beta u, \tag{C.33}$$

$$q = \int Dz \Big(Y^{-1} \int Dw\, \frac{g}{u} \sinh \beta u \Big)^2, \tag{C.34}$$

$$R = \int Dz\, Y^{-1} \Big(\int Dw \left(\frac{g}{u} \right)^2 \cosh \beta u + \frac{(\tilde{m}^x)^2}{\beta} \int Dw\, \frac{1}{u^3} \sinh \beta u \Big)^2, \tag{C.35}$$

$$\tilde{m}^x = 1 - s - 2s(1-\lambda) m^x, \tag{C.36}$$

$$\tilde{q} = \frac{(s\lambda)^2 q}{\{1 - \beta s \lambda (R-q)\}^2}, \tag{C.37}$$

$$\tilde{R} = \tilde{q} + \frac{(s\lambda)^2 (R-q)}{1 - \beta s \lambda (R-q)}. \tag{C.38}$$

The order parameter R is greater than or equal to q, since

$$\begin{aligned}
R &\geq \int Dz\, Y^{-1} \int Dw \left(\frac{g}{u} \right)^2 \cosh \beta u \\
&= \int Dz\, \frac{Y^{-2}}{2\pi} \int dw\, e^{-w^2/2} \cosh \beta u \int dw\, e^{-w^2/2} \Big(\frac{g}{u} \Big)^2 \cosh \beta u \\
&\geq \int Dz\, \frac{Y^{-2}}{2\pi} \Big\{ \int dw (e^{-w^2/2} \cosh \beta u)^{1/2} \Big(e^{-w^2/2} \Big(\frac{g}{u} \Big)^2 \cosh \beta u \Big)^{1/2} \Big\}^2 \\
&= \int Dz \left\{ Y^{-1} \int Dw\, \frac{g}{u} \cosh \beta u \right\}^2 \\
&\geq \int Dz \left\{ Y^{-1} \int Dw\, \frac{g}{u} \sinh \beta u \right\}^2 \\
&= q.
\end{aligned} \tag{C.39}$$

In particular, q is equal to R in the limit $\beta \to \infty$ as shown below. Assuming that $R > q$, we have $\tilde{q} = \tilde{R} = 0$ from Eqs. (C.37) and (C.38). Then, Eqs. (C.34) and (C.35) read

$$q = \left\{ \frac{g}{u} \tanh \beta u \right\}^2 \to \left(\frac{g}{u} \right)^2, \tag{C.40}$$

$$R = \left(\frac{g}{u} \right)^2 + \frac{(\tilde{m}^x)^2 \tanh \beta u}{\beta u^3} \to \left(\frac{g}{u} \right)^2, \tag{C.41}$$

which is in conflict with the assumption. Hence, the relation $q = R$ holds in the low-temperature limit. From Eq. (C.38), we have $\tilde{q} = \tilde{R}$. It follows that the integrands in the self-consistent equations are independent of w; the integrals with respect to w are taken

easily. Consequently, the self-consistent equations in the low-temperature limit are

$$m = \int Dz \frac{s\lambda m + \sqrt{\alpha\tilde{q}}z}{\sqrt{(s\lambda m + \sqrt{\alpha\tilde{q}}z)^2 + (1 - s - 2s(1-\lambda)m^x)^2}}, \tag{C.42}$$

$$m^x = \int Dz \frac{1 - s - 2s(1-\lambda)m^x}{\sqrt{(s\lambda m + \sqrt{\alpha\tilde{q}}z)^2 + (1 - s - 2s(1-\lambda)m^x)^2}}, \tag{C.43}$$

$$q = \int Dz \frac{(s\lambda m + \sqrt{\alpha\tilde{q}}z)^2}{(s\lambda m + \sqrt{\alpha\tilde{q}}z)^2 + (1 - s - 2s(1-\lambda)m^x)^2}. \tag{C.44}$$

Although q is equal to R, the factor $\beta(R-q)$ converges to

$$\lim_{\beta\to\infty} \beta(R-q) = \int Dz \frac{\{1 - s - 2s(1-\lambda)m^x\}^2}{\{(s\lambda m + \sqrt{\alpha\tilde{q}}z)^2 + (1 - s - 2s(1-\lambda)m^x)^2\}^{3/2}} \equiv C. \tag{C.45}$$

For this reason, we obtain

$$\tilde{q} = \frac{(s\lambda)^2 q}{(1 - s\lambda C)^2}. \tag{C.46}$$

The pseudo free energy is written as

$$\begin{aligned} f = {} & \frac{1}{2}s\lambda m^2 - s(1-\lambda)(m^x)^2 - \frac{\alpha}{2}s\lambda + \frac{\alpha}{2}\tilde{q}C \\ & - \int Dz \sqrt{(s\lambda m + \sqrt{\alpha\tilde{q}})^2 + (1 - s - 2s(1-\lambda)m^x)^2}. \end{aligned} \tag{C.47}$$

Appendix D.

Self-consistent equations for the Hopfield model with many-body interactions and with many patterns

We derive Eqs. (4.22)–(4.24) in this Appendix. We closely follow the calculation in Ref. [38]. The target Hamiltonian is given by Eq. (4.1) and (4.2). The number of patterns must be $p = \alpha N^{k-1}$ so that the free energy is extensive. We consider the case where the system has a single non-vanishing overlap again.

The replicated partition function for a Trotter number M is calculated in the same way as in the case of $k = 2$ except that the spin-product term for $\sigma^z_{i\rho}(\alpha)$ is linearized by using the delta function:

$$
\begin{aligned}
[Z_M^n] = \int \prod_{\alpha,\mu,\rho} & dm_\rho(\alpha)\, d\tilde{m}_\rho(\alpha)\, dm^x_\rho(\alpha)\, d\tilde{m}^x_\rho(\alpha) \\
& \times \mathrm{Tr}\Big[\exp -\frac{\beta}{M}\sum_{\alpha,\rho}\tilde{m}_\rho(\alpha)\Big(Nm_\rho(\alpha) - \sum_i \xi^1_i \sigma^z_{i\rho}(\alpha)\Big)\Big] \\
& \times \exp -\frac{\beta}{M}\sum_{\alpha,\rho}\tilde{m}^x_\rho(\alpha)\Big(Nm^x_\rho(\alpha) - \sum_i \sigma^x_{i\rho}(\alpha)\Big) \\
& \times \exp \frac{\beta s\lambda N}{M}\sum_{\alpha,\rho}\big(m_\rho(\alpha)\big)^k \prod_{\mu\geq 2}\Big[\exp \frac{\beta s\lambda}{MN^{k-1}}\sum_{\alpha,\rho}\sum_{i_1<\cdots<i_k}\xi^\mu_{i_1}\sigma^z_{i_1\rho}(\alpha)\cdots\xi^\mu_{i_k}\sigma^z_{i_k\rho}(\alpha)\Big] \\
& \times \exp \frac{\beta N}{M}\sum_{\alpha,\rho}\Big\{-s(1-\lambda)\big(m^x_\rho(\alpha)\big)^2 + (1-s)m^x_\rho(\alpha)\Big\} \\
& \times \prod_{\alpha,\rho,i}\langle\sigma^z_{i\rho}(\alpha)|\sigma^x_{i\rho}(\alpha)\rangle\langle\sigma^x_{i\rho}(\alpha)|\sigma^z_{i\rho}(\alpha+1)\rangle. \qquad \text{(D.1)}
\end{aligned}
$$

Note that only the spin-product term for the pattern with non-vanishing overlap is linearized. The other spin-product term is evaluated as follows. Expanding the exponential, we find that the linear term in the series vanishes. The contribution from the second term is

$$
\begin{aligned}
& \frac{1}{2}\Big(\frac{\beta s\lambda}{MN^{k-1}}\Big)^2 \sum_{\alpha,\rho,\alpha',\rho'}\sum_{i_1<\cdots<i_k}\sigma^z_{i_1\rho}(\alpha)\sigma^z_{i_1\rho'}(\alpha')\cdots\sigma^z_{i_k\rho}(\alpha)\sigma^z_{i_k\rho'}(\alpha') \\
& = \frac{1}{2}\Big(\frac{\beta s\lambda}{MN^{k-1}}\Big)^2 \sum_{\alpha,\rho,\alpha',\rho'}\Big\{\Big(\sum_i \sigma^z_{i\rho}(\alpha)\sigma^z_{i\rho'}(\alpha')\Big)^k + \mathrm{O}(N^{k-1})\Big\} \\
& = \frac{1}{2}\Big(\frac{\beta s\lambda}{M}\Big)^2 \sum_{\alpha,\rho,\alpha',\rho'}\frac{1}{N^{k-2}}\Big(\frac{1}{N}\sum_i \sigma^z_{i\rho}(\alpha)\sigma^z_{i\rho'}(\alpha')\Big)^k + \mathrm{O}\Big(\frac{1}{N^{k-1}}\Big). \qquad \text{(D.2)}
\end{aligned}
$$

Since the contribution from the lth term is of the order of $N^{l(1-k/2)}$, the correction to the $\mathrm{O}(N^{2-k})$ term in the series, ϵ_k, is the greater one of $\mathrm{O}(N^{1-k})$ and $\mathrm{O}(N^{3(1-k/2)})$: For $k=3$, $\epsilon_3=\mathrm{O}(N^{-3/2})$, and for $k>3$, $\epsilon_k=\mathrm{O}(N^{1-k})$. Thus, the series reads

$$\begin{aligned}
&\prod_{\mu\geq 2}\Big\{1+\frac{1}{2}\Big(\frac{\beta s\lambda}{M}\Big)^2\frac{1}{N^{k-2}}\sum_{\alpha,\rho,\alpha',\rho'}\Big(\frac{1}{N}\sum_i\sigma^z_{i\rho}(\alpha)\sigma^z_{i\rho'}(\alpha')\Big)^k+\epsilon_k\Big\}\\
&=\exp\sum_{\mu\geq 2}\Big\{\frac{1}{2}\Big(\frac{\beta s\lambda}{M}\Big)^2\frac{1}{N^{k-2}}\sum_{\alpha,\rho,\alpha',\rho'}\Big(\frac{1}{N}\sum_i\sigma^z_{i\rho}(\alpha)\sigma^z_{i\rho'}(\alpha')\Big)^k+\epsilon_k\Big\}\\
&=\exp\Big\{\frac{\alpha N}{2}\Big(\frac{\beta s\lambda}{M}\Big)^2\sum_{\alpha,\rho,\alpha',\rho'}\Big(\frac{1}{N}\sum_i\sigma^z_{i\rho}(\alpha)\sigma^z_{i\rho'}(\alpha')\Big)^k+\alpha N^{k-1}\epsilon_k\Big\}. \qquad \text{(D.3)}
\end{aligned}$$

Here, we have used $p=\alpha N^{k-1}$. The correction term is $\mathrm{O}(N^{1/2})$ for $k=3$, and $\mathrm{O}(N^0)$ for $k>3$; hence, this term is negligible in the thermodynamic limit. Linearizing the spin-product term in Eq. (D.3) by using the delta functions (C.9) and (C.10), we can write the integrand in $[Z_M^n]$ as $\exp(-N\beta\tilde{f})$ with

$$\begin{aligned}
\tilde{f}=&-\frac{s\lambda}{M}\sum_{\alpha\rho}\big(m_\rho(\alpha)\big)^k+\frac{s(1-\lambda)}{M}\sum_{\alpha\rho}\big(m^x_\rho(\alpha)\big)^2-\frac{1-s}{M}\sum_{\alpha\rho}m^x_\rho(\alpha)\\
&+\frac{1}{M}\sum_{\alpha\rho}\tilde{m}_\rho(\alpha)m_\rho(\alpha)+\frac{1}{M}\sum_{\alpha\rho}\tilde{m}^x_\rho(\alpha)m^x_\rho(\alpha)\\
&-\frac{\alpha\beta}{2M^2}(s\lambda)^2\sum_{(\alpha\rho,\alpha'\rho')}\big(q_{\rho\rho'}(\alpha,\alpha')\big)^k-\frac{\alpha\beta}{2M^2}(s\lambda)^2\sum_{\alpha\alpha'\rho}\big(R_\rho(\alpha,\alpha')\big)^k\\
&+\frac{\alpha\beta}{2M^2}\sum_{(\alpha\rho,\alpha'\rho')}\tilde{q}_{\rho\rho'}(\alpha,\alpha')q_{\rho\rho'}(\alpha,\alpha')+\frac{\alpha\beta}{2M^2}\sum_{\alpha\alpha'\rho}\tilde{R}_\rho(\alpha,\alpha')R_\rho(\alpha,\alpha')\\
&-\frac{1}{\beta}\Big[\ln\mathrm{Tr}\exp\Big\{\frac{\beta}{M}\sum_{\alpha\rho}\xi\tilde{m}_\rho(\alpha)\sigma^z_\rho(\alpha)+\frac{\beta}{M}\sum_{\alpha\rho}\tilde{m}^x_\rho(\alpha)\sigma^x_\rho(\alpha)\\
&+\frac{\alpha\beta^2}{2M^2}\sum_{(\alpha\rho,\alpha'\rho')}\tilde{q}_{\rho\rho'}(\alpha,\alpha')\sigma^z_\rho(\alpha)\sigma^z_{\rho'}(\alpha')+\frac{\alpha\beta^2}{2M^2}\sum_{(\alpha\alpha'\rho)}\tilde{R}_\rho(\alpha,\alpha')\sigma^z_\rho(\alpha)\sigma^z_\rho(\alpha')\Big\}\\
&\times\prod_{\alpha\rho}\langle\sigma^z_\rho(\alpha)|\sigma^x_\rho(\alpha)\rangle\langle\sigma^x_\rho(\alpha)|\sigma^z_\rho(\alpha+1)\rangle\Big]. \qquad \text{(D.4)}
\end{aligned}$$

In a similar manner to the case of $k=2$, we look for the RS solution, and use the static ansatz. The spin-product term in Eq. (D.4) is linearized by using a Gaussian integral. Expanding the configurational term in Eq. (D.4) in powers of n, we have,

$$\begin{aligned}
&n\Big[\int Dz\ln\int Dw\,\mathrm{Tr}\exp\Big\{\frac{\beta}{M}\sum_\alpha\xi\tilde{m}\sigma^z(\alpha)+\frac{\beta}{M}\sum_\alpha\tilde{m}^x\sigma^x(\alpha)\\
&+\sqrt{\alpha\tilde{q}}\frac{\beta}{M}\sum_\alpha\sigma^z(\alpha)z+\sqrt{\alpha(\tilde{R}-\tilde{q})}\frac{\beta}{M}\sum_\alpha\sigma^x(\alpha)w\Big\}\\
&\times\prod_\alpha\langle\sigma^z(\alpha)|\sigma^x(\alpha)\rangle\langle\sigma^x(\alpha)|\sigma^z(\alpha+1)\rangle\Big]+\mathrm{O}(n^2). \qquad \text{(D.5)}
\end{aligned}$$

The inverse operation of the Trotter decomposition leads to

$$n \int Dz \ln \int Dw \, 2\cosh \beta \sqrt{\left(\tilde{m} + \sqrt{\alpha \tilde{q}} z + \sqrt{\alpha(\tilde{R} - \tilde{q})} w\right)^2 + (\tilde{m}^x)^2} + \mathrm{O}(n^2). \tag{D.6}$$

Using the replica trick, we finally obtain the following pseudo free energy:

$$\begin{aligned} f = & -s\lambda m^k + s(1-\lambda)(m^x)^2 - (1-s)m^x + \tilde{m}m + \tilde{m}^x m^x \\ & + \frac{\alpha}{2}\beta(s\lambda)^2 q^k - \frac{\alpha}{2}\beta(s\lambda)^2 R^k - \frac{\alpha}{2}\beta\tilde{q}q + \frac{\alpha}{2}\beta\tilde{R}R \\ & - \frac{1}{\beta}\int Dz \ln \int Dw \, 2\cosh \beta \sqrt{\left(\tilde{m} + \sqrt{\alpha \tilde{q}} z + \sqrt{\alpha(\tilde{R} - \tilde{q})} w\right)^2 + (\tilde{m}^x)^2}. \end{aligned} \tag{D.7}$$

The saddle-point conditions for the pseudo free energy (D.7) yield the self-consistent equations. Let

$$g \equiv s\lambda k m^{k-1} + \sqrt{\alpha \tilde{q}} z + \sqrt{\alpha(\tilde{R} - \tilde{q})} w, \tag{D.8}$$

and u in the same way as in Eq. (C.30), and Y as in Eq. (C.31). Then the self-consistent equations are given by Eqs. (C.32)–(C.36) with Eq. (D.8) and

$$\tilde{q} = (s\lambda)^2 k q^{k-1}, \tag{D.9}$$

$$\tilde{R} = (s\lambda)^2 k R^{k-1}. \tag{D.10}$$

In the same way as the case of $k = 2$, we find $R \geq q$. If $R > q$, the free energy diverges in the limit $\beta \to \infty$. Accordingly, R must be equal to q. It follows that $\tilde{R} = \tilde{q}$, so that the integrands in the self-consistent equations are independent of w. Hence, the self-consistent equations in the low-temperature limit are

$$m = \int Dz \, \frac{s\lambda(km^{k-1} + \sqrt{\alpha k q^{k-1}} z)}{\sqrt{(s\lambda[km^{k-1} + \sqrt{\alpha k q^{k-1}} z])^2 + (1 - s - 2s(1-\lambda)m^x)^2}}, \tag{D.11}$$

$$m^x = \int Dz \, \frac{1 - s - 2s(1-\lambda)m^x}{\sqrt{(s\lambda[km^{k-1} + \sqrt{\alpha k q^{k-1}} z])^2 + (1 - s - 2s(1-\lambda)m^x)^2}}, \tag{D.12}$$

$$q = \int Dz \, \frac{(s\lambda[km^{k-1} + \sqrt{\alpha k q^{k-1}} z])^2}{(s\lambda[km^{k-1} + \sqrt{\alpha k q^{k-1}} z])^2 + (1 - s - 2s(1-\lambda)m^x)^2}. \tag{D.13}$$

The factor $\beta(R - q)$ converges to

$$C \equiv \lim_{\beta \to \infty} \beta(R - q) = \int Dz \, \frac{\{1 - s - 2s(1-\lambda)m^x\}^2}{\{(s\lambda[km^{k-1} + \sqrt{\alpha k q^{k-1}} z])^2 + (1 - s - 2s(1-\lambda)m^x)^2\}^{3/2}}. \tag{D.14}$$

Since the factor $\beta(R^k - q^k)$ converges to Ckq^{k-1}, the pseudo free energy in the low-temperature limit is

$$\begin{aligned} f = & \, s\lambda(k-1)m^k - s(1-\lambda)(m^x)^2 + \frac{\alpha}{2}k(k-1)(s\lambda)^2 C q^{k-1} \\ & - \int Dz \sqrt{(s\lambda[km^{k-1} + \sqrt{\alpha k q^{k-1}} z])^2 + (1 - s - 2s(1-\lambda)m^x)^2}. \end{aligned} \tag{D.15}$$

Appendix E.

Pseudo free energy of the Wajnflasz-Pick model with antiferromagnetic transverse interactions and transverse field

We derive the pseudo free energy (5.11) by using the mean-field analysis. The calculation is similar to that of the ferromagnetic p-spin model described in Chap. 3. The difference is that we have to use three types of closures to convert the quantum Hamiltonian (5.10) to a classical Hamiltonian.

The Hamiltonian is

$$\hat{H}(s,\lambda) = -s\lambda N\left(\frac{1}{N}\sum_i \hat{\tau}_i^z\right)^2 - s\lambda h\sum_i \hat{\tau}_i^z + s(1-\lambda)N\left(\frac{1}{N}\sum_i \hat{\tau}_i^{x,2}\right)^2 - (1-s)\sum_i \hat{\tau}_i^{x,1}, \tag{E.1}$$

where s and λ are control parameters, and N is the number of variables corresponding to the spin variable of the usual spin-1/2 system. The operators τ^z, $\tau^{x,1}$, and $\tau^{x,2}$ are defined by Eqs. (5.5) and (5.8). The partition function for a Trotter number M is given as

$$Z_M = \mathrm{Tr}\left(\exp\left\{\frac{\beta s\lambda N}{M}\left[\left(\frac{1}{N}\sum_i \hat{\tau}_i^z\right)^2 + h\sum_i \hat{\tau}_i^z\right]\right\}\exp\left\{-\frac{\beta s(1-\lambda)N}{M}\left(\frac{1}{N}\sum_i \hat{\tau}_i^{x,2}\right)^2\right\}\right.$$
$$\left.\times\exp\left\{\frac{\beta(1-s)}{M}\sum_i \hat{\tau}_i^{x,1}\right\}\right)^M. \tag{E.2}$$

Here, β denotes inverse temperature.

We use the following three types of closures:

$$\hat{1}^z(\alpha) \equiv \sum_{\{\tau_i^z(\alpha)\}} |\{\tau_i^z(\alpha)\}\rangle\langle\{\tau_i^z(\alpha)\}|, \tag{E.3}$$

$$\hat{1}^{x,1}(\alpha) \equiv \sum_{\{\tau_i^{x,1}(\alpha)\}} |\{\tau_i^{x,1}(\alpha)\}\rangle\langle\{\tau_i^{x,1}(\alpha)\}|, \tag{E.4}$$

$$\hat{1}^{x,2}(\alpha) \equiv \sum_{\{\tau_i^{x,2}(\alpha)\}} |\{\tau_i^{x,2}(\alpha)\}\rangle\langle\{\tau_i^{x,2}(\alpha)\}|, \tag{E.5}$$

in order to convert the system to a classical system. Here, α is an integer between unity and M. The quantum state $|\{\tau_i^z(\alpha)\}\rangle$ denotes an orthogonal basis that diagonalizes the operators $\hat{\tau}_i^z(\alpha)$ for $i = 1,\ldots,N$. The summation $\sum_{\{\tau_i^z(\alpha)\}}$ is taken over all orthogonal

basis. In a similar way, we define $|\{\hat{\tau}_i^{x,1}(\alpha)\}\rangle$ and $|\{\hat{\tau}_i^{x,2}(\alpha)\}\rangle$, and summations with regards to them. Introducing the closures (E.3)–(E.5) to Eq. (E.2), we have

$$\begin{aligned} Z_M = \prod_\alpha \sum_{\{\tau_i^z(\alpha)\}} \sum_{\{\tau_i^{x,1}(\alpha)\}} \sum_{\{\tau_i^{x,2}(\alpha)\}} \exp\Bigg\{ & \frac{\beta s\lambda N}{M}\left[\left(\frac{1}{N}\sum_i \tau_i^z(\alpha)\right)^2 + h\sum_i \tau_i^z(\alpha)\right] \\ & - \frac{\beta s(1-\lambda)N}{M}\left(\frac{1}{N}\sum_i \tau_i^{x,2}(\alpha)\right)^2 + \frac{\beta(1-s)}{M}\sum_i \tau_i^{x,1}(\alpha)\Bigg\} \\ & \times \prod_i \langle \tau_i^z(\alpha)|\tau_i^{x,2}(\alpha)\rangle\langle\tau_i^{x,2}(\alpha)|\tau_i^{x,1}(\alpha)\rangle\langle\tau_i^{x,1}(\alpha)|\tau_i^z(\alpha+1)\rangle, \end{aligned} \tag{E.6}$$

with periodic boundary conditions $\tau_i^z(M+1) = \tau_i^z(1)$ for all i.

The spin-product terms in Eq. (E.6) can be linearized by using integral representation of the delta functions:

$$\delta\left(Nm^z(\alpha) - \sum_i \tau_i^z(\alpha)\right) = \int d\tilde{m}^z(\alpha) \exp\left\{-\frac{\beta}{M}\tilde{m}^z(\alpha)\left(Nm^z(\alpha) - \sum_i \tau_i^z(\alpha)\right)\right\}, \tag{E.7}$$

$$\delta\left(Nm^x(\alpha) - \sum_i \tau_i^{x,2}(\alpha)\right) = \int d\tilde{m}^x(\alpha) \exp\left\{-\frac{\beta}{M}\tilde{m}^x(\alpha)\left(Nm^x(\alpha) - \sum_i \tau_i^{x,2}(\alpha)\right)\right\}, \tag{E.8}$$

leading to the partition function for a single-particle system:

$$\begin{aligned} Z_M = \int\cdots\int \prod_\alpha & dm^z(\alpha)\, d\tilde{m}^z(\alpha)\, dm^x(\alpha)\, d\tilde{m}^x(\alpha) \\ & \times \exp\left\{\frac{\beta N}{M}\sum_\alpha (s\lambda\{[m^z(\alpha)]^2 + hm^z(\alpha)\} - \tilde{m}^z(\alpha)m^z(\alpha) - s(1-\lambda)[m^x(\alpha)]^2 - \tilde{m}^x(\alpha)m^x(\alpha))\right\} \\ & \times \exp\Bigg\{N\ln \prod_\alpha \sum_{\{\tau^z(\alpha)\}} \sum_{\{\tau^{x,1}(\alpha)\}} \sum_{\{\tau^{x,2}(\alpha)\}} \\ & \quad \times \exp\frac{\beta}{M}[\tilde{m}^z(\alpha)\tau^z(\alpha) + \tilde{m}^x(\alpha)\tau^{x,2}(\alpha) + (1-s)\tau^{x,1}(\alpha)] \\ & \quad \times \langle\tau^z(\alpha)|\tau^{x,2}(\alpha)\rangle\langle\tau^{x,2}(\alpha)|\tau^{x,1}(\alpha)\rangle\langle\tau^{x,1}(\alpha)|\tau^z(\alpha+1)\rangle\Bigg\}. \end{aligned} \tag{E.9}$$

We evaluate the integral by using the saddle-point method. The saddle-point conditions for $m^z(\alpha)$ and $m^x(\alpha)$ yields

$$\tilde{m}^z(\alpha) = s\lambda(2m^z(\alpha) + h), \tag{E.10}$$

$$\tilde{m}^x(\alpha) = -2s(1-\lambda)m^x(\alpha). \tag{E.11}$$

Using the static ansatz, we can take the summations in Eq. (E.9) by the inverse operation of the Trotter decomposition. Then, we finally obtain the partition function

$$Z = \iint dm^z\, dm^x \exp\{-N\beta f\}, \tag{E.12}$$

where f is a pseudo free energy given by

$$f = s\lambda\big(m^z\big)^2 - s(1-\lambda)\big(m^x\big)^2 - \frac{1}{\beta}\ln \mathrm{Tr}\exp\beta\big(\tilde{m}^z\hat{\tau}^z + \tilde{m}^x\hat{\tau}^{x,2} + (1-s)\hat{\tau}^{x,1}\big). \tag{E.13}$$

Bibliography

[1] T. Kadowaki and H. Nishimori, Phys. Rev. E **58**, 5355 (1998).

[2] A. Finnila, M. Gomez, C. Sebenik, C. Stenson, and J. D. Doll, Chem. Phys. Lett. **219**, 1994 (1994).

[3] A. Das and B. Chakrabarti, Rev. Mod. Phys. **80**, 1061 (2008).

[4] G. E. Santoro and E. Tosatti, J. Phys. A: Math. Gen. **39**, R393 (2006).

[5] S. Morita and H. Nishimori, J. Math. Phys. **49**, 125210 (2008).

[6] V. Bapst, L. Foini, F. Krzakala, G. Semerjian, and F. Zamponi, Phys. Rep. **523**, 127 (2013).

[7] A. K. Hartmann and M. Weigt, *Phase Transitions in Combinatorial Optimization Problems: Basics, Algorithms and Statistical Mechanics*, WILEY-VCH, 2005.

[8] S. Kirkpatrick, C. D. Gelatt, and M. P. Vecchi, Science **220**, 671 (1983).

[9] A. Perdomo-Ortiz, N. Dickson, and M. Drew-Brook, Sci. Rep. **2**, 1 (2012).

[10] J. Hopfield and D. Tank, Science **233**, 625 (1986).

[11] Y. Fu and P. Anderson, J. Phys. A: Math. Gen. **19**, 1605 (1986).

[12] S. Geman and D. Geman, IEEE Trans. Pattern Anal. Mach. Intell. **6**, 721 (1984).

[13] A. Messiah, *Quantum Mechanics*, DOVER, 1999.

[14] S. Suzuki, J.-i. Inoue, and B. K. Chakrabarti, *Quantum Ising Phases and Transitions in Transverse Ising Models*, Springer, 2012.

[15] R. Schützhold and G. Schaller, Phys. Rev. A **74**, 060304 (2006).

[16] T. Jörg, F. Krzakala, J. Kurchan, and A. C. Maggs, Phys. Rev. Lett. **101**, 147204 (2008).

[17] T. Jörg, F. Krzakala, G. Semerjian, and F. Zamponi, Phys. Rev. Lett. **104**, 207206 (2010).

[18] T. Jörg, F. Krzakala, J. Kurchan, A. C. Maggs, and J. Pujos, Europhys. Lett. **89**, 40004 (2010).

[19] A. Young, S. Knysh, and V. Smelyanskiy, Phys. Rev. Lett. **104**, 020502 (2010).

[20] J. Tsuda, Y. Yamanaka, and H. Nishimori, J. Phys. Soc. Japan **82**, 1 (2013).

[21] J. J. Hopfield and D. W. Tank, Biol. Cybern. **52**, 141 (1985).

[22] H. Nishimori and Y. Nonomura, J. Phys. Soc. Japan **65**, 3780 (1996).

[23] E. Farhi et al., Science **292**, 472 (2001).

[24] S. Sachdev, *Quantum Phase Transitions*, CAMBRIDGE, 2011.

[25] H. Nishimori, J. Tsuda, and S. Knysh, Phys. Rev. E **91**, 012104 (2015).

[26] R. Somma, D. Nagaj, and M. Kieferová, Phys. Rev. Lett. **109**, 050501 (2012).

[27] M. A. Nielsen and I. L. Chuang, *Quantum Computation and Quantum Information*, CAMBRIDGE, 2010.

[28] D. Aharonov, W. V. Dam, J. Kempe, and Z. Landau, SIAM Rev. **50**, 755 (2008).

[29] W. Van Dam, M. Mosca, and U. Vazirani, How powerful is adiabatic quantum computation?, in *Proceedings of the 42nd IEEE Symposium on Foundations of Computer Science*, pages 279–287, IEEE, 2001.

[30] Y. Seki and H. Nishimori, Phys. Rev. E **85**, 051112 (2012).

[31] M. Suzuki, Prog. Theor. Phys. **56**, 1454 (1976).

[32] H. Nishimori and G. Ortiz, *Elements of Phase Transitions and Critical Phenomena*, OXFORD, 2010.

[33] E. Farhi, J. Goldstone, S. Gutmann, and M. Sipser, arXiv Prepr. quant-ph/0001106 (2000).

[34] J. Roland and N. Cerf, Phys. Rev. A **65**, 042308 (2002).

[35] J. Hopfield, Proc. Natl. Acad. Sci. **79**, 2554 (1982).

[36] D. Amit, H. Gutfreund, and H. Sompolinsky, Phys. Rev. A **32**, 1007 (1985).

[37] D. Amit, H. Gutfreund, and H. Sompolinsky, Ann. Phys. **173**, 30 (1987).

[38] E. Gardner, J. Phys. A: Math. Gen. **20**, 3453 (1987).

[39] Y.-q. Ma and C.-d. Gong, Phys. Rev. E **51**, 1573 (1995).

[40] J. A. Hertz, A. S. Krogh, and R. G. Palmer, *Introduction to the Theory of Neural Computation*, CITESEER, 1991.

[41] B. Seoane and H. Nishimori, J. Phys. A: Math. Theor. **45**, 435301 (2012).

[42] J. Wajnflasz and R. Pick, J. Phys. **32**, C1 (1971).

[43] S. Miyashita et al., **114**, 19 (2005).

[44] K. Kurihara, S. Tanaka, and S. Miyashita, Proc. 25th Conf. Uncertain. Artif. Intell. , 8 (2009).

[45] I. Sato, K. Kurihara, S. Tanaka, H. Nakagawa, and S. Miyashita, Proc. 25th Conf. Uncertain. Artif. Intell. , 9 (2009).

[46] B. Altshuler, H. Krovi, and J. Roland, Proc. Natl. Acad. Sci. **107**, 12446 (2010).